

Discovery of a small-molecule bromodomain-containing protein 4 (BRD4) inhibitor that induces AMP-activated protein kinase-modulated autophagy-associated cell death in breast cancer

Liang Ouyang, Lan Zhang, Jie Liu, Leilei Fu, Dahong Yao,
Yuqian Zhao, Shouyue Zhang, Guan Wang, Gu He, and Bo Liu

J. Med. Chem., **Just Accepted Manuscript** • DOI: 10.1021/acs.jmedchem.7b00275 • Publication Date (Web): 27 Nov 2017

Downloaded from <http://pubs.acs.org> on November 29, 2017

Just Accepted

“Just Accepted” manuscripts have been peer-reviewed and accepted for publication. They are posted online prior to technical editing, formatting for publication and author proofing. The American Chemical Society provides “Just Accepted” as a free service to the research community to expedite the dissemination of scientific material as soon as possible after acceptance. “Just Accepted” manuscripts appear in full in PDF format accompanied by an HTML abstract. “Just Accepted” manuscripts have been fully peer reviewed, but should not be considered the official version of record. They are accessible to all readers and citable by the Digital Object Identifier (DOI®). “Just Accepted” is an optional service offered to authors. Therefore, the “Just Accepted” Web site may not include all articles that will be published in the journal. After a manuscript is technically edited and formatted, it will be removed from the “Just Accepted” Web site and published as an ASAP article. Note that technical editing may introduce minor changes to the manuscript text and/or graphics which could affect content, and all legal disclaimers and ethical guidelines that apply to the journal pertain. ACS cannot be held responsible for errors or consequences arising from the use of information contained in these “Just Accepted” manuscripts.

1
2
3 **Discovery of a small-molecule bromodomain-containing**
4 **protein 4 (BRD4) inhibitor that induces AMP-activated**
5 **protein kinase-modulated autophagy-associated cell**
6 **death in breast cancer**
7
8
9
10
11
12

13 Liang Ouyang[#], Lan Zhang[#], Jie Liu, Leilei Fu, Dahong Yao, Yuqian Zhao, Shouyue
14 Zhang, Guan Wang, Gu He^{*}, Bo Liu^{*}

15
16
17 *State Key Laboratory of Biotherapy and Cancer Center, West China Hospital, Sichuan*
18 *University, and Collaborative Innovation Center of Biotherapy, Chengdu 610041, China*
19
20
21
22

23 **ABSTRACT**
24

25 Based upon The Cancer Genome Atlas (TCGA) dataset, we identified that several
26 autophagy-related proteins such as AMP-activated protein kinase (AMPK) was
27 remarkably downregulated in breast cancer. Combined with co-immunoprecipitation
28 assay, we demonstrated that BRD4 might interact with AMPK. After analyses of the
29 pharmacophore and WPF interaction optimization, we designed a small-molecule inhibitor
30 of BRD4 **9f** (FL-411) which was validated by co-crystal structure with BD1 of BRD4.
31 Subsequently, **9f** was discovered to induce ATG5-dependent autophagy-associated cell
32 death (ACD) by blocking BRD4-AMPK interaction, and thus activating
33 AMPK-mTOR-ULK1-modulated autophagic pathway in breast cancer cells. Interestingly,
34 the iTRAQ-based proteomics analyses revealed that **9f** induced ACD pathways, involved
35 in HMGB1, VDAC1/2 and eEF2. Moreover, **9f** displayed a therapeutic potential on both
36 breast cancer xenograft mouse and zebrafish models. Together, these results
37 demonstrate that a novel small-molecule inhibitor of BRD4 induces
38 BRD4-AMPK-modulated ACD in breast cancer, which may provide a candidate drug for
39 future cancer therapy.
40
41
42
43
44
45
46
47
48
49
50
51
52
53
54
55
56
57
58
59
60

Key words: Bromodomain-containing protein 4 (BRD4); BRD4-AMPK interaction; Small-molecule inhibitor of BRD4; Autophagy-associated cell death (ACD); Breast cancer

INTRODUCTION

Bromodomain-containing protein 4 (BRD4) is a member of the bromodomain and extra-terminal (BET) protein family, functioning as a central element in transmission of epigenetic memory across cell division and transcription regulation.¹⁻² Besides BRD4, there are other three members of BET family, such as BRD2, BRD3 and BRDT, which may regulate many cellular processes by the interactions of bromodomain.^{3,4} BRD4 is a ubiquitously expressed nuclear protein of 200 kDa that contains two tandem bromodomains (BD1 and BD2) which are structurally conserved but not functionally equivalent, and an extra-terminal domain.⁵⁻⁷ BRD4 may participate in oncogenic rearrangements, leading to highly oncogenic fusion proteins, and thus playing a key role in development of many types of cancer, including breast cancer.⁸⁻¹⁰ Recently, BRD4 has been reported to regulate breast cancer cell metastasis through modulating the enzymatic activity of Sipa1 in ER+ breast cancer.^{11,12} In addition, BRD4 is reported to modulate extracellular matrix gene expression, frequently presented in metastasis-predictive gene signature; thereby robustly predicting progression and survival through its activation signature in breast cancer.¹³ Therefore, targeting BRD4 inhibition would be a potential strategy in breast cancer therapy.

Of note, autophagy is an evolutionarily conserved, multi-step lysosomal degradation process for the clearance of damaged or superfluous proteins and organelles.¹⁴⁻¹⁷ In the autophagy process, mammalian target of rapamycin (mTOR) and AMP-activated protein kinase (AMPK) are able to oppositely regulate UNC-51-like kinase 1 (ULK1) activity by direct phosphorylation.¹⁸ AMPK-mTOR-ULK1 axis may play a key role in autophagosome formation and autophagy regulation.¹⁹ The function of AMPK, mTOR and ULK1 and their associations with breast cancer, has been gradually elucidated.²⁰⁻²² More recently, compound **1** (JQ1),²³ as the famous and first inhibitor of BET, has been reported to induce the AMPK-ULK1-modulated cytoprotective autophagy in acute myeloid leukemia (AML) stem cells.²⁴ On the contrary, **1** has been also reported to inhibit cytoprotective autophagy

1
2
3 via increasing NPM1 and HEXIM1 expression in AML cells.²⁵

4 For better elucidation of the role of BRD4 inhibition in autophagy and discovery of a
5 novel BRD4 inhibitor in breast cancer, we firstly identified the potential BRD4-AMPK axis
6 in autophagy by the combination of TCGA analyses and co-immunoprecipitation assays.
7
8 Based on the structure-based design, we finally discovered a new small-molecule inhibitor
9 of BRD4 that induced BRD4-AMPK-modulated autophagy/autophagic cell death of breast
10 cancer *in vitro* and *in vivo*.
11
12
13
14
15
16
17

18 **RESULTS**

19 **Identification of BRD4-AMPK interaction in autophagy to breast cancer therapy**

20 We constructed the protein-protein interactions (PPI) network of BRD4 by the
21 predicted and experimentally determined protein-protein interactions (PrePPI), in which
22 382 hub proteins were identified to potentially interact with BRD4. Based upon the PPI
23 network, BRD4 was shown to interact with 28 autophagy-related genes/proteins, which
24 are annotated by Gene Ontology (GO), indicating that BRD4, as an attractive cancer
25 target is related to some autophagic genes/proteins by regulation of the autophagic
26 process (Figure 1A). Subsequently, to attest the impact of autophagy in breast cancer, the
27 expression differences of autophagic genes were identified between normal and cancer
28 tissues in breast cancer dataset from The Cancer Genome Atlas (TCGA). Some key
29 autophagic genes, which were involved in the PPI network of BRD4, such as MAP1LC3A
30 ($p=1.10e-4$), MAP1LC3B ($p=2.02e-11$), PRKAA1 ($p=2.06e-11$) and ATG4C ($p=1.46e-8$)
31 were identified to have lower expression in tumor tissues than normal ones (Figure 1B).
32 Amongst them, we demonstrated that AMPK (PRKAA1), which is a key autophagic
33 regulator triggering AMPK-mTOR-ULK1 pathway, might interact with BRD4 by reciprocal
34 co-immunoprecipitation (Figure 1C). Interestingly, we found that AMPK did not interact
35 with c-Myc, a targeted transcription factor regulated by BRD4 (Figure S1), indicating there
36 may be a direct interaction between BRD4 and AMPK. Recently, decreased expression of
37 some autophagy-related genes, such as ULK1 and Beclin-1 has been revealed to be
38 closely associated with poor prognosis in breast cancer.^{26,27} It is well-known that BRD4,
39
40
41
42
43
44
45
46
47
48
49
50
51
52
53
54
55
56
57
58
59
60

as an attractive cancer target, can be combined with PI3K inhibition to induce cell death and overcomes resistance in breast cancer, indicating that combination of BRD4 and other kinase may be also a therapeutic avenue in breast cancer.²⁸ Interestingly, BRD4 has been demonstrated as a negative regulator of autophagy gene expression, and its dissociation from autophagy gene promoters can lead to transcriptional activation of autophagy genes.²⁹ Thus, induction of ACD is a possible strategy to sensitize breast cancer cells to therapy or kill them. As mentioned above, we identified the BRD4-AMPK interaction, which might play a key autophagy-modulating role in breast cancer. Thus, we put forward a hypothesis to design a small-molecule inhibitor of BRD4 that induces BRD4-AMPK-modulated ACD of breast cancer *in vitro* and *in vivo* (Figure 1D).

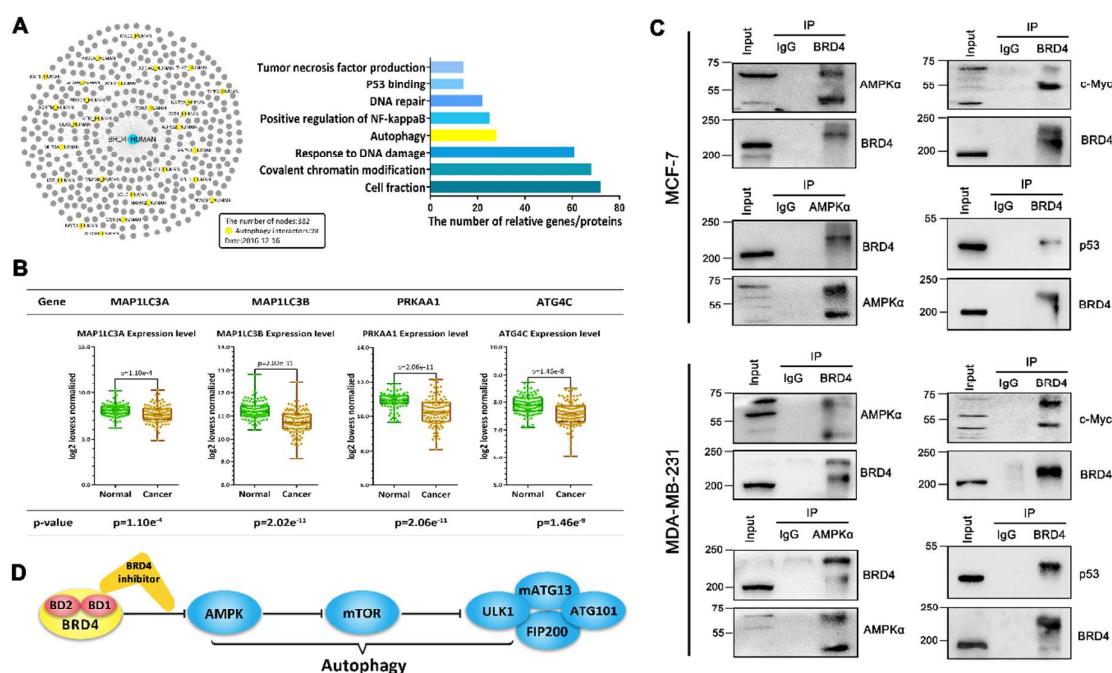


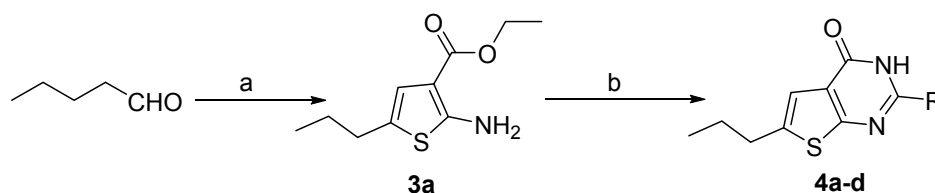
Figure.1 Identification of the BRD4-AMPK interaction in autophagy to breast cancer therapy. (A) The BRD4 related protein-protein network and autophagy-related enrichment analyses. (B) Comparison of autophagy related genes expression level between normal and cancer in TCGA breast cancer dataset. (C) Cell extracts of MCF-7 or MDA-MB-231 cells were subjected to immunoprecipitation with BRD4 (upper, left panel) and AMPK α (lower, left panel) antibodies, then detected by western blot using AMPK α and BRD4 antibodies. The expressions of BRD4 and AMPK α were determined in the input. C-Myc and p53 were immunoprecipitated with BRD4 as the positive control. (D) Model of BRD4 inhibitor-modulating autophagy, via inhibiting BRD4 and activating AMPK-mTOR-ULK complex axis.

Design and synthesis of candidate BRD4 inhibitors

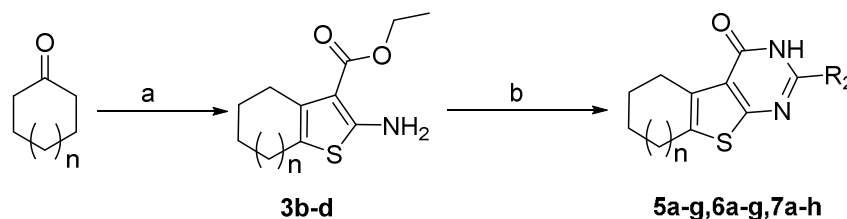
We performed two-step molecular docking on the candidate small-molecule compounds from ZINC database, which is a free public resource for ligand discovery that contains over twenty million commercially available molecules. We utilized the crystal structure of BRD4(1) from the RSCB (PDB ID: 3MXF) and defined the binding site referred to that of **1**. Other parameters were set as default values. In the first step, the top 500 hits were selected by LibDock protocol mainly according to the LibDock Score. Subsequently, the top 20 hits determining by CDOCKER protocol were selected by the interaction energy (Figure S2). And ZINC96907903 was shown to exhibit the best score and binding mode, suggesting this compound may have the priority as a candidate inhibitor of BRD4.

To obtain more potent analogues, we designed various substituents on the phenyl group to explore the chemical space for affinity improvement (Figure 2A). We preferentially determined the *m*-methoxyphenyl, *m*-bromophenyl, *p*-hydroxyphenyl when preserving the *n*-propyl on thiophene (Scheme 1), revealing that **4c**, with a *p*-hydroxyphenyl, showing the most potent inhibitory activity ($IC_{50} = 8.59 \mu M$). Whereas other compounds (**4a**, **4b**, **4d**) showed a weak inhibitory activity, suggesting that a hydrogen bond acceptor group forming a key hydrogen bond with Asn140 plays an important role for inhibitory potency. Subsequently, a cyclopentyl was incorporated into the thiophene and 7 compounds with different substituted phenyls were synthesized (Scheme 2). The AlphaScreen assay indicated that most of these compounds showed a certain extent improvement in potency. Especially **5a**, **5b** and **5f** have 1 to 10 fold improvement compared with **4c**. We speculated that the replacement of cyclopentyl with *n*-propyl might have a favorable contribution to compound activity. To further confirm SAR, on one hand, some greater groups in size were induced into the thiophene, including cyclohexyl, cycloheptyl, 4-methylcyclohexyl, nitromethylpiperidine and nitrobenzylpiperidine; on the other hand, various substituents on the phenyl group were preserved (Scheme 2 and 3). The AlphaScreen assay presented that all compounds

(except for **10b**) containing 4-hydroxy-3,5-dimethylbenzyl group had potent inhibitory activity against BRD4, and the change of substituents on thiophene from *n*-propyl to nitromethylpiperidine, led to a remarkable potency improvement, such as **5f** ($IC_{50} = 6.38 \mu\text{M}$), **8h** ($IC_{50} = 3.23 \mu\text{M}$) and **9f** (FL-411) ($IC_{50} = 0.43 \mu\text{M}$) (Table 1). However, further extension of the substituent decreased the activity, such as **10b** ($IC_{50} > 10 \mu\text{M}$). We demonstrated that 4-hydroxy-3,5-dimethylbenzyl was a favorable group to fit the acetyl-lysine binding site, the OH group as a hydrogen bond acceptor could interact with Asn140 to form a conserved hydrogen bond, and the ortho methyl of **9f** could function as the methyl of acetylated lysine to occupy the small hydrophobic pocket. Thus, the 4-hydroxy-3,5-dimethylbenzyl seems to be an optimal acetyl mimic fragment. The substituents on thiophene made hydrophobic interactions or hydrogen bonds with residues located in the ZA loop, especially the WPF shelf (Trp81, Pro82 and Phe83), which is key to the affinity and selectivity. Based upon the multiple biological evaluation screening, we eventually discovered that **9f** possessed the best BRD4(1) inhibition activity ($IC_{50}=0.43 \mu\text{M}$), anti-proliferative activity (MCF-7: $IC_{50}=1.62 \mu\text{M}$, MDA-MB-231: $IC_{50}=3.27 \mu\text{M}$) and autophagic activity (42.29% in MCF-7 cells), as well as displayed a low toxicity against MCF10A cells (Figure 2B and C, Table 1, Figure S2). In addition, **9f** had a better anti-proliferative activity than **1** and **2a** (RVX-208)³⁰ although it showed lower BRD4(1) inhibition activity than **1** (Table 1).



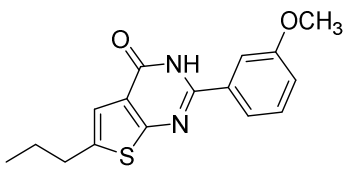
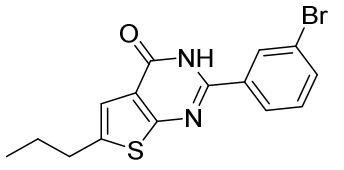
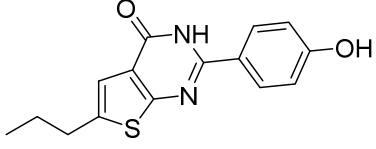
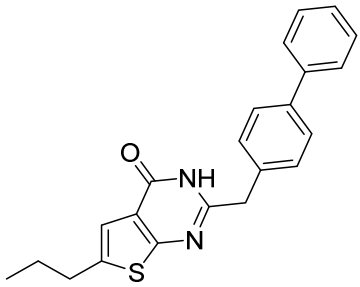
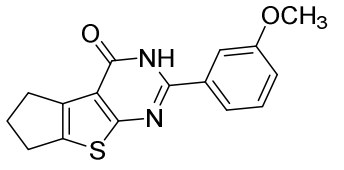
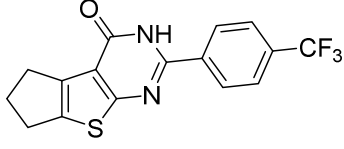
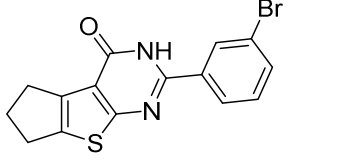
Scheme 1. Reagents and conditions: (a) $\text{NCCH}_2\text{CO}_2\text{Et}$, S_8 , EtOH, Et_3N , reflux, 12 h; (b) nitrile, dioxane/HCl, $100 \text{ }^\circ\text{C}$, 12 h.

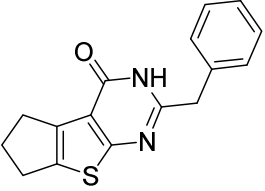
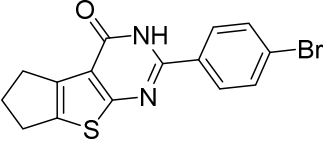
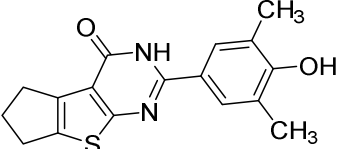
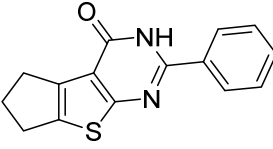
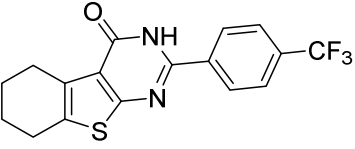
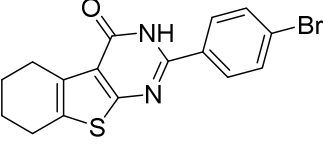
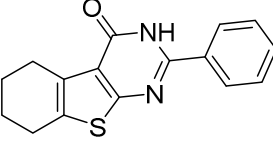
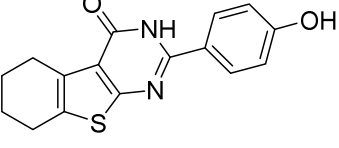
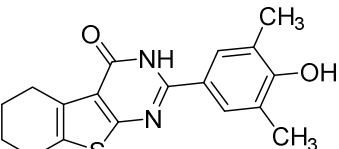


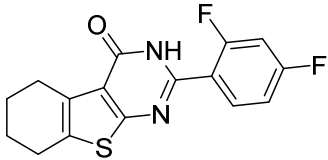
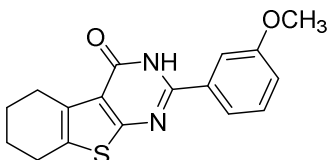
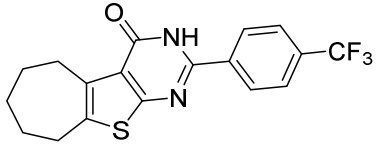
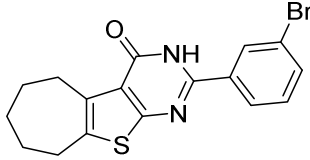
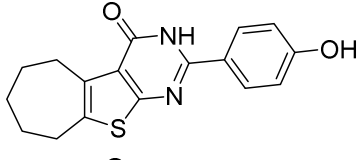
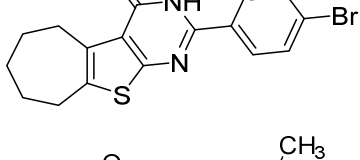
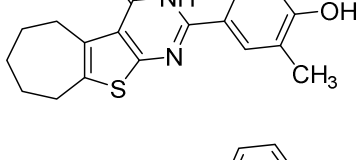
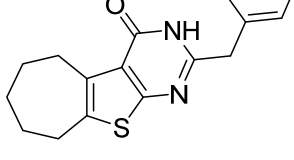
Scheme 2. Reagents and conditions: (a) $\text{NCCH}_2\text{CO}_2\text{Et}$, S_8 , EtOH, Et_3N , reflux, 12 h; (b) nitrile,

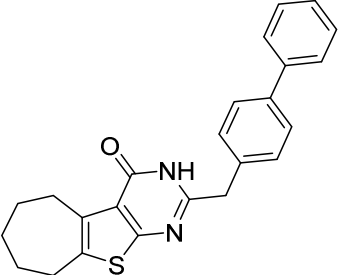
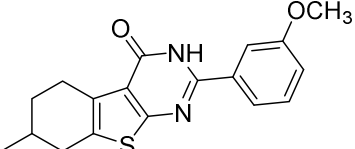
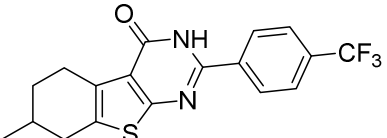
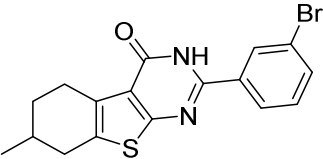
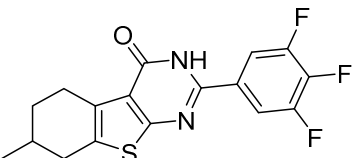
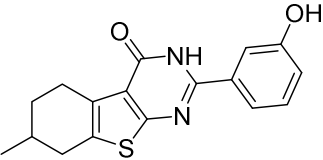
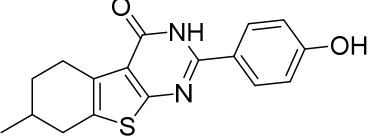
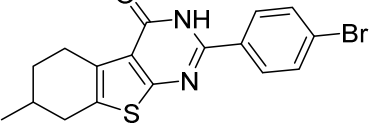
solid).

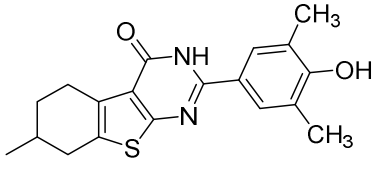
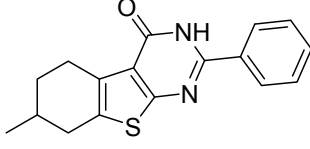
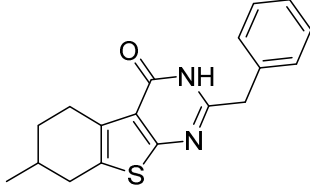
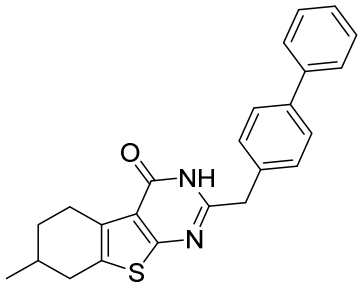
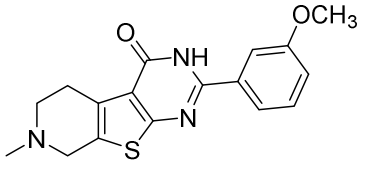
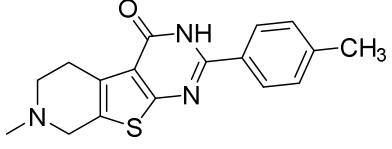
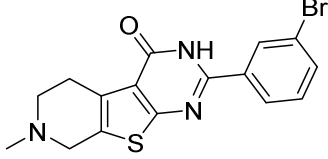
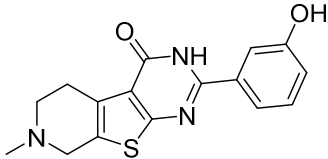
Table 1. Biochemical and biological evaluations of candidate compounds

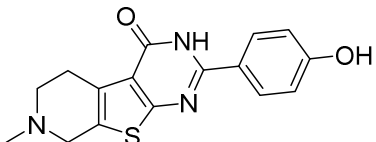
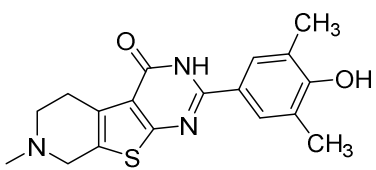
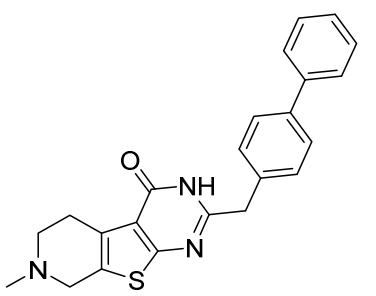
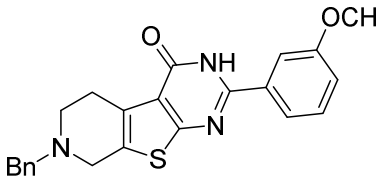
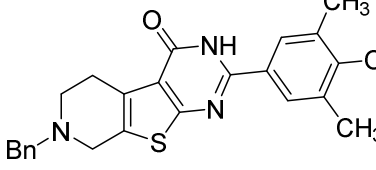
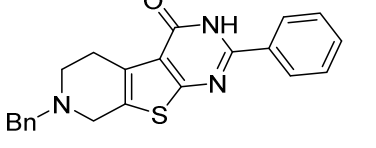
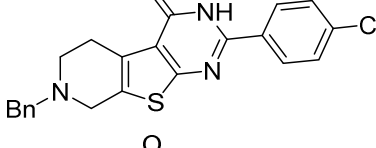
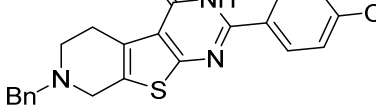
No.	Structure	BRD4(1) AlphaScreen (IC ₅₀ , μM) ^a	Anti-proliferative activity (IC ₅₀ , μM) ^b		MDC positive ratio% (5 μM) ^c
			MCF-7	MDA-MB-231	
4a		>10.00	>30.00	>30.00	9.58±1.02
4b		>10.00	>30.00	>30.00	6.35±0.59
4c		8.59±0.32	>30.00	28.35±1.66	18.77±0.78
4d		>10.00	>30.00	>30.00	5.90±0.68
5a		0.78±0.04	2.22±0.82	5.34±0.37	26.66±0.92
5b		1.53±0.08	8.39±1.34	14.69±0.72	25.21±0.41
5c		>10.00	>30.00	>30.00	11.79±0.95

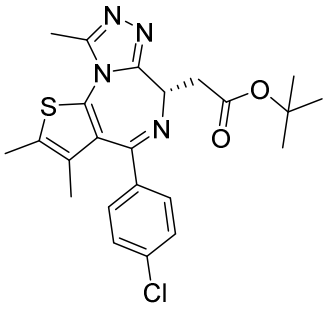
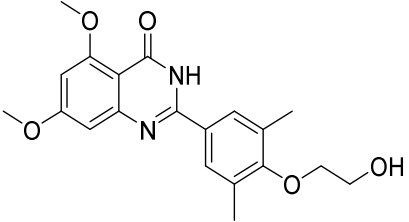
1						
2						
3						
4						
5						
6	5d		>10.00	>30.00	>30.00	9.05±0.43
7						
8						
9						
10						
11						
12	5e		8.94±0.11	21.29±1.95	>30.00	20.31±0.87
13						
14						
15						
16						
17	5f		6.38±0.22	18.47±1.27	23.12±1.81	26.98±1.32
18						
19						
20						
21						
22						
23	5g		>10.00	>30.00	>30.00	10.43±0.74
24						
25						
26						
27						
28	6a		>10.00	28.11±1.28	>30.00	13.11±0.81
29						
30						
31						
32	6b		>10.00	>30.00	>30.00	11.70±0.49
33						
34						
35						
36						
37	6c		>10.00	>30.00	>30.00	7.51±0.32
38						
39						
40						
41						
42	6d		7.32±0.37	22.75±2.02	>30.00	18.81±0.99
43						
44						
45						
46						
47	6e		6.93±0.28	24.91±1.85	27.76±2.11	25.62±1.05
48						
49						
50						
51						
52						
53						
54						
55						
56						
57						
58						
59						
60						

6f		>10.00	>30.00	>30.00	14.48±0.60
6g		>10.00	>30.00	>30.00	12.59±0.83
7a		>10.00	>30.00	>30.00	10.55±0.97
7b		5.73±0.12	18.52±1.01	>30.00	19.79±1.38
7c		3.98±0.27	13.23±1.06	17.42±1.76	25.99±0.82
7d		0.56±0.03	1.56±0.26	3.29±0.29	33.17±0.47
7e		>10.00	>30.00	>30.00	19.21±0.37
7f		0.49±0.06	2.81±0.32	8.31±0.99	38.37±0.97
7g		0.82±0.08	4.50±0.81	5.80±1.08	27.36±0.85

7h		>10.00	>30.00	>30.00	9.79±0.69
8a		>10.00	>30.00	>30.00	14.78±0.77
8b		>10.00	>30.00	>30.00	17.55±0.68
8c		1.02±0.09	2.69±0.37	16.26±1.11	27.22±0.51
8d		>10.00	>30.00	>30.00	13.59±0.94
8e		>10.00	>30.00	>30.00	15.24±0.89
8f		4.31±0.22	12.19±0.81	22.85±1.21	20.47±0.34
8g		>10.00	>30.00	>30.00	15.26±0.57

1						
2						
3						
4						
5	8h		3.24±0.23	5.59±0.76	9.42±0.48	30.79±0.91
6						
7						
8						
9						
10	8i		>10.00	>30.00	>30.00	8.38±0.50
11						
12						
13						
14						
15						
16	8j		>10.00	>30.00	>30.00	10.32±0.31
17						
18						
19						
20						
21						
22						
23						
24						
25	8k		>10.00	>30.00	>30.00	9.64±0.73
26						
27						
28						
29						
30						
31						
32						
33	9a		2.47±0.31	5.60±0.43	8.19±0.63	22.47±1.49
34						
35						
36						
37						
38						
39	9b		>10.00	>30.00	22.21±0.88	10.78±0.71
40						
41						
42						
43	9c		1.04±0.06	2.17±0.28	8.31±1.08	21.26±0.45
44						
45						
46						
47						
48						
49	9d		>10.00	>30.00	>30.00	13.61±0.32
50						
51						
52						
53						
54						
55						
56						
57						
58						
59						
60						

1						
2						
3						
4	9e		0.72±0.08	5.48±0.84	8.29±0.71	33.18±0.58
5						
6						
7						
8						
9	9f		0.43±0.09	1.62±0.06	3.27±0.14	42.29±0.91
10						
11						
12						
13						
14						
15						
16						
17						
18	9g		>10.00	>30.00	>30.00	10.34±0.29
19						
20						
21						
22						
23						
24						
25	10a		>10.00	>30.00	>30.00	8.62±0.63
26						
27						
28						
29						
30						
31	10b		>10.00	>30.00	>30.00	12.58±0.58
32						
33						
34						
35						
36						
37	10c		>10.00	>30.00	>30.00	5.87±0.48
38						
39						
40						
41						
42	10d		>10.00	>30.00	>30.00	11.30±0.39
43						
44						
45						
46						
47	10e		6.37±0.11	17.01±1.26	>30.00	6.74±0.56
48						
49						
50						
51						
52						
53						
54						
55						
56						
57						
58						
59						
60						

1		0.073±0.006	28.75±1.97	33.04±2.66	12.30±1.23
2a		>10.00	140.10 ± 2.71	155.40 ± 1.89	8.70±0.95

^a Each compound was tested in triplicate; the data are presented as the mean ± SEM (n=3).

^b IC₅₀ values obtained with cell viability assay for 24 h.

^c MDC positive ratio was detected by flow cytometry analysis using MDC staining on MCF-7 cells, the data are presented as the mean ± SEM (n=3).

Identification of **9f** as a selective BRD4 inhibitor

To demonstrate the direct binding of this small-molecule inhibitor, we set up a co-crystallization assay and elucidated the tertiary structure for **9f** (PDB ID: 4ZW1)³¹ in complex with the BD1 of BRD4 (Table S1). The 3,5-dimethylphenol moiety of **9f** penetrated deeply into the *N*-acetylated lysine pocket and occupied the same position as the acetyl head group of the acetylated lysine present in the histone tail peptides, initiating a direct hydrogen bond with the conserved asparagine (Asn140). One water molecule was located at the bottom of the active pocket, as observed in the *N*-acetylated lysine peptide complex structure (PDB ID: 3UVW).³² The water molecule hydrogen bond network contributed to stabilizing the ligand through additional hydrogen bonds. The pyrimidone moiety occupied the WPF shelf site composed of the residues Trp81, Pro82, and Phe83. The pyrimidone formed a Pi-Pi interaction with the indole side chain of Trp81 and two hydrogen bonds were observed in amide scaffold with residues Pro82, Gln85. The carbonyl group establishes a water bridged hydrogen bond interaction with residues Pro86 and Asp88 stabilizing the complex (Figure 3A). Subsequently, 100ns molecular dynamics (MD) simulations were performed on BRD4(1)-**9f** complex. The fluctuations of

1
2
3 RMSD (root-mean-square deviation) of MD trajectories were relative low, as well as the
4 energies, temperatures, and pressures of the systems suggested the systems were stable
5 and robust (Figure S4). To further characterize the selectivity of **9f** to other BET family
6 proteins, we determined the binding affinity of **9f** to BRD2(1), BRD2(2), BRD3(1),
7 BRD3(2), BRD4(1), BRD4(2) and BRDT(1) by using TR-FRET. **9f** displayed a high
8 selectivity for BRD4 instead of other BET family proteins, with IC₅₀ of 0.47 μM and 0.93
9 μM against BRD4(1) and BRD4(2), respectively (Figure 3B). To explain the selectivity of
10 **9f** over BRD4, we superimposed the structures of BRD2(1) (PDB ID: 1X0J), BRD3(1)
11 (PDB ID: 3S91), BRD4(1) (PDB ID: 4ZW1) and BRDT(1) (PDB ID: 4FLP) and performed
12 the molecular docking (Figure 3C and Figure S5). The results revealed that the overlay of
13 structures were almost consistent with the docked pose. Intriguingly, despite the highly
14 conservative sequences, we found that there were two potential key residues (Gln85,
15 Pro82) contributing to the selectivity of **9f**. The Gln residue is highly conserved in BD1 of
16 BRD2-4, but the amide side chain of Gln residues possess different orientations which
17 result in the failure of the hydrogen bond formed by the oxygen atom of **9f** and Gln
18 residues in BRD2(1) and BRD3(1). In BRDT(1), the corresponding Gln residue is replaced
19 by Arg residue, which may reduce the binding affinity of **9f** (Figure 3C and Figure S5). In
20 addition, the conformation of Pro residue is also different in BD1 of BRD2-4 and BRDT. A
21 hydrogen bond could be observed in BRD2(1), BRD4(1) and BRDT(1), but the deviation
22 of Pro residue in BRD3(1) resulted in the failure of a hydrogen bond (Figure 3C and Figure
23 S5). Collectively, the Gln85 residue plays a key role in selectivity of **9f** over BRD4. To
24 further illuminate the selectivity of **9f** over BRD4, we performed the MD simulations on the
25 docked pose of **9f** to monitor the RMSD of Cα atoms for the residues in 5 Å around ligand,
26 and it can be seen that this system is stable within 20 ns (Figure S6). Subsequently, we
27 calculated the binding free energy of the four systems, the results revealed that **9f** showed
28 the strongest binding affinity against BRD4 (Table 2), which is consistent with the assay
29 results. Taken together, **9f** is a potent and selective BRD4 inhibitor.

30
31
32
33
34
35
36
37
38
39
40
41
42
43
44
45
46
47
48
49
50
51
52
53
54 Moreover, we determined whether **9f** had direct modulatory effect on
55 autophagy-associated kinases such as AMPK and ULK1 by using ADP-Glo kinase assay.
56
57
58
59
60

1
2
3 As expected, **9f** did not activate or inhibit the kinase activities of AMPK and ULK1 in a
4 series of concentrations (Figure S7A and B). To demonstrate that **9f** inhibits BRD4 and
5 blocks the interaction of BRD4-AMPK, we examined the expression and interaction status
6 of BRD4 and AMPK. Interestingly, we found that **9f** markedly inhibited the expression of
7 BRD4 and its downstream target c-Myc, while activating the phosphorylation of AMPK α at
8 thr172 site (Figure 4A). Further co-immunoprecipitation results showed that **9f** could
9 reduce the binding capacity between BRD4 and AMPK α (Figure 4B). Since p53 can
10 interact with BRD4 and regulated by AMPK,^{33,34} we next employed
11 co-immunoprecipitation assay to examine whether **9f** disrupts the interaction between
12 BRD4 and AMPK via p53. Intriguingly, we found that **9f** attenuated the interaction
13 between BRD4 and p53, whereas the interaction between p53 and AMPK was
14 augmented after treatment of **9f** in MCF-7 cells (Figure 4C). However, **9f** did not disrupt
15 the interaction between BRD4 and p53, as well as the interaction between p53 and AMPK.
16 Thus, we deduce that the p53 is not a key factor for BRD4-AMPK interaction. Taken
17 together, these results suggest that **9f**, as a potent and selective BRD4 inhibitor, might
18 block the interaction of BRD4-AMPK; thereby activating AMPK-modulated autophagy in
19 breast cancer.
20
21
22
23
24
25
26
27
28
29
30
31
32
33
34
35
36
37
38
39
40
41
42
43
44
45
46
47
48
49
50
51
52
53
54
55
56
57
58
59
60

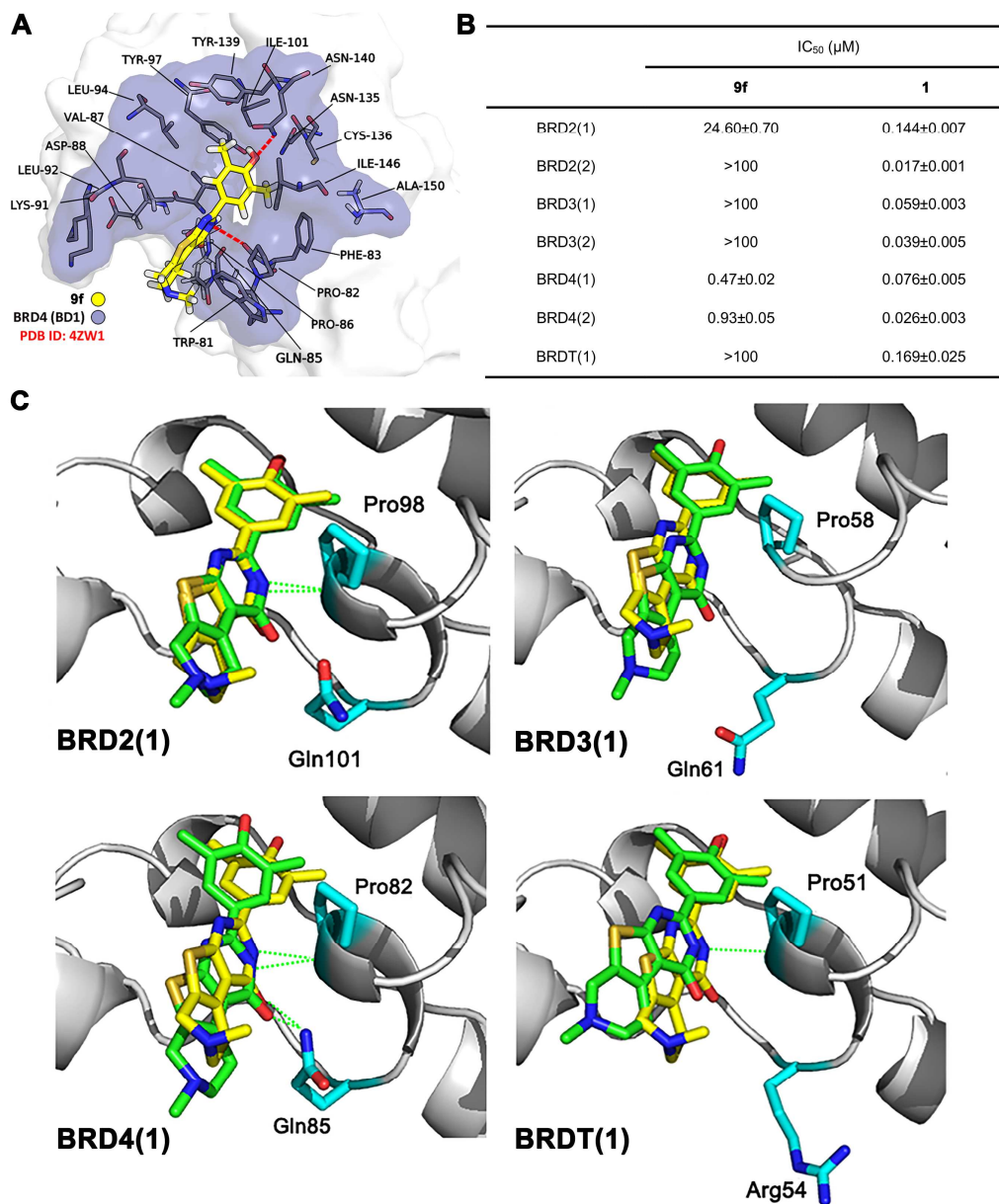


Figure.3 Identification of **9f** as a selective BRD4 inhibitor. (A) Binding model of **9f** with the BRD4 (white)/BD1 (deep blue). **9f** (light yellow) in receptor residues is illustrated. (B) Binding affinities of **9f** were measured by TR-FRET against the first and second bromodomains of BRD2, BRD3, BRD4 and BRDT. (C) The comparisons of the docked pose of **9f** with the co-crystal structures of BRD2(1), BRD3(1), BRD4(1) and BRDT(1), the docked conformation of **9f** was shown in green and the co-crystallized conformation was shown in yellow.

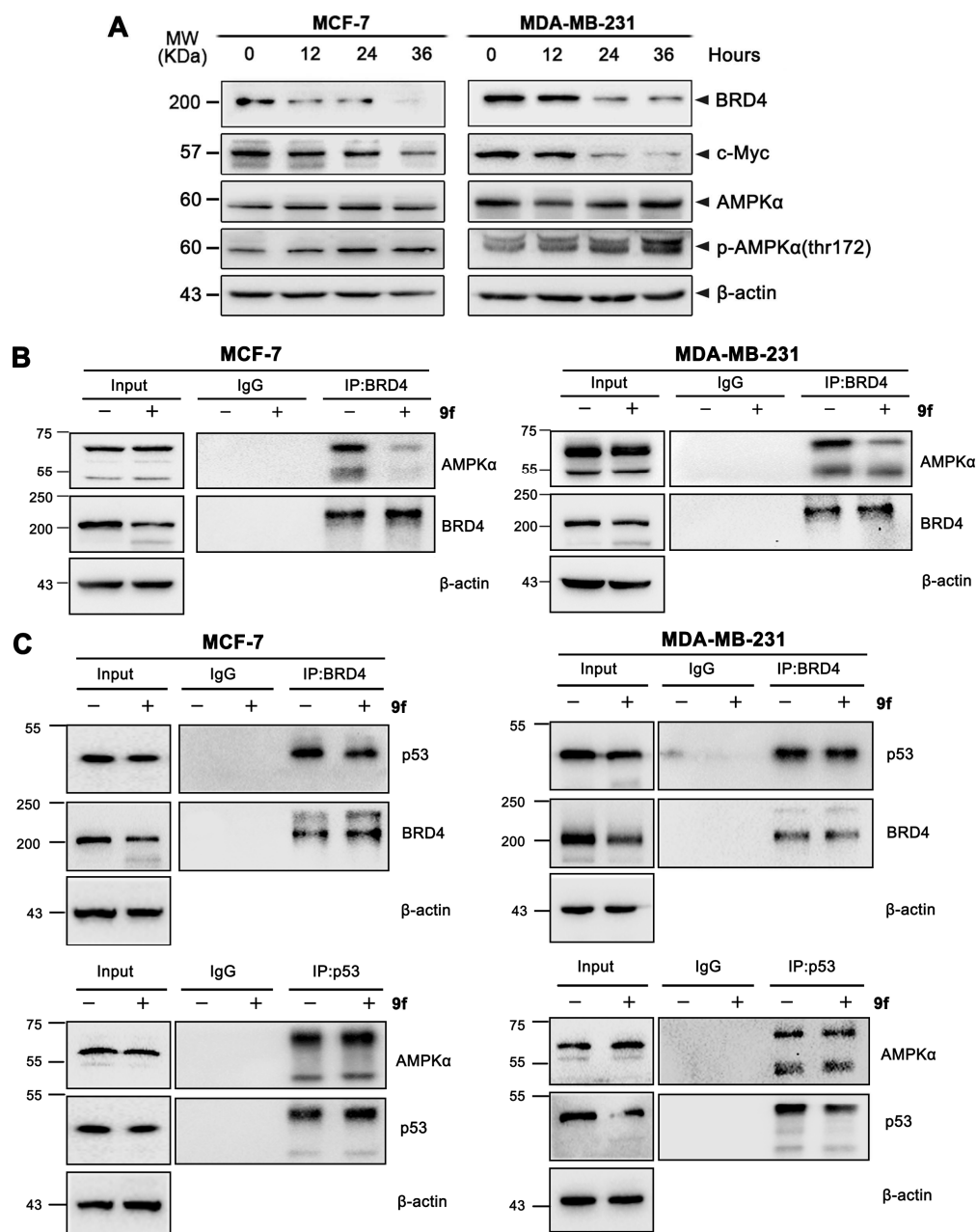


Figure.4 **9f** activates AMPK and blocks the interaction between BRD4 and AMPK. (A) MCF-7 or MDA-MB-231 cells were treated with 1.5 or 3 μ M of **9f** for indicated times, respectively. Then, the expression levels of BRD4, c-Myc, AMPK α and p-AMPK α were detected by western blot analysis. (B) MCF-7 or MDA-MB-231 cells were treated without or with **9f**. Cell extracts were subjected to immunoprecipitation with BRD4 antibody, then detected by western blot using AMPK α antibody. The expressions of BRD4 and AMPK α were determined in the input. (C) MCF-7 or MDA-MB-231 cells were treated without or with **9f**. Cell extracts were subjected to immunoprecipitation with BRD4 and p53 antibodies, then detected by western blot using p53 and AMPK α antibody. BRD4, p53 and AMPK α expressions were determined in the input.

Table 2. Binding free energy predicted by MM/GBSA methods (kcal/mol)

	BRD4	BRD3	BRD2	BRDT
ΔE_{ele}	-13.15	-9.98	-11.69	-9.09
ΔE_{vdw}	-31.60	-30.04	-30.66	-31.21
ΔE_{MM}	-44.75	-40.02	-42.35	-40.30
$\Delta G_{\text{sol-np}}$	-4.19	-4.10	-4.10	-3.95
$\Delta G_{\text{sol-ele}}$	20.67	19.15	20.42	21.16
ΔG_{sol}	16.48	15.05	16.32	17.21
$\Delta G_{\text{polar}}^{\text{a}}$	7.52	9.17	8.73	12.07
$\Delta G_{\text{nonpolar}}^{\text{b}}$	-35.79	-34.14	-34.76	-35.16
ΔH_{bind}	-28.27	-24.97	-26.03	-23.09

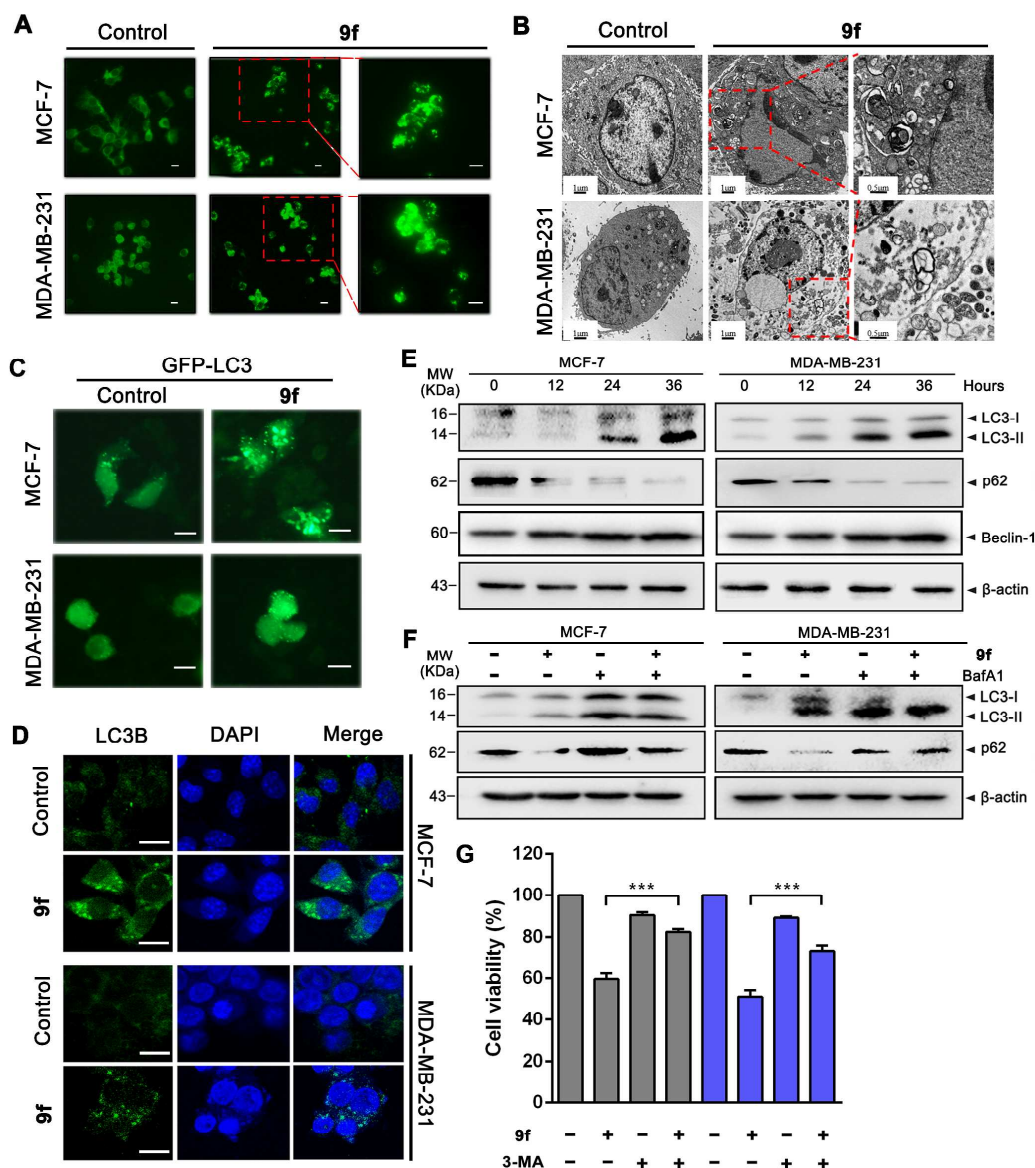
$$^{\text{a}} \Delta G_{\text{nonpolar}} = \Delta E_{\text{vdw}} + \Delta G_{\text{sol-np}}$$

$$^{\text{b}} \Delta G_{\text{polar}} = \Delta E_{\text{ele}} + \Delta G_{\text{sol-ele}}$$

9f induces ACD in breast cancer cells

We observed **9f** could induce massive cytoplasmic vacuolization in the treated MCF-7 and MDA-MB-231 cells (data not shown), which is closely associated with autophagy. Thus, we examined whether **9f** could induce autophagy in breast cancer cells. Monodansylcadaverine (MDC), a probe for the detection of autophagic vacuoles, was applied to **9f** treated cells, and the green fluorescent dots were observed and photographed under fluorescence microscopy (Figure 5A). Subsequently, we observed the morphologic signs of autophagy under electron microscope, characterized by the extensive vacuoles in the cytoplasm (Figure 5B). The induction of autophagy was further confirmed by GFP-LC3 transfection and immunofluorescence of LC3, which showed an increase in the LC3 puncta in the cells treated with **9f** (Figure 5C and D). To further confirm that **9f** induces autophagy, we found that treatment with **9f** resulted in increased expression of Beclin-1, downregulation of autophagy substrate p62/SQSTM1, as well as a time-dependent elevation of LC3-II in MCF-7 and MDA-MB-231 cells (Figure 5E). Intriguingly, our results suggested that **9f** did not increase the expression of Beclin-1, whereas increased the transformation of LC3-I to LC3-II in MDA-MB-468 cells (Figure S8). This phenomenon may be due to **9f** induced autophagy through a non-canonical pathway in MDA-MB-468 cells, which is independent on Beclin-1. Next, we used the lysosomal inhibitor, Bafilomycin A1 (BafA1), to validate the induction of autophagic flux. We found

that LC3-II and p62/SQSTM1 were significantly accumulated in the presence of BafA1, indicating that autophagic flux is enhanced by treatment with **9f** (Figure 5F). To further determine whether **9f**-induced autophagy is cytotoxic or cytoprotective autophagy, we applied the autophagy inhibitor 3-methyladenine (3-MA), which inhibits autophagy by blocking autophagosome formation via inhibiting type III phosphatidylinositol 3-kinases (PI3KIII), to block the induction of autophagy. The MTT assay was carried out to assess the cell viability. We found that the cell viabilities were significantly increased following treatment with 2 mM 3-MA ($p < 0.01$) (Figure 5G). These results suggest that **9f** induces ACD in both MCF-7 and MDA-MB-231 cells.



1
2
3 **Figure.5** **9f** induces ACD in breast cancer cells. (A) MCF-7 or MDA-MB-231 cells were treated with 1.5 or
4 3 μM of **9f** for indicated times, respectively. Then, the cells were detected by MDC fluorescence staining
5 under a fluorescence microscope. Scale bar: 50 μm (left panel), 20 μm (right panel). (B) MCF-7 or
6 MDA-MB-231 cells were treated with 1.5 or 3 μM of **9f** for indicated times, respectively. Then cells were
7 processed for electron microscopy. Scale bar=1 μm . (C) MCF-7 or MDA-MB-231 cells were transfected
8 with a GFP-LC3 plasmid, followed by treatment with 1.5 or 3 μM of **9f**, respectively. Then, the cells were
9 inspected under a fluorescence microscope. Scale bar=20 μm . (D) MCF-7 or MDA-MB-231 cells were
10 treated with 1.5 or 3 μM of **9f** for 24h, respectively. Then, the expression of LC3B puncta were detected
11 by immunocytochemistry. Green: anti-LC3B; Blue: DAPI. Scale bar=20 μm . (E) MCF-7 or MDA-MB-231
12 cells were treated with **9f** for the indicated times. The expression levels of LC3, p62 and Beclin-1 were
13 examined by western blot analysis. (F) MCF-7 or MDA-MB-231 cells were treated with **9f** for 24 h in the
14 presence or absence of BafA1, the autophagy flux was detected by western blot analysis of LC3 and p62,
15 β -actin was used as a loading control. (G) MCF-7 or MDA-MB-231 cells were treated with 1.5 and 3 μM
16 of **9f**, respectively. 3-MA (1 mM) was added 1 h before treated with **9f**. After treatment, cell viabilities were
17 detected by MTT assay. *** $p < 0.001$ compared with **9f**-treated group.
18
19
20
21
22
23
24
25
26
27
28

29 **9f induces autophagy via BRD4-AMPK-mTOR-ULK complex axis**

30
31 Next, we examined the upstream of autophagy signaling to illuminate the mechanism
32 for **9f**-induced autophagy. Firstly, we detected the expressions of Akt, p-Akt (ser473),
33 p-Akt (thr308), mTOR and p-mTOR (ser2448) after **9f** treatment. And **9f** markedly
34 reduced the expression levels of p-Akt (ser473), p-Akt (thr308) and p-mTOR (ser2448),
35 while the expressions of Akt and mTOR were unchanged (Figure 6A). Because the ULK
36 complex (ULK1-mATG13-FIP200) is closely related with autophagosome formation, we
37 subsequently examined the expression of ULK1, p-ULK1 (ser317), ATG13, p-ATG13
38 (ser318) and FIP200. The results showed that after treatment with **9f** the phosphorylation
39 of ULK1 and ATG13 were increased, while ULK1, ATG13 and FIP200 were slightly
40 downregulated, suggesting that **9f** may regulate autophagy through the ULK1 complex
41 (Figure 6B). To demonstrate whether **9f**-induced autophagy is only associated with BRD4
42 inhibition, we used two specific siRNAs to knockdown the expression of BRD4.
43 Interestingly, we found that silence of BRD4 decreased the expression of c-Myc, which
44 was consistent with **9f** treatment. However, different from **9f** treatment, the expression
45
46
47
48
49
50
51
52
53
54
55
56
57
58
59
60

and phosphorylation of AMPK α and ULK1, as well as the LC3-II accumulation and p62 degradation were merely changed after knocking down of BRD4, indicating silencing of BRD4 cannot induce obvious activation of autophagy (Figure 6C). To explore whether **9f**-induced autophagy is dependent on ATG5, we used specific siRNA to knockdown the expression of ATG5 in cells (Figure 6D). Interestingly, we found that silencing of ATG5 did not disrupt the activation of AMPK but could block the degradation of p62 and lipidation of LC3 (Figure 6D). Taken together, these results indicate that **9f** induces ATG5-dependent autophagy via BRD4-AMPK-mTOR-ULK complex axis.

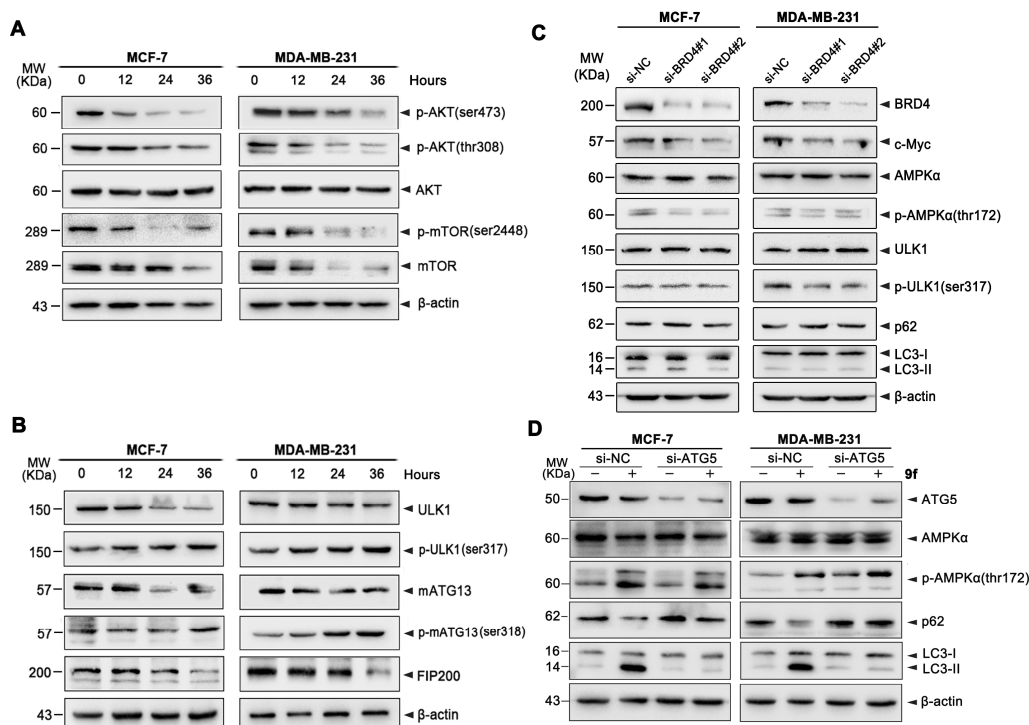


Figure.6 **9f** induces autophagy via BRD4-AMPK-mTOR-ULK1 axis. (A) MCF-7 or MDA-MB-231 cells were treated with 1.5 or 3 μ M of **9f** for indicated times, respectively. Then the expression levels of AKT, p-AKT, mTOR, p-mTOR, p70S6K and p-p70S6K were detected by western blot analysis. (B) MCF-7 or MDA-MB-231 cells were treated with 1.5 or 3 μ M of **9f** for indicated times, respectively. Then the expression levels of the ULK1, p-ULK1, ATG13, p-ATG13 and FIP200 were detected by western blot analysis. (C) MCF-7 or MDA-MB-231 cells were transfected with two specific siRNAs of BRD4 or negative control siRNA for indicated times, respectively. After treatment, the expression levels of BRD4, c-Myc, AMPK α , p-AMPK α , ULK1, p-ULK1, p62 and LC3 were detected by western blot analysis. (D) MCF-7 or MDA-MB-231 cells were transfected with specific siRNA of ATG5 or negative control siRNA for

1
2
3 indicated times, respectively. After treatment, the expression levels of ATG5, AMPK α , p-AMPK α , p62 and
4 LC3 were detected by western blot analysis. β -actin was used as a loading control.
5
6
7

8 **Proteomics-based identification of BRD4-modulating autophagic mechanisms in 9f** 9 **treatment** 10

11 Previous studies reported that **1** induced AMPK-ULK1 modulated cytoprotective
12 autophagy, thereby conferring resistance to AML stem cells.²⁴ As a consequence, in our
13 study, we found that **9f** showed more potent autophagic activity than **1** and **2a** at
14 concentration of 5 μ M (Figure 2C and Table 1). Interestingly, 3 μ M of **9f** could markedly
15 increase the LC3 puncta and LC3 lipidation, as well as the degradation of p62. However,
16 10 μ M of **1** induced weak autophagy in both MCF-7 and MDA-MB-231 cells. And high
17 concentration of **2a** (150 μ M) also lead to obvious autophagy in breast cancer cells,
18 especially in MCF-7 cells (Figure 7A and B). To further reveal the potential mechanisms
19 underlying **9f**-induced ACD with BRD4, iTRAQ-based proteomics analysis was employed
20 to profile differentially expressed proteins in MCF-7 and MDA-MB-231 cells treated with **9f**,
21 respectively. Hundreds of proteins were retrieved from the proteomics results, among
22 which only differentially expressed proteins (>1.2, <0.8) were selected (Table S2 and S3).
23 We identified some differentially expressed proteins that interacted with BRD4. In MCF-7
24 cells, three differential expression proteins HMGB1, VDAC1 and eEF2, were predicted to
25 interact with BRD4 or to be affected by BRD4. While in MDA-MB-231 cells, two differential
26 expression proteins VDAC2 and eEF2, were predicted to interact with BRD4 or to be
27 affected by BRD4 (Figure 8A and B). Next, in the MCF-7 cells, we found that **9f** induced
28 the downregulation of HMGB1, as well as a decreased phosphorylation of eEF2 and
29 upregulation of VDAC1. Otherwise, we found that the phosphorylation of eEF2 was also
30 downregulated after **9f** treatment in the MDA-MB-231 cells, while the expression of
31 VDAC2 was simultaneously increased (Figure 8C and D). To further validate the possible
32 mechanisms under BRD4 inhibition, we used **1** to compare with **9f**. Interestingly, we found
33 that **1** only displayed some similar results with **9f** on the expression of HMGB1, but not
34 affected the phosphorylation of eEF2, as well as the expressions of VDAC1 and VDAC2
35
36
37
38
39
40
41
42
43
44
45
46
47
48
49
50
51
52
53
54
55
56
57
58
59
60

(Figure 8E and F). These results indicate that the **9f**-induced autophagy is involved HMGB1, VDAC1, VDAC2 and eEF2, which still needs to be further explored whether these proteins can be directly regulated by BRD4.

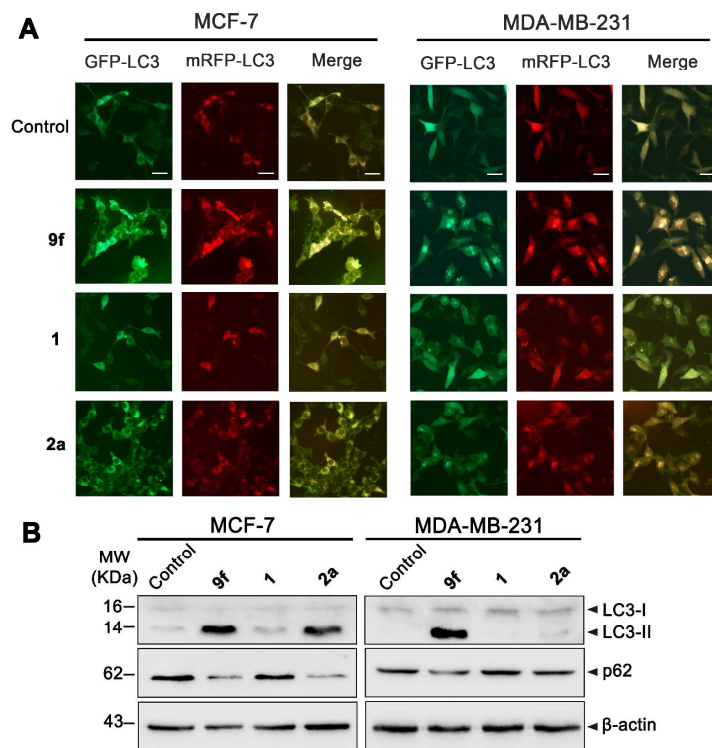


Figure 7. **9f** induces more obvious autophagy compared with **1** and **2a**. (A) MCF-7 or MDA-MB-231 cells were transfected with GFP/mRFP-LC3 plasmid, followed by treatment with 3.0 μ M of **9f**, 10 μ M of **1** or 150 μ M of **2a** for indicated times, respectively. Then, the GFP-LC3 puncta were observed by fluorescence microscope. Scale bar = 20 μ m. (B) MCF-7 or MDA-MB-231 cells were treated with 3.0 μ M of **9f**, 10 μ M of **1** or 150 μ M of **2a** for indicated times, respectively. Then the expression levels of LC3 and p62 were detected. β -actin was measured as loading control.

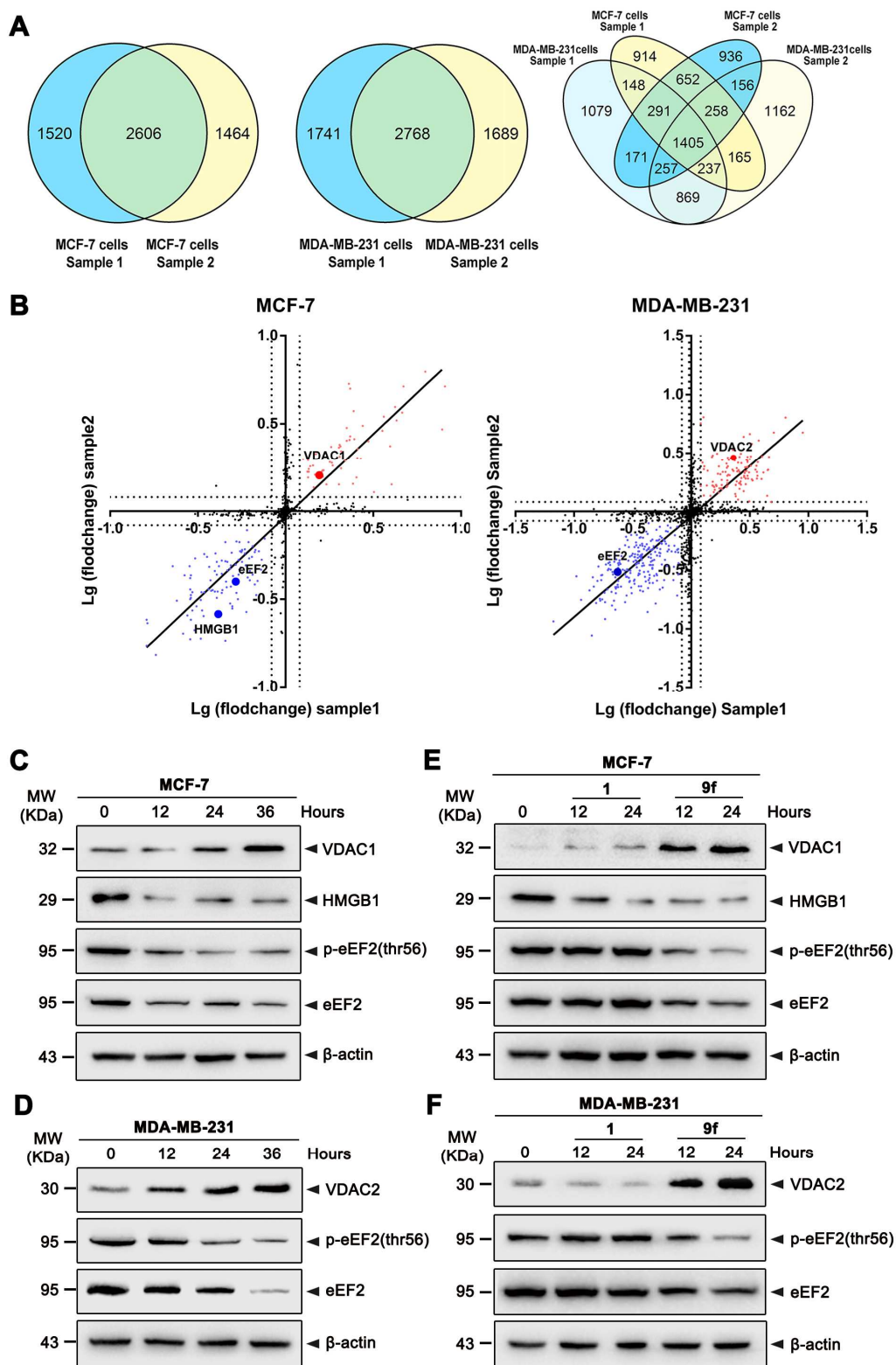


Figure.8 Proteomics-based identification of **9f**-induced ACD mechanisms. (A) Venn diagram showed the consensus proteins that were remarkably changed in both **9f**-treated MCF-7 and MDA-MB-231 cells. (B)

1
2
3 Correlation of log₁₀ fold changes between the two samples across all changed proteins in both MCF-7
4 and MDA-MB-231 cells by Deming linear regression. The proteins that were validated by subsequent
5 experiments were highlighted. (C) MCF-7 cells were treated with 1.5 μM of **9f** for indicated times, then
6 the expression levels of HMGB1, VDAC1, p-eEF2 and eEF2 were detected by western blot analysis. (D)
7 MDA-MB-231 were treated with 3.0 μM of **9f** for indicated times, then the expression levels of VDAC2,
8 p-eEF2 and eEF2 were detected by western blot analysis. (E) MCF-7 cells were treated with 1.5 μM of **9f**
9 or 10 μM of **1** for indicated times, respectively. Then the expression levels of HMGB1, VDAC1, p-eEF2
10 and eEF2 were detected by western blot analysis. (F) MDA-MB-231 cells were treated with 3.0 μM of **9f**
11 or 10 μM of **1** for indicated times, respectively. Then the expression levels of VDAC2, p-eEF2 and eEF2
12 were detected by western blot analysis. β-actin was used as a loading control.
13
14
15
16
17
18
19
20

21 **9f has a therapeutic potential by targeting BRD4-modulated autophagy *in vivo***

22
23 To evaluate the anti-tumor activity of **9f** *in vivo*, two breast tumor xenograft models namely
24 MCF-7, and MDA-MB-231 cell lines models were used. We conducted the *in vivo* study
25 using three different doses of **9f**: 25 mg/kg, 50 mg/kg and 100 mg/kg. In all the models, **9f**
26 showed significant tumor growth inhibition in a dose-dependent manner as determined by
27 80% and 76% tumor growth inhibition ratio in MCF-7 and MDA-MB-231 cell models,
28 respectively (Figure 9A and B). And we observed a remarkable loss of tumor weights in all
29 dose groups ($p < 0.001$) (Figure 9C). Moreover, **9f** displayed no obvious effects on the
30 body weight of all the treatment groups (Figure 9D). To examine whether **9f**-mediated
31 inhibition of tumor growth *in vivo* was associated with reduced cell proliferation and the
32 increased autophagy-associated cell death, tumor tissues from control and **9f**-treated
33 mice were processed for the immunohistochemical analysis of Ki-67 and LC3. We found
34 that **9f** treatment obviously reduced the number of Ki-67 ($p < 0.001$) positive cells as well as
35 increased autophagy levels, which was determined by increased LC3 expression
36 ($p < 0.001$) (Figure 9E). Next, we carried out western blot analysis to further clarify the
37 mechanism of **9f** *in vivo*. We found that **9f** increased LC3-II accumulation and cleavage of
38 caspase3 *in vivo*, as well as inhibit expressions of BRD4 and c-Myc, which was almost
39 consistent with the immunohistochemical analysis and the results obtained *in vitro* (Figure
40 9F). Moreover, we used a zebrafish xenograft model to further assess the anti-tumor
41
42
43
44
45
46
47
48
49
50
51
52
53
54
55
56
57
58
59
60

effect of **9f**. Interestingly, we found that all three doses of **9f** caused obvious decrease of tumor growth (12.5 μM : $p < 0.01$, 25 and 50 μM : $p < 0.001$) compared to the control group (Figure 10A and B). Together, these results suggest that **9f** bears a good anti-tumor activity in both mouse and zebrafish xenograft models.

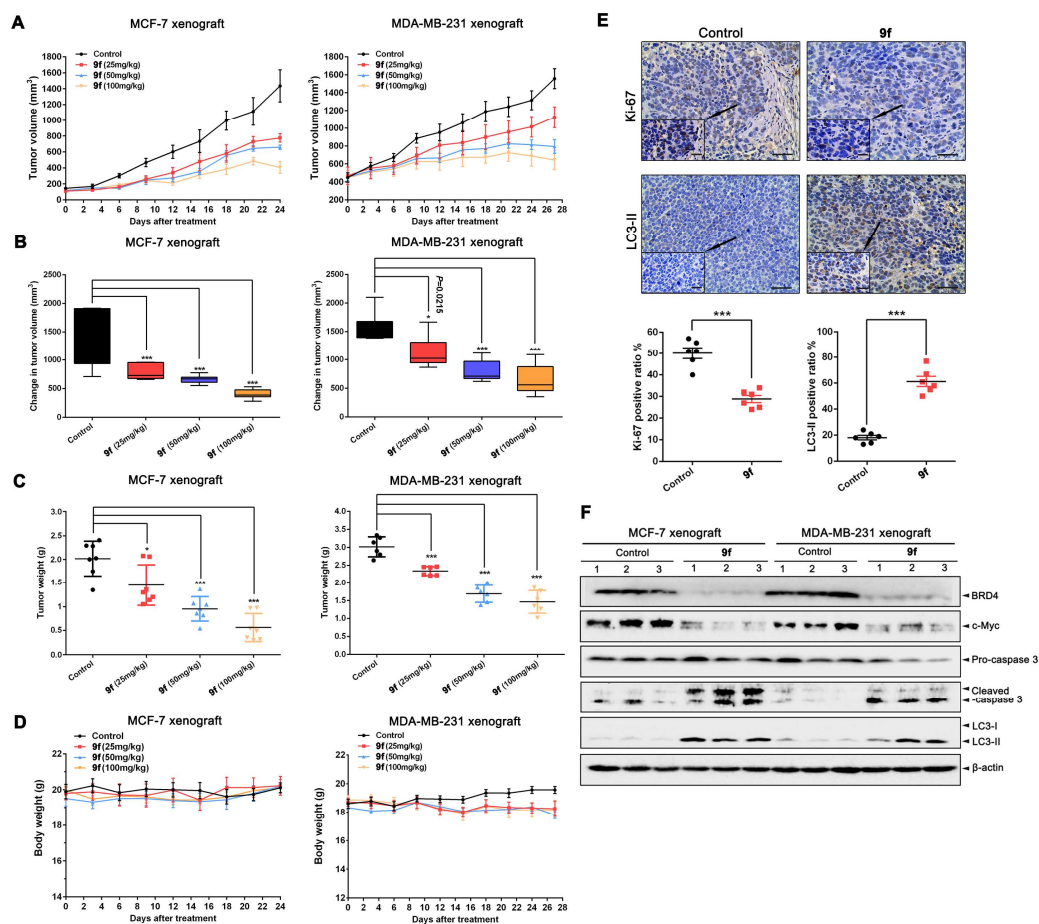


Figure.9 **9f** has an anti-tumor effect in mouse xenograft models via inducing ACD. (A) Mice bearing MCF-7 ($n = 7$ per group) or MDA-MB-231 ($n = 6$ per group) tumor xenograft were treated with vehicle control or indicated dose of **9f** once a day. Tumor volume data were presented as mean \pm SEM. (B) Analysis of tumor volume change on final study day. * $p < 0.05$, *** $p < 0.001$, compared with control group. (C) Tumor weight change of mice in different group. * $p < 0.05$, *** $p < 0.001$, compared with control group. (D) Body weight of mice during **9f** treatment. (E) Immunohistochemical analysis of proliferative marker Ki-67, and LC3-II. Representative images and quantitative analysis of percentage of positive staining are shown. Tumor tissues were excised from the control and **9f** (100mg/kg) treated mice; *** $p < 0.001$ compared with control group. Scale bar=200 μm . (F) Tumor tissues excised from the MCF-7 or MDA-MB-231 xenograft mice were lysed. Then the expression levels of BRD4, c-Myc, LC3, and caspase3 were detected by western blot analysis, β -actin was used as a loading control.

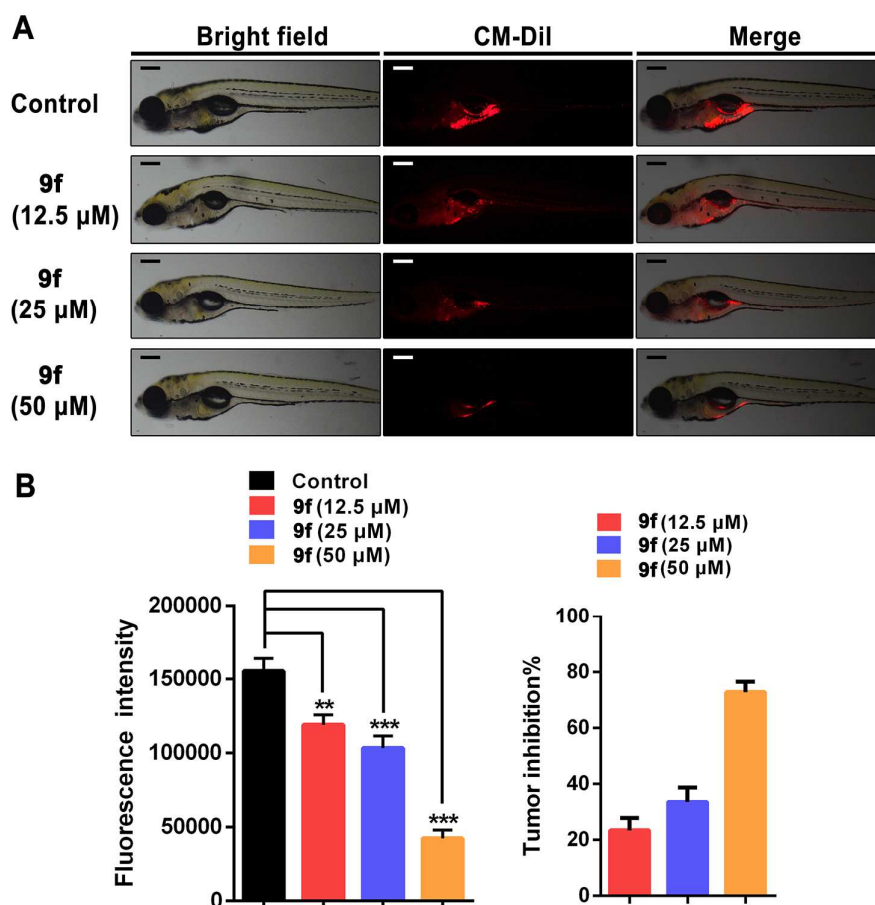


Figure.10 **9f** has an anti-tumor effect on zebrafish xenograft model. (A) Anti-tumor activity of **9f** in zebrafish xenograft model. Representative images for bright field and fluorescent images of zebrafish implanted with CM-Dil-labeled MCF-7 cells after treatment with vehicle control or different concentrations of **9f** (12.5, 25, 50 μ M). (B) Tumor fluorescence intensities (mean \pm SEM) and percentages of inhibition in tumor volumes of treated embryos after 48 h. ** p <0.01, *** p <0.001, compared with control group. Scale bar=200 μ m.

DISCUSSION

BRD4, which is an attractive epigenetic target for cancer therapy, engages in direct regulatory interactions with some DNA-binding transcription factors, such as Mediator, Jmjd6, and P-TEFb to influence their functions.³⁵ Some PPI employed by BRD4 have been shown to be crucial to the potential therapeutic effects of a BRD4 inhibitor; however, its regulatory mechanisms for PPI still remain in its infancy. In our study, we constructed the PPI network of BRD4 with a function enrichment, and identified BRD4 could interact

1
2
3 with 28 autophagic proteins including AMPK that were annotated by GO, suggesting
4 BRD4 may function as a regulator in the autophagic pathways. In TCGA dataset, we
5 identified that some autophagic proteins such as AMPK, LC3A, LC3B and ATG4C were
6 remarkably downregulated in breast cancer tissues, which is different from the known
7 overexpression of BRD4, suggesting that BRD4 might play an inhibitory role in autophagy
8 and thus inhibition of BRD4 may activate AMPK-modulated autophagy/ACD. Our results
9 of network predication, TCGA analyses and co-immunoprecipitation together revealed
10 that BRD4 might interact with AMPK. However, we consider that above-mentioned result
11 is insufficient to confirm the direct interaction between BRD4 and AMPK, additional
12 studies such as structural biology study would help us to clarify the intrinsic mechanism of
13 BRD4-AMPK-modulated autophagy. More recently, a study have been revealed that
14 BRD4 represses autophagy and lysosome gene expression. This repression is alleviated
15 during nutrient deprivation through AMPK-SIRT1 signaling, allowing autophagy
16 activation.²⁹ These findings might indicate that disrupting the interaction between BRD4
17 and AMPK by small-molecule inhibitor of BRD4, thereby activating AMPK-modulated
18 autophagy will be a new therapeutic approach to breast cancer therapy.

19
20
21
22
23
24
25
26
27
28
29
30
31
32
33 Of note, AMPK, mTOR and ULK1 together form a complex, which comprises both
34 key positive- and negative-feedback regulation in autophagy.¹⁸ mTOR and AMPK can
35 oppositely regulate ULK1 kinase activity by direct phosphorylation.¹⁹ In our study, we
36 found that BRD4 might interact with AMPK and thus indicating that there might be the
37 interaction between BRD4 and AMPK, which subsequently regulates
38 mTOR-ULK1-modulated autophagy. Accumulating evidence for ACD has been emerging
39 now.^{21,22} To our knowledge, not any BRD4 inhibitor has been reported to induce ACD in
40 cancer. Thus, targeting BRD4 inhibition and thereby activating
41 BRD4-AMPK-mTOR-ULK1-modulated ACD will fill in the gap in breast cancer therapy.

42
43
44
45
46
47
48
49
50 We designed a small-molecule inhibitor of BRD4 (**9f**) according to the
51 pharmacophore of the BRD4 (1) and WPF interaction, which was further validated by the
52 co-crystal structure of **9f**-BRD4 and other multiple biological evaluation. In addition, we
53 found that the part B of **9f** was a pharmacophore of BRD4, which was similar to the
54
55
56
57
58
59
60

1
2
3 chemical structures of **2a** and its derivative **2b** (RVX-OH).³⁰ However, **2a** has been
4 revealed to bind selectively to the BD2 of BET proteins and thus being developing into a
5 BET inhibitor for the treatment of cardiovascular diseases.^{30, 36, 37} In this study, we
6 designed WPF interaction optimization in the part A, which was validated by BRD4
7 inhibition activity and autophagic activity. As mentioned above, we discovered a
8 small-molecule inhibitor of BRD4 that not only impeded BRD4 activity, but disrupted the
9 BRD4-AMPK interaction, and thus activating AMPK-mTOR-ULK1-modulated ACD.

16 Intriguingly, combined with iTRAQ-based proteomics analyses, we identified some
17 potential BRD4 interactors in **9f**-treated breast cancer cells. Among these interactors,
18 eEF2 as a downstream target of eEF2K, controls the protein synthesis of cancer cells.³⁸
19 And eEF2K can be positively regulated by mTOR and Akt inhibition, leading to a
20 suppression of eEF2.^{39,40} In our study, eEF2 were downregulated simultaneously in
21 MCF-7 and MDA-231 cells, indicating it may be served as a key component of **9f**-induced
22 autophagy that fills the gaps between inhibition of mTOR and Akt as well as the activation
23 of the ULK complex. Moreover, VDAC1 and VDAC2 have been reported that participate in
24 the recruitment of Parkin to mitochondria to promote mitochondrial autophagy. And
25 another study showed VDAC1 along with p62/SQSTM1 are essential for mitophagy.^{41,42}
26 Further, our results showed that VDAC1 was upregulated in MCF-7 cells, while VDAC2
27 was increased in MDA-MB-231 cells. Thus, we hypothesize that **9f**-induced ACD may also
28 be associated with mitophagy, which is a selective degradation
29 of mitochondria by autophagy. Moreover, we found that **9f** has a potent anti-tumor effect
30 on xenograft breast cancer mouse models by targeting BRD4 without remarkable toxicity.
31 Also, **9f** was shown to have a therapeutic effect on zebrafish xenograft model. These
32 results indicate that **9f** has an anti-tumor therapeutic potency as a lead drug of breast
33 cancer *in vivo*.

50 In conclusion, based upon PrePPI network, TCGA analysis and our
51 co-immunoprecipitation results, we found that BRD4 might interact with AMPK. These
52 results have led to the discovery of
53 2-(4-hydroxy-3,5-dimethylphenyl)-7-methyl-5,6,7,8-tetrahydropyrido[4',3':4,5]thieno[2,3-d]

1
2
3 pyrimidin-4(3*H*)-one (**9f**), which possessed relatively high affinity with BRD4 rather than
4 other BET family proteins, as well as the function of autophagy activation. Additionally, we
5 demonstrated that **9f** could induce ATG5-dependent autophagy/ACD via
6 BRD4-AMPK-mTOR-ULK complex axis. Moreover, we found that **9f** had a good
7 therapeutic potential on breast cancer xenograft mouse and zebrafish models *in vivo*.
8 These findings demonstrate that **9f** would be a useful tool for dissecting the
9 autophagy-modulating role of BRD4 and further exploited as a novel candidate drug for
10 breast cancer therapeutics.
11
12
13
14
15
16
17
18
19

20 **EXPERIMENTAL SECTION**

21 **Materials and measurements**

22 ¹H-NMR spectra were recorded at 400 MHz. The chemical shifts were recorded in ppm
23 relative to tetramethylsilane and with the solvent resonance as the internal standard. Data
24 were reported as follows: chemical shift, multiplicity (s = singlet, d = doublet, t = triplet, q =
25 quartet, m = multiplet), coupling constants (Hz), integration. ¹³C-NMR data were collected
26 at 100 MHz with complete proton decoupling. Chemical shifts were reported in ppm from
27 the tetramethylsilane with the solvent resonance as internal standard. ESI-HRMS spectra
28 were recorded on a commercial apparatus and methanol was used to dissolve the sample.
29 All chemicals were obtained from commercial sources and used without further
30 purification. Column chromatography was carried out on silica gel (300-400 mesh,
31 Qingdao Marine Chemical Ltd, Qingdao, China). Thin layer chromatography (TLC) was
32 performed on TLC silica gel 60 F254 plates. The purity of compounds was determined to
33 be over 95% (>95%) by reverse-phase high performance liquid chromatography (HPLC)
34 analysis. HPLC instrument: SHIMADZU HPLC (Column: Diamonsil C18-WR, 5.0 μm, 4.6
35 x 250 mm (WondaSil); Detector: SPD-20A Photodiode Array; Injector: SIL-20A
36 Autoinjector; Pump: LC-20AT). Elution: MeOH in water; Flow rate: 1.0 mL/min.
37
38
39
40
41
42
43
44
45
46
47
48
49
50
51

52 **General procedure for the synthesis of compounds**

53
54 Procedure A: To a solution of ketone or aldehyde (30.0 mmol), ethyl cyanoacetate (30.0
55 mmol), and sulfur (30.0 mmol) in anhydrous ethanol (200 mL) was added triethylamine
56
57
58
59
60

(35.0 mmol). The resulting was allowed to refluxed for 12 h. The suspension was filtered through a pad of Celite and washed with absolute ethyl alcohol (30 ml x 3). The combined filtrate was concentrated to dryness. The crude product was purified by silica gel chromatography eluted with PE : EtOAc = 5:1 to give the product as a white solid.

Procedure B: To a solution of 2-amino-3-carbethoxythiophene derivatives (2.0 mmol) in anhydrous dioxane (4 mL) saturated by HCl gas was added appropriate nitriles (2.2 mmol). The resulting was allowed to heat to 100 °C for 6-12 h. After reaction was cooled to room temperature, quenched by addition of saturated sodium bicarbonate solution 20 ml. The solid was collected by filtration and washed by methanol to give the product.

Ethyl 2-amino-5-propylthiophene-3-carboxylate (3a). Preparation by Procedure A, white solid, yield 79.3%. ¹H-NMR (400 MHz, CDCl₃-d₆), δ (ppm): 5.73(1H, s), 4.18 (2H, q, *J* = 7.1 Hz), 2.47 (2H, m), 1.53 (2H, m), 1.25 (3H, t, *J* = 7.0 Hz), 0.87 (3H, t, *J* = 7.2 Hz).

Ethyl 2-amino-5,6-dihydro-4H-cyclopenta[b]thiophene-3-carboxylate (3b). Preparation by Procedure A, white solid, yield 88.4%. ¹H-NMR (400 MHz, CDCl₃), δ (ppm): 5.85 (2H, s), 4.24 (2H, m), 2.84 (2H, m), 2.72 (2H, m), 2.30 (2H, m), 1.32 (3H, t, *J* = 7.1 Hz).

Ethyl 2-amino-4,5,6,7-tetrahydrobenzo[b]thiophene-3-carboxylate (3c). Preparation by Procedure A, white solid, yield 85.6%. ¹H-NMR (400 MHz, DMSO-*d*₆), δ (ppm): 7.19 (2H, s), 4.15 (2H, q, *J* = 7.1 Hz), 2.60 (2H, br s), 2.41 (2H, br s), 1.67 (4H, br s), 1.24 (3H, t, *J* = 7.0 Hz).

Ethyl 2-amino-5,6,7,8-tetrahydro-4H-cyclohepta[b]thiophene-3-carboxylate (3d). Preparation by Procedure A, white solid, yield 86.8%. ¹H-NMR (400 MHz, CDCl₃), δ(ppm): 5.73 (2H, s), 4.26 (2H, q, *J* = 6.9 Hz), 2.94 (2H, t, *J* = 5.3 Hz), 2.55 (2H, t, *J* = 5.3 Hz), 1.79 (2H, m), 1.60 (4H, m), 1.32 (3H, t, *J* = 7.2 Hz).

Ethyl 2-amino-6-methyl-4,5,6,7-tetrahydrobenzo[b]thiophene-3-carboxylate (3e). Preparation by Procedure B, off-white solid, yield 58.8%. ¹H-NMR (400 MHz, DMSO-*d*₆), δ (ppm): 5.92 (2H, s), 4.26 (2H, q, *J* = 14.2, 7.13 Hz), 2.87 (1H, m), 2.56 (2H, m), 2.12 (1H, m), 1.81 (2H, m), 1.33 (4H, t, *J* = 7.1 Hz), 1.04 (3H, d, *J* = 6.5 Hz).

Ethyl 2-amino-6-methyl-4,5,6,7-tetrahydrothieno[2,3-*c*]pyridine-3-carboxylate (3f).

1
2
3 Preparation by Procedure B, white solid, yield 79.0%. $^1\text{H-NMR}$ (400 MHz, CDCl_3), δ (ppm):
4 5.98 (2H, s), 4.26 (2H, m), 3.37 (2H, t, $J=2.0$ Hz), 2.84 (2H, m), 2.66 (2H, t, $J = 5.9$ Hz),
5 2.44 (3H, s), 1.33 (3H, t, $J=7.1$ Hz).
6
7

8 **2-(3-Methoxyphenyl)-6-propylthieno[2,3-d]pyrimidin-4(3H)-one (4a)**. Preparation by
9
10 Procedure B, off-white solid, m.p. 239-242 °C, yield 66.2%. $^1\text{H-NMR}$ (400 MHz, $\text{DMSO-}d_6$),
11 δ (ppm): 7.85 (2H, m), 7.25 (1H, t, $J = 7.9$ Hz), 6.88 (1H, ddd, $J = 8.4, 2.7, 1.0$ Hz), 6.78
12 (1H, br s), 3.80 (3H, s), 2.71 (2H, t, $J = 7.3$ Hz), 1.65 (2H, m), 0.94 (3H, t, $J = 7.3$ Hz);
13
14 $^{13}\text{C-NMR}$ (100 MHz, CF_3COOD), δ (ppm): 160.6, 155.2, 150.5, 149.1, 131.7, 124.3, 123.9,
15 123.0, 120.4, 118.4, 118.0, 112.4, 55.1, 31.6, 23.6, 11.4; HRMS (ESI) $^+$ calculated for
16 $\text{C}_{16}\text{H}_{17}\text{N}_2\text{O}_2\text{S}$, $[\text{M}+\text{H}]^+$: m/z 301.1011, found 301.1020; Purity: 95.4% (HPLC, t_R 11.93
17 min).
18
19

20 **2-(3-Bromophenyl)-6-propylthieno[2,3-d]pyrimidin-4(3H)-one (4b)**. Preparation by
21 Procedure B, off-white solid, m.p. 265-268 °C, yield 69.7%. $^1\text{H-NMR}$ (400 MHz, $\text{DMSO-}d_6$),
22 δ (ppm): 8.42(1H, t, $J = 1.6$ Hz), 8.26 (1H, dt, $J = 7.8, 1.3$ Hz), 7.49 (1H, dq, $J = 7.8, 1.0$
23 Hz), 7.32 (1H, t, $J = 7.8$ Hz), 6.79 (1H, br s), 2.71 (2H, t, $J=7.0$ Hz), 1.65 (2H, m), 0.94 (3H,
24 t, $J=7.3$ Hz); $^{13}\text{C-NMR}$ (100 MHz, CF_3COOD), δ (ppm): 159.5, 156.6, 153.2, 151.8, 141.5,
25 133.8, 133.0, 128.5, 127.6, 126.8, 126.5, 120.4, 34.0, 26.0, 13.8; HRMS (ESI) $^+$ calculated
26 for $\text{C}_{15}\text{H}_{14}\text{BrN}_2\text{OS}$, $[\text{M}+\text{H}]^+$: m/z 349.0010, found 349.0017; Purity: 98.1% (HPLC, t_R 10.24
27 min).
28
29

30 **2-(4-Hydroxyphenyl)-6-propylthieno[2,3-d]pyrimidin-4(3H)-one (4c)**. Preparation by
31 Procedure B, off-white solid, m.p. 290-292 °C, yield 52.9%. $^1\text{H-NMR}$ (400 MHz,
32 $\text{DMSO-}d_6$), δ (ppm): 8.09 (2H, d, $J = 8.3$ Hz), 6.72 (2H, t, $J = 8.2$ Hz), 2.69 (2H, t, $J = 7.4$
33 Hz), 1.63 (2H, q, $J = 14.4, 7.1$ Hz), 0.93 (3H, t, $J = 7.5$ Hz); $^{13}\text{C-NMR}$ (100 MHz,
34 CF_3COOD), δ (ppm): 159.5, 156.6, 153.2, 151.8, 141.5, 133.8, 133.0, 128.5, 127.6, 124.8,
35 113.8, 111.6, 34.0, 26.0, 13.8; HRMS (ESI) $^+$ calculated for $\text{C}_{15}\text{H}_{15}\text{N}_2\text{O}_2\text{S}$, $[\text{M}+\text{H}]^+$: m/z
36 287.0854, found 287.0863; Purity: 96.0% (HPLC, t_R 8.59 min).
37
38

39 **2-([1,1'-Biphenyl]-4-ylmethyl)-6-propylthieno[2,3-d]pyrimidin-4(3H)-one (4d)**.
40

41 Preparation by Procedure B, off-white solid, m.p. 278-280 °C, yield 72.3%. $^1\text{H-NMR}$ (400
42
43
44
45
46
47
48
49
50
51
52

1
2
3 MHz, DMSO- d_6), δ (ppm): 7.62 (2H, dd, J = 8.4, 1.3 Hz), 7.55 (2H, d, J =8.4 Hz), 7.41 (4H,
4 m), 7.32 (1H, m), 6.81 (1H, s), 3.80 (2H, s), 2.70 (2H, t, J = 7.0 Hz), 1.61 (1H, m), 0.91 (3H,
5 t, J = 7.5 Hz); ^{13}C -NMR (100 MHz, CF_3COOD), δ (ppm): 162.1, 152.6, 152.6, 150.7, 145.6,
6 141.5, 132.3, 132.3, 130.8, 130.8, 130.6, 130.6, 130.0, 128.8, 128.8, 126.5, 120.3, 120.3,
7 39.8, 33.9, 26.1, 13.9; HRMS (ESI) $^+$ calculated for $\text{C}_{22}\text{H}_{21}\text{N}_2\text{OS}$, $[\text{M}+\text{H}]^+$: m/z 361.1375,
8 found 361.1381; Purity: 97.2% (HPLC, t_R 13.58 min).

13
14 **2-(2-Methoxyphenyl)-3,5,6,7-tetrahydro-4H-cyclopenta[4,5]thieno[2,3-d]pyrimidin-4-**

15 **one (5a)**. Preparation by Procedure B, off-white solid, m.p. 241-243 $^\circ\text{C}$, yield 48.5%.

16
17 ^1H -NMR (400 MHz, DMSO- d_6), δ (ppm): 12.60 (1H, s), 7.71 (2H, m), 7.45 (1H, dd, J = 8.8,
18 6.1 Hz), 7.13 (1H, d, J = 6.1 Hz), 3.86 (3H, s), 2.41 (4H, m), 2.95 (2H, m); ^{13}C -NMR (100
19 MHz, CF_3COOD), δ (ppm): 161.6, 155.5, 151.2, 150.7, 146.4, 142.7, 132.7, 125.5, 124.0,
20 121.4, 113.2, 112.6, 56.1, 29.4, 28.6, 28.4; HRMS (ESI) $^+$ calculated for $\text{C}_{16}\text{H}_{15}\text{N}_2\text{O}_2\text{S}$,
21 $[\text{M}+\text{H}]^+$: m/z 299.0854, found 299.0860; Purity: 99.4% (HPLC, t_R 12.75 min).

22
23 **2-(4-(Trifluoromethyl)phenyl)-3,5,6,7-tetrahydro-4H-cyclopenta[4,5]thieno[2,3-d]pyri**

24
25 **midin-4-one (5b)**. Preparation by Procedure B, off-white solid, m.p. 301-303 $^\circ\text{C}$, yield

26
27 54.8%. ^1H -NMR (400 MHz, DMSO- d_6), δ (ppm): 12.83 (1H, s), 8.33 (2H, d, J = 8.1 Hz),
28 7.90 (2H, d, J = 8.1 Hz), 2.96 (4H, m), 2.95 (2H, m); ^{13}C -NMR (100 MHz, CF_3COOD), δ
29 (ppm): 159.7, 157.3, 153.1, 151.8, 136.4, 136.4, 135.2, 135.2, 131.3, 131.3, 126.4, 124.5,
30 120.6, 34.2, 26.2, 14.0; HRMS (ESI) $^+$ calculated for $\text{C}_{16}\text{H}_{12}\text{F}_3\text{N}_2\text{OS}$, $[\text{M}+\text{H}]^+$: m/z 337.0622,
31 found 337.0630; Purity: 95.5% (HPLC, t_R 11.96 min).

32
33 **2-(3-Bromophenyl)-3,5,6,7-tetrahydro-4H-cyclopenta[4,5]thieno[2,3-d]pyrimidin-4-o**

34
35 **ne (5c)**. Preparation by Procedure B, off-white solid, m.p. 273-275 $^\circ\text{C}$, yield 67.7%.

36
37 ^1H -NMR (400 MHz, DMSO- d_6), δ (ppm): 12.69 (1H, s), 8.34 (1H, dd, J = 1.8, 1.7 Hz), 8.12
38 (1H, d, J = 8.0 Hz), 7.73 (1H, d, J = 7.8 Hz), 7.47 (1H, dd, J = 8.0, 7.8 Hz), 2.93 (4H, m),
39 2.40 (2H, m); ^{13}C -NMR (100 MHz, CF_3COOD), δ (ppm): 161.3, 159.2, 155.5, 152.1, 151.6,
40 130.3, 130.3, 129.1, 129.1, 128.8, 125.8, 116.4, 30.4, 29.5, 29.3; HRMS (ESI) $^+$ calculated
41 for $\text{C}_{15}\text{H}_{12}\text{BrN}_2\text{OS}$, $[\text{M}+\text{H}]^+$: m/z 346.9854, found 346.9863; Purity: 97.5% (HPLC, t_R 12.32
42 min).

2-Benzyl-3,5,6,7-tetrahydro-4H-cyclopenta[4,5]thieno[2,3-d]pyrimidin-4-one (5d).

Preparation by Procedure B, off-white solid, m.p. 250-253 °C, yield 62.9%. ¹H-NMR (400 MHz, DMSO-*d*₆), δ (ppm): 12.54 (1H, s), 7.32 (4H, m), 7.25 (1H, m), 3.93 (2H, s), 2.88 (4H, m), 2.36 (2H, m); ¹³C-NMR (100 MHz, CF₃COOD), δ (ppm): 168.8, 158.7, 156.2, 139.8, 137.2, 137.0, 129.3, 129.3, 129.0, 129.0, 127.3, 118.6, 29.4, 29.1, 27.9; HRMS (ESI)⁺ calculated for C₁₆H₁₅N₂OS, [M+H]⁺: m/z 283.0905, found 283.0914; Purity: 96.2% (HPLC, *t*_R 11.98 min).

2-(4-Bromophenyl)-3,5,6,7-tetrahydro-4H-cyclopenta[4,5]thieno[2,3-d]pyrimidin-4-one (5e).

Preparation by Procedure B, off-white solid, m.p. 317-319 °C, yield 66.3%. ¹H-NMR (400 MHz, DMSO-*d*₆), δ(ppm): 12.70 (1H, s), 8.07 (2H, d *J* = 8.6 Hz), 7.73 (2H, d *J* = 8.6 Hz), 2.95 (4H, m), 2.41 (2H, m); ¹³C-NMR (100 MHz, CF₃COOD), δ (ppm): 161.3, 159.2, 155.5, 152.1, 151.6, 130.3, 130.3, 129.1, 129.1, 128.8, 125.8, 116.4, 30.4, 29.5, 29.3; HRMS (ESI)⁺ calculated for C₁₅H₁₂BrN₂OS, [M+H]⁺: m/z 346.9854, found 346.9864; Purity: 97.4% (HPLC, *t*_R 12.31 min).

2-(4-Hydroxy-3,5-dimethylphenyl)-3,5,6,7-tetrahydro-4H-cyclopenta[4,5]thieno[2,3-d]pyrimidin-4-one (5f).

Preparation by Procedure B, off-white solid, m.p. 307-309 °C, yield 52.1%. ¹H-NMR (400 MHz, DMSO-*d*₆), δ (ppm): 12.22 (1H, s), 8.99 (1H, s), 7.81 (2H, s), 2.92 (4H, m), 2.39 (2H, m), 2.23 (6H, s); ¹³C-NMR (100 MHz, CF₃COOD), δ (ppm): 162.8, 156.7, 155.6, 146.4, 144.0, 136.5, 131.1, 130.9, 130.9, 129.6, 125.0, 116.5, 30.8, 30.1, 29.9, 16.5, 16.5; HRMS (ESI)⁺ calculated for C₁₇H₁₇N₂O₂S, [M+H]⁺: m/z 313.1011, found 313.1020; Purity: 98.4% (HPLC, *t*_R 8.97 min).

2-Phenyl-3,5,6,7-tetrahydro-4H-cyclopenta[4,5]thieno[2,3-d]pyrimidin-4-one (5g).

Preparation by Procedure B, off-white solid, m.p. 251-253 °C, yield 69.2%. ¹H-NMR (400 MHz, DMSO-*d*₆), δ (ppm): 12.61 (1H, s), 8.13 (2H, m), 7.55 (3H, m), 2.96 (4H, m), 2.41 (2H, m); ¹³C-NMR (100 MHz, CF₃COOD), δ (ppm): 162.9, 157.3, 151.8, 133.6, 133.6, 129.3, 129.3, 128.1, 128.1, 126.9, 121.6, 117.0, 29.8, 29.0, 28.8; HRMS (ESI)⁺ calculated for C₁₅H₁₃N₂OS, [M+H]⁺: m/z 269.0749, found 269.0753; Purity: 96.2% (HPLC, *t*_R 13.52 min).

2-(4-(Trifluoromethyl)phenyl)-5,6,7,8-tetrahydrobenzo[4,5]thieno[2,3-d]pyrimidin-4(3H)-one (6a).

Preparation by Procedure B, off-white solid, m.p. 327-329 °C, yield 55.2%.

¹H-NMR (400 MHz, DMSO-*d*₆), δ (ppm): 12.74 (1H, s), 8.32 (2H, d, *J* = 8.2 Hz), 7.90 (2H, d, *J* = 8.2 Hz), 2.93 (2H, t, *J* = 5.0 Hz), 2.79 (2H, t, *J* = 5.0 Hz), 1.81 (4H, m); ¹³C-NMR (100 MHz, CF₃COOD), δ (ppm): 162.4, 157.3, 153.7, 148.7, 140.5, 138.0, 133.0, 128.3, 128.3, 127.1, 127.1, 126.6, 122.6, 24.2, 24.2, 21.4, 20.5; HRMS (ESI)⁺ calculated for C₁₇H₁₄F₃N₂OS, [M+H]⁺: m/z 351.0079, found 351.0084; Purity: 96.0% (HPLC, *t*_R 11.38 min).

2-(4-Bromophenyl)-5,6,7,8-tetrahydrobenzo[4,5]thieno[2,3-d]pyrimidin-4(3H)-one (6b).

Preparation by Procedure B, off-white solid, m.p. 320-322 °C, yield 49.6%. ¹H-NMR

(400 MHz, DMSO-*d*₆), δ (ppm): 12.59 (1H, s), 8.08 (2H, d, *J* = 8.2 Hz), 7.34 (2H, d, *J* = 8.2 Hz), 2.91 (2H, t, *J* = 5.0 Hz), 2.77 (2H, t, *J* = 5.0 Hz), 1.80 (4H, m); ¹³C-NMR (100 MHz, CF₃COOD), δ (ppm): 162.7, 157.6, 154.4, 148.9, 140.2, 134.1, 134.1, 133.0, 128.9, 128.9, 122.5, 122.0, 24.5, 24.4, 21.7, 20.8; HRMS (ESI)⁺ calculated for C₁₆H₁₄BrN₂OS, [M+H]⁺: m/z 361.0010, found 361.0018; Purity: 97.2% (HPLC, *t*_R 12.51 min).

2-(4-Hydroxyphenyl)-5,6,7,8-tetrahydrobenzo[4,5]thieno[2,3-d]pyrimidin-4(3H)-one (6c).

Preparation by Procedure B, off-white solid, m.p. 259-261 °C, yield 73.6%. ¹H-NMR

(400 MHz, DMSO-*d*₆), δ(ppm): 12.45 (1H, s), 7.33-7.23 (5H, m), 2.84 (2H, t, *J* = 5.2 Hz), 2.70 (2H, t, *J* = 5.2 Hz), 1.80 (4H, m); ¹³C-NMR (100 MHz, CF₃COOD), δ(ppm): 163.0, 159.2, 156.9, 147.9, 139.5, 132.7, 129.8, 129.8, 129.4, 129.4, 127.5, 122.3, 24.2, 24.0, 21.5, 20.6; HRMS (ESI)⁺ calculated for C₁₆H₁₅N₂OS, [M+H]⁺: m/z 283.0905, found 283.0911; Purity: 98.4% (HPLC, *t*_R 12.09 min).

2-(4-Hydroxyphenyl)-5,6,7,8-tetrahydrobenzo[4,5]thieno[2,3-d]pyrimidin-4(3H)-one (6d).

Preparation by Procedure B, off-white solid, m.p. 299-301 °C, yield 57.3%. ¹H-NMR

(400 MHz, DMSO-*d*₆), δ (ppm): 12.25 (1H, s), 10.16 (1H, s), 8.01 (2H, d, *J* = 8.8 Hz), 6.86 (2H, d, *J* = 8.8 Hz), 2.89 (2H, t, *J* = 5.8 Hz), 2.74 (2H, t, *J* = 5.8 Hz), 1.76 (4H, m); ¹³C-NMR (100 MHz, CF₃COOD), δ (ppm): 163.0, 157.8, 154.3, 149.0, 139.0, 133.0, 130.4, 130.4, 121.6, 117.7, 117.7, 115.1, 25.5, 24.2, 21.7, 20.7; HRMS (ESI)⁺ calculated for

1
2
3 $C_{16}H_{15}N_2O_2S$, $[M+H]^+$: m/z 299.0854, found 299.0864; Purity: 99.4% (HPLC, t_R 8.32 min).

4 **2-(4-Hydroxy-3,5-dimethylphenyl)-5,6,7,8-tetrahydrobenzo[4,5]thieno[2,3-d]pyrimidin-4(3H)-one (6e)**

5
6 **n-4(3H)-one (6e)**. Preparation by Procedure B, off-white solid, m.p. 311-313 °C, yield

7
8 63.7%. 1H -NMR (400 MHz, $DMSO-d_6$), δ (ppm): 12.12 (1H, s), 8.97 (1H, s), 7.80 (2H, s),

9
10 2.89 (2H, t, $J = 5.8$ Hz), 2.74 (2H, t, $J = 5.8$ Hz), 2.23 (2H, s), 1.79 (4H, m); ^{13}C -NMR (100

11
12 MHz, CF_3COOD), δ (ppm): 162.8, 156.7, 155.6, 146.4, 144.0, 136.5, 131.1, 130.9, 130.9,

13
14 129.6, 125.0, 116.5, 30.8, 30.1, 29.9, 28.45, 16.5, 16.5; HRMS (ESI) $^+$ calculated for

15
16 $C_{18}H_{19}N_2O_2S$, $[M+H]^+$: m/z 327.1167, found 327.1175; Purity: 95.0% (HPLC, t_R 8.59 min).

17
18 **2-(2,4-Difluorophenyl)-5,6,7,8-tetrahydrobenzo[4,5]thieno[2,3-d]pyrimidin-4(3H)-one**

19
20 **(6f)**. Preparation by Procedure B, off-white solid, m.p. 238-241 °C, yield 52.8%. 1H -NMR

21
22 (400 MHz, $DMSO-d_6$), δ (ppm): 12.58 (1H, s), 7.85-7.79 (1H, m), 7.49-7.43 (1H, m), 7.25

23
24 (2H, td, $J = 8.8, 2.7$ Hz), 2.91 (2H, t, $J = 5.8$ Hz), 2.77 (2H, t, $J = 5.8$ Hz), 1.80 (4H, m);

25
26 ^{13}C -NMR (100 MHz, CF_3COOD), δ (ppm): 162.0, 159.3, 152.1, 150.7, 142.6, 135.2, 134.0,

27
28 124.7, 116.4, 113.8, 110.5, 108.2, 26.4, 26.4, 23.6, 22.7; HRMS (ESI) $^+$ calculated for

29
30 $C_{16}H_{13}F_2N_2OS$, $[M+H]^+$: m/z 319.0717, found 319.0722; Purity: 98.4% (HPLC, t_R 12.48

31
32 min).

33
34 **2-(3-Methoxyphenyl)-5,6,7,8-tetrahydrobenzo[4,5]thieno[2,3-d]pyrimidin-4(3H)-one**

35
36 **(6g)**. Preparation by Procedure B, off-white solid, m.p. 242-246 °C, yield 49.1%. 1H -NMR

37
38 (400 MHz, $DMSO-d_6$), δ (ppm): 12.51 (1H, s), 7.73 (1H, d, $J = 7.9$ Hz), 7.69 (1H, br s),

39
40 7.43 (1H, t, $J = 7.9$ Hz), 7.12 (1H, dd, $J = 7.9, 2.0$ Hz), 3.85 (3H, s), 2.92 (2H, t, $J = 5.8$ Hz),

41
42 2.77 (2H, t, $J = 5.8$ Hz), 1.80 (4H, m); ^{13}C -NMR (100 MHz, CF_3COOD), δ (ppm): 160.6,

43
44 157.5, 154.6, 149.6, 139.8, 133.0, 131.7, 124.3, 123.0, 122.2, 120.3, 112.1, 55.1, 24.3,

45
46 24.2, 21.5, 20.6; HRMS (ESI) $^+$ calculated for $C_{17}H_{17}N_2O_2S$, $[M+H]^+$: m/z 313.1011, found

47
48 313.1020; Purity: 95.7% (HPLC, t_R 13.01 min).

49
50 **2-(4-(Trifluoromethyl)phenyl)-3,5,6,7,8,9-hexahydro-4H-cyclohepta[4,5]thieno[2,3-d]**

51
52 **pyrimidin-4-one (7a)**. Preparation by Procedure B, off-white solid, m.p. 317-319 °C, yield

53
54 69.5%. 1H -NMR (400 MHz, $DMSO-d_6$), δ (ppm): 12.73 (1H, s), 8.32 (2H, d, $J = 8.0$ Hz),

55
56 7.90 (2H, d, $J = 8.0$ Hz), 3.28 (2H, m), 2.87 (2H, m), 1.87 (2H, m), 1.60 (4H, m); ^{13}C -NMR

(100 MHz, CF₃COOD), δ (ppm): 160.9, 157.8, 153.3, 146.7, 144.7, 138.9, 138.0, 128.3, 127.1, 126.5, 123.8, 122.8, 121.1, 31.3, 29.2, 26.8, 26.8, 25.8; HRMS (ESI)⁺ calculated for C₁₈H₁₆F₃N₂O₅, [M+H]⁺: m/z 365.0935, found 365.0942; Purity: 97.3% (HPLC, t_R 13.69 min).

2-(3-Bromophenyl)-3,5,6,7,8,9-hexahydro-4H-cyclohepta[4,5]thieno[2,3-d]pyrimidin-4-one (7b). Preparation by Procedure B, off-white solid, m.p. 287-290 °C, yield 60.0%.

¹H-NMR (400 MHz, DMSO-*d*₆), δ (ppm): 8.33 (1H, m), 8.15 (1H, d, *J* = 7.8 Hz), 7.70 (1H, d, *J* = 7.8 Hz), 7.44 (1H, t, *J* = 7.8 Hz), 3.29 (2H, m), 2.83 (2H, m), 1.85 (2H, m), 1.61 (4H, m); ¹³C-NMR (100 MHz, CF₃COOD), δ (ppm): 160.1, 155.6, 149.0, 146.7, 141.4, 141.2, 133.8, 132.8, 128.4, 127.3, 126.8, 125.0, 33.7, 31.6, 29.2, 28.8, 28.1; HRMS (ESI)⁺ calculated for C₁₇H₁₆BrN₂O₅, [M+H]⁺: m/z 375.0167, found 375.0174; Purity: 99.1% (HPLC, t_R 12.74 min).

2-(3-Hydroxyphenyl)-3,5,6,7,8,9-hexahydro-4H-cyclohepta[4,5]thieno[2,3-d]pyrimidin-4-one (7c). Preparation by Procedure B, off-white solid, m.p. 295-297 °C, yield 71.3%.

¹H-NMR (400 MHz, DMSO-*d*₆), δ (ppm): 12.39 (1H, s), 9.71 (1H, s), 7.52 (2H, m), 7.30 (1H, t, *J* = 7.5 Hz), 6.95 (1H, d, *J* = 6.7 Hz), 3.29 (2H, br s), 2.84 (2H, br s), 1.85 (2H, br s), 1.64 (4H, m); ¹³C-NMR (100 MHz, CF₃COOD), δ (ppm): 160.6, 158.3, 158.3, 156.4, 149.0, 146.3, 141.0, 134.2, 126.8, 125.8, 123.0, 116.5, 33.6, 31.4, 29.1, 28.7, 28.1; HRMS (ESI)⁺ calculated for C₁₇H₁₇N₂O₅S, [M+H]⁺: m/z 313.1011, found 313.1020; Purity: 97.4% (HPLC, t_R 9.72 min).

2-(4-Hydroxyphenyl)-3,5,6,7,8,9-hexahydro-4H-cyclohepta[4,5]thieno[2,3-d]pyrimidin-4-one (7d). Preparation by Procedure B, off-white solid, m.p. 293-296 °C, yield 54.8%.

¹H-NMR (400 MHz, DMSO-*d*₆), δ (ppm): 12.20 (1H, s), 10.04 (1H, s), 8.00 (2H, d, *J* = 8.8 Hz), 6.86 (2H, d, *J* = 8.8 Hz), 3.27 (2H, m), 2.82 (2H, m), 1.85 (2H, br s), 1.62 (4H, m); ¹³C-NMR (100 MHz, CF₃COOD), δ (ppm): 160.4, 157.6, 155.8, 149.3, 147.0, 141.4, 132.5, 132.5, 125.3, 125.3, 125.1, 124.9, 34.0, 31.8, 29.4, 29.0, 28.4; HRMS (ESI)⁺ calculated for C₁₇H₁₇N₂O₅S, [M+H]⁺: m/z 313.1011, found 313.1019; Purity: 95.5% (HPLC, t_R 9.09 min).

2-(4-Bromophenyl)-3,5,6,7,8,9-hexahydro-4H-cyclohepta[4,5]thieno[2,3-d]pyrimidin-

1
2
3 **4-one (7e)**. Preparation by Procedure B, off-white solid, m.p. 310-312 °C, yield 63.3%.

4
5 ¹H-NMR (400 MHz, DMSO-*d*₆), δ (ppm): 12.61 (1H, s), 8.07 (2H, d, *J* = 8.1 Hz), 7.75 (2H,
6
7 d, *J* = 8.1 Hz), 3.32 (2H, m), 2.88 (2H, m), 1.89 (2H, br s), 1.65 (4H, m); ¹³C-NMR (100
8
9 MHz, CF₃COOD), δ (ppm): 160.5, 156.3, 152.7, 146.6, 141.3, 136.3, 136.3, 135.0, 131.2,
10
11 131.2, 124.9, 116.9, 33.9, 31.7, 29.3, 29.0, 28.3; HRMS (ESI)⁺ calculated for
12
13 C₁₇H₁₆BrN₂OS, [M+H]⁺: m/z 375.0167, found 375.0174; Purity: 97.3% (HPLC, *t*_R 13.23
14
15 min).

16 **2-(4-Hydroxy-3,5-dimethylphenyl)-3,5,6,7,8,9-hexahydro-4H-cyclohepta[4,5]thieno[2**
17
18 **,3-d]pyrimidin-4-one (7f)** Preparation by Procedure B, off-white solid, m.p. 316-318 °C,
19

20 yield 48.5%. ¹H-NMR (400 MHz, DMSO-*d*₆), δ (ppm): 12.11 (1H, s), 8.97 (1H, s), 7.80 (2H,
21
22 s), 3.28 (2H, m), 2.83 (2H, m), 2.23 (6H, s), 1.86 (2H, br s), 1.63 (4H, m); ¹³C-NMR (100
23
24 MHz, CF₃COOD), δ (ppm): 162.6, 156.2, 152.6, 149.6, 145.0, 140.9, 136.3, 130.9, 130.8,
25
26 130.8, 129.5, 129.5, 33.9, 31.5, 29.3, 28.9, 28.3, 16.4, 16.4; HRMS (ESI)⁺ calculated for
27
28 C₁₉H₂₁N₂O₂S, [M+H]⁺: m/z 341.1324, found 341.1331; Purity: 97.0% (HPLC, *t*_R 9.33 min).

29 **2-Benzyl-3,5,6,7,8,9-hexahydro-4H-cyclohepta[4,5]thieno[2,3-d]pyrimidin-4-one (7g)**.

30 Preparation by Procedure B, off-white solid, m.p. 252-254 °C, yield 68.3%. ¹H-NMR (400
31
32 MHz, DMSO-*d*₆), δ (ppm): 12.52 (1H, s), 7.41-7.29 (4H, m), 7.25 (1H, br s) 3.91 (2H, s),
33
34 3.23 (2H, br s), 2.80 (2H, br s), 1.84 (2H, s), 1.59 (4H, m); ¹³C-NMR (100 MHz,
35
36 CF₃COOD), δ (ppm): 160.8, 152.4, 151.9, 131.9, 131.9, 131.8, 131.8, 131.6, 131.6, 129.8,
37
38 129.8, 116.6, 39.7, 33.6, 31.1, 29.0, 28.7, 28.0; HRMS (ESI)⁺ calculated for C₁₈H₁₉N₂OS,
39
40 [M+H]⁺: m/z 311.1218, found 311.1223; Purity: 97.3% (HPLC, *t*_R 13.21 min).

41 **2-([1,1'-Biphenyl]-4-ylmethyl)-3,5,6,7,8,9-hexahydro-4H-cyclohepta[4,5]thieno[2,3-d]**
42
43 **pyrimidin-4-one (7h)**. Preparation by Procedure B, off-white solid, m.p. 284-286 °C, yield
44
45

46 66.5%. ¹H-NMR (400 MHz, DMSO-*d*₆), δ (ppm): 7.63 (4H, m), 7.44 (4H, m), 7.34 (1H, m),
47
48 3.92 (2H, s), 3.23 (2H, m), 2.77 (2H, m), 1.82 (2H, m), 1.56 (4H, m); ¹³C-NMR (100 MHz,
49
50 CF₃COOD), δ(ppm): 160.2, 158.6, 157.4, 145.9, 143.6, 143.1, 139.2, 138.5, 129.8, 129.8,
51
52 128.4, 128.4, 128.2, 128.2, 127.6, 126.4, 126.4, 122.5, 37.2, 31.4, 29.0, 26.8, 26.5, 25.8;
53
54 HRMS (ESI)⁺ calculated for C₂₄H₂₃N₂OS, [M+H]⁺: m/z 387.1531, found 387.1540; Purity:
55
56
57
58
59
60

1
2
3 98.7% (HPLC, t_R 14.07 min).

4 **2-(2-Methoxyphenyl)-7-methyl-5,6,7,8-tetrahydrobenzo[4,5]thieno[2,3-d]pyrimidin-4(**

5 **3H)-one (8a).** Preparation by Procedure B, off-white solid, m.p. 261-263 °C, yield 63.7%.

6
7
8 $^1\text{H-NMR}$ (400 MHz, $\text{DMSO-}d_6$), δ (ppm): 12.51 (1H, s), 7.73 (1H, d, $J = 7.9$ Hz), 7.68 (1H, t,
9 $J = 1.9$ Hz), 7.42 (1H, t, $J = 8.2$ Hz), 7.13 (1H, dq, $J = 8.2, 0.7$ Hz), 3.85 (3H, s), 3.13 (1H,
10 m), 2.87 (1H, dd, $J = 16.5, 4.9$ Hz), 2.76 (1H, m), 2.36 (1H, m), 1.89 (2H, m), 1.41 (1H, m),
11 1.07 (3H, d, $J = 6.6$ Hz); $^{13}\text{C-NMR}$ (100 MHz, CF_3COOD), δ (ppm): $^{13}\text{C-NMR}$ (100 MHz,
12 CF_3COOD), δ (ppm): 163.0, 160.0, 157.0, 151.2, 142.0, 135.1, 134.1, 126.7, 125.4, 124.5,
13 122.8, 114.6, 57.5, 34.5, 31.3, 31.1, 26.5, 21.6; HRMS (ESI) $^+$ calculated for $\text{C}_{18}\text{H}_{19}\text{N}_2\text{O}_2\text{S}$,
14 $[\text{M}+\text{H}]^+$: m/z 327.1167, found 327.1170; Purity: 97.4% (HPLC, t_R 13.98 min).

15
16
17
18 **7-Methyl-2-(4-(trifluoromethyl)phenyl)-5,6,7,8-tetrahydrobenzo[4,5]thieno[2,3-d]pyri**

19 **midin-4(3H)-one (8b).** Preparation by Procedure B, off-white solid, m.p. 321-324 °C,

20
21
22 yield 58.4%. $^1\text{H-NMR}$ (400 MHz, $\text{DMSO-}d_6$), δ (ppm): 12.74 (1H, s), 8.33 (2H, d, $J = 8.4$
23 Hz), 7.90 (2H, d, $J = 8.4$ Hz), 3.13 (1H, m), 2.90 (1H, dd, $J = 17.8, 5.5$ Hz), 2.83(1H, m),
24 2.40 (1H, m), 1.90 (2H, m), 1.40 (1H, m), 1.07 (3H, d, $J = 6.5$ Hz); $^{13}\text{C-NMR}$ (100 MHz,
25 CF_3COOD), δ (ppm): 159.9, 156.3, 151.4, 142.8, 135.3, 130.9, 130.9, 129.7, 129.6, 129.2,
26 126.3, 125.0, 123.6, 34.7, 31.4, 31.1, 26.5, 21.7; HRMS (ESI) $^+$ calculated for
27 $\text{C}_{18}\text{H}_{16}\text{F}_3\text{N}_2\text{OS}$, $[\text{M}+\text{H}]^+$: m/z 365.0935, found 365.0941; Purity: 99.1% (HPLC, t_R 12.54
28 min).

29
30
31
32 **2-(3-Bromophenyl)-7-methyl-5,6,7,8-tetrahydrobenzo[4,5]thieno[2,3-d]pyrimidin-4(3**

33 **H)-one (8c).** Preparation by Procedure B, off-white solid, m.p. 280-282 °C, yield 60.3%.

34
35
36 $^1\text{H-NMR}$ (400 MHz, $\text{DMSO-}d_6$), δ (ppm): 12.60 (1H, s), 8.31 (1H, s), 8.13 (1H, d, $J = 8.0$
37 Hz), 7.77 (1H, d, $J = 7.9$ Hz), 7.48 (1H, t, $J = 8.0$ Hz), 3.13 (1H, m), 2.88 (1H, dd, $J = 17.2,$
38 4.7 Hz), 2.80 (1H, m), 2.38 1H, m), 1.90 (2H, m), 1.38 (1H, m), 1.07 (3H, d, $J = 6.4$ Hz);
39 $^{13}\text{C-NMR}$ (100 MHz, CF_3COOD), δ (ppm): 161.0, 156.0, 151.2, 142.4, 141.5, 141.5, 135.1,
40 133.9, 133.9, 133.0, 128.5, 127.4, 126.8, 34.5, 31.3, 31.0, 26.5, 21.6; HRMS (ESI) $^+$
41 calculated for $\text{C}_{17}\text{H}_{16}\text{BrN}_2\text{OS}$, $[\text{M}+\text{H}]^+$: m/z 375.0167, found 375.0178; Purity: 96.2%
42 (HPLC, t_R 12.83 min).

43
44
45
46 **7-Methyl-2-(3,4,5-trifluorophenyl)-5,6,7,8-tetrahydrobenzo[4,5]thieno[2,3-d]pyrimidi**

n-4(3H)-one (8d). Preparation by Procedure B, off-white solid, m.p. 305-307 °C, yield 58.6%. ¹H-NMR (400 MHz, DMSO-*d*₆), δ (ppm): 12.65 (1H, m), 8.10 (2H, m), 3.13 (1H, m), 2.89 (1H, m), 2.78 (1H, m), 2.39 (1H, m), 1.89 (2H, m), 1.38 (1H, m), 1.07 (3H, d, *J* = 6.7 Hz); ¹³C-NMR (100 MHz, CF₃COOD), δ (ppm): 159.9, 156.2, 154.5, 153.7, 151.8, 148.8, 146.1, 142.9, 135.2, 124.9, 122.1, 115.8, 34.7, 31.4, 31.1, 26.6, 21.7; HRMS (ESI)⁺ calculated for C₁₇H₁₄F₃N₂O₅, [M+H]⁺: *m/z* 351.0779, found 351.0087; Purity: 96.7% (HPLC, *t*_R 12.01 min).

2-(3-Hydroxyphenyl)-7-methyl-5,6,7,8-tetrahydrobenzo[4,5]thieno[2,3-d]pyrimidin-4(3H)-one (8e). Preparation by Procedure B, off-white solid, m.p. 291-293 °C, yield 63.4%. ¹H-NMR (400 MHz, DMSO-*d*₆), δ (ppm): 12.4 (1H, s), 9.73 (1H, s), 7.55 (2H, m), 7.30 (1H, t, *J* = 7.7 Hz), 6.95 (1H, ddd, *J* = 8.1, 2.4, 0.8 Hz), 3.12 (1H, m), 2.83 (1H, dd, *J* = 16.6, 4.7 Hz), 2.75 (1H, m), 2.36 (1H, m), 1.87 (2H, m), 1.38 (1H, m), 1.06 (3H, d, *J* = 6.6 Hz); ¹³C-NMR (100 MHz, CF₃COOD), δ (ppm): 159.9, 158.6, 157.2, 151.2, 142.2, 135.2, 134.5, 127.1, 126.1, 124.7, 123.3, 116.7, 34.7, 31.4, 31.2, 26.6, 21.7; HRMS (ESI)⁺ calculated for C₁₇H₁₇N₂O₂S, [M+H]⁺: *m/z* 313.1011, found 313.1020; Purity: 97.3% (HPLC, *t*_R 9.18 min).

2-(4-Hydroxyphenyl)-7-methyl-5,6,7,8-tetrahydrobenzo[4,5]thieno[2,3-d]pyrimidin-4(3H)-one (8f). Preparation by Procedure B, off-white solid, m.p. 288-289 °C, yield 48.7%. ¹H-NMR (400 MHz, DMSO-*d*₆), δ (ppm): 12.25(1H, s), 10.15(1H, s), 8.01 (2H, d, *J* = 8.7 Hz), 6.87 (2H, d, *J* = 8.7 Hz), 6.87 (2H, d, *J* = 8.7 Hz), 3.11 (1H, m), 2.84 (1H, m), 2.75 (1H, m), 2.35 (1H, m), 1.88 (2H, m), 1.40 (1H, m), 1.06 (3H, d, *J* = 6.5 Hz); ¹³C-NMR (100 MHz, CF₃COOD), δ (ppm): 165.2, 160.0, 156.5, 151.3, 141.1, 134.9, 132.6, 132.6, 123.7, 119.9, 119.9, 117.4, 34.4, 31.3, 31.1, 26.4, 21.6; HRMS (ESI)⁺ calculated for C₁₇H₁₇N₂O₂S, [M+H]⁺: *m/z* 313.1011, found 313.1022; Purity: 99.1% (HPLC, *t*_R 9.52 min).

2-(4-Bromophenyl)-7-methyl-5,6,7,8-tetrahydrobenzo[4,5]thieno[2,3-d]pyrimidin-4(3H)-one (8g). Preparation by Procedure B, off-white solid, m.p. 311-313 °C, yield 61.1%. ¹H-NMR (400 MHz, DMSO-*d*₆), δ (ppm): 12.59 (1H, s), 8.07 (2H, d, *J* = 8.5 Hz), 7.73 (2H, dt, *J* = 8.7, 1.9 Hz), 3.13 (1H, m), 2.88 (1H, dd, *J* = 16.6, 4.8 Hz), 2.78 (1H, m), 2.33 (1H, m), 1.88 (2H, m), 1.39 (1H, m), 1.07 (3H, d, *J* = 6.6 Hz); ¹³C-NMR (100 MHz, CF₃COOD),

1
2
3 δ (ppm): 160.3, 156.7, 151.5, 142.2, 136.4, 136.4, 135.2, 135.1, 131.2, 131.2, 124.6,
4 124.3, 34.6, 31.4, 31.1, 26.5, 21.7; HRMS (ESI)⁺ calculated for C₁₇H₁₆BrN₂OS, [M+H]⁺:
5 m/z 375.0088, found 375.0093; Purity: 95.1% (HPLC, *t*_R 13.49 min).
6
7

8 **2-(4-Hydroxy-3,5-dimethylphenyl)-7-methyl-5,6,7,8-tetrahydrobenzo[4,5]thieno[2,3-**
9 **d]pyrimidin-4(3*H*)-one (8h).** Preparation by Procedure B, off-white solid, m.p.
10 305-307 °C, yield 58.5%. ¹H-NMR (400 MHz, DMSO-*d*₆), δ (ppm): 12.12 (1H, s), 8.97 (1H,
11 s), 7.79 (2H, s), 3.10 (1H, m), 2.83 (1H, dd, *J* = 16.6, 4.6 Hz), 2.73 (1H, m), 2.34 (1H, m),
12 2.22 (6H, s), 1.87 (2H, m), 1.37 (1H, m), 1.06 (3H, d, *J* = 6.5 Hz); ¹³C-NMR (100 MHz,
13 CF₃COOD), δ (ppm): 162.7, 160.2, 156.6, 151.5, 140.7, 134.9, 130.9, 130.9, 129.6, 129.6,
14 123.5, 116.4, 34.5, 31.4, 31.1, 26.5, 21.6, 16.4, 16.4; HRMS (ESI)⁺ calculated for
15 C₁₉H₂₁N₂O₂S, [M+H]⁺: m/z 341.1324, found 341.1330; Purity: 98.3% (HPLC, *t*_R 9.36 min).
16
17
18
19

20 **7-Methyl-2-phenyl-5,6,7,8-tetrahydrobenzo[4,5]thieno[2,3-d]pyrimidin-4(3*H*)-one (8i).**
21 Preparation by Procedure B, off-white solid, m.p. 263-265 °C, yield 50.0%. ¹H-NMR (400
22 MHz, DMSO-*d*₆), δ (ppm): 12.57 (1H, s), 9.78 (1H, s), 7.52 (2H, m), 7.32 (1H, t, *J* = 7.9 Hz),
23 6.98 (1H, ddd, *J* = 8.1, 2.4, 0.6 Hz), 4.03 (2H, s), 3.11 (4H, s), 2.66 (3H, s); ¹³C-NMR (100
24 MHz, CF₃COOD), δ (ppm): 159.6, 158.8, 154.4, 134.6, 134.6, 131.5, 129.6, 127.1, 126.7,
25 123.7, 123.4, 117.1, 54.4, 54.1, 45.3, 45.3, 24.6; HRMS (ESI)⁺ calculated for C₁₇H₁₇N₂OS,
26 [M+H]⁺: m/z 297.1062, found 297.1071; Purity: 97.4% (HPLC, *t*_R 12.99 min).
27
28
29
30
31
32
33
34
35

36 **2-Benzyl-7-methyl-5,6,7,8-tetrahydrobenzo[4,5]thieno[2,3-d]pyrimidin-4(3*H*)-one (8j).**
37 Preparation by Procedure B, off-white solid, m.p. 256-258 °C, yield 64.8%. ¹H-NMR (400
38 MHz, DMSO-*d*₆), δ (ppm): 12.45 (1H, s), 7.31 (4H, m), 7.24 (1H, m), 3.90 (2H, s), 3.01 (1H,
39 m), 2.77 (1H, dd, *J* = 16.8, 4.8 Hz), 2.69 (1H, m), 2.31 (1H, m), 1.84 (2H, m), 1.34 (1H, m),
40 1.03 (3H, d, *J* = 6.6 Hz); ¹³C-NMR (100 MHz, CF₃COOD), δ (ppm): 161.8, 159.4, 150.5,
41 141.7, 134.9, 132.3, 132.3, 132.1, 131.9, 131.9, 130.1, 124.7, 40.1, 34.5, 31.4, 31.1, 26.5,
42 21.6; HRMS (ESI)⁺ calculated for C₁₈H₁₉N₂OS, [M+H]⁺: m/z 311.1218, found 311.1222;
43 Purity: 96.4% (HPLC, *t*_R 13.06 min).
44
45
46
47
48
49
50
51

52 **2-([1,1'-Biphenyl]-4-ylmethyl)-7-methyl-5,6,7,8-tetrahydrobenzo[4,5]thieno[2,3-d]pyr**
53 **imidin-4(3*H*)-one (8k).** Preparation by Procedure B, off-white solid, m.p. 288-291 °C,
54
55
56
57
58
59
60

1
2
3 yield 64.5%. ¹H-NMR (400 MHz, DMSO-*d*₆), δ (ppm): 12.50 (1H, s), 7.64 (4H, m), 7.45
4 (4H, m), 7.34 (1H, m), 3.96 (2H, s), 3.06 (1H, m), 2.81 (1H, dd, *J* = 16.6, 4.7 Hz), 2.71 (1H,
5 m), 2.32 (1H, m), 1.85 (2H, m), 1.35 (1H, m), 1.03 (3H, d, *J* = 6.5 Hz); ¹³C-NMR (100 MHz,
6 CF₃COOD), δ (ppm): 161.4, 159.4, 150.5, 145.4, 141.7, 141.6, 134.8, 132.4, 132.4, 130.9,
7 130.9, 130.6, 130.6, 130.1, 129.4, 128.8, 128.8, 124.7, 39.7, 34.5, 31.4, 31.1, 26.5, 21.7;
8 HRMS (ESI)⁺ calculated for C₂₄H₂₃N₂O₂S, [M+H]⁺: *m/z* 387.1531, found 387.1540; Purity:
9 98.7% (HPLC, *t*_R 13.85 min).

10
11
12 **2-(2-Methoxyphenyl)-7-methyl-5,6,7,8-tetrahydropyrido[4',3':4,5]thieno[2,3-d]pyrimi**
13 **din-4(3*H*)-one (9a).** Preparation by Procedure B, off-white solid, m.p. 259-262 °C, yield
14 60.5%. ¹H-NMR (400 MHz, DMSO-*d*₆), δ (ppm): 12.57 (1H, s), 7.73 (1H, d, *J* = 7.8 Hz),
15 7.69 (1H, m), 7.44 (1H, dd, *J* = 8.5, 7.8 Hz), 7.13 (1H, dd, *J* = 8.5, 2.5 Hz), 3.85 (3H, s),
16 3.60 (2H, s), 2.99 (2H, m), 2.70 (2H, m), 2.39 (3H, s); ¹³C-NMR (100 MHz, CF₃COOD), δ
17 (ppm): 160.1, 158.6, 156.3, 141.8, 134.0, 133.4, 131.4, 129.4, 128.9, 128.4, 127.0, 123.4,
18 54.5, 54.3, 45.4, 45.4, 24.7; HRMS (ESI)⁺ calculated for C₁₇H₁₈N₃O₂S, [M+H]⁺: *m/z*
19 328.1120, found 328.1131; Purity: 95.3% (HPLC, *t*_R 11.94 min).

20
21
22 **7-Methyl-2-(4-(trifluoromethyl)phenyl)-5,6,7,8-tetrahydropyrido[4',3':4,5]thieno[2,3-d**
23 **]pyrimidin-4(3*H*)-one (9b).** Preparation by Procedure B, off-white solid, m.p. 249-252 °C,
24 yield 67.6%. ¹H-NMR (400 MHz, DMSO-*d*₆), δ (ppm): 12.83 (1H, s), 8.34 (2H, d, *J* = 8.2
25 Hz), 7.96 (2H, d, *J* = 8.2 Hz), 3.61 (2H, s), 2.99 (2H, m), 2.69 (2H, m), 2.39 (3H, s);
26 ¹³C-NMR (100 MHz, CF₃COOD), δ (ppm): 160.0, 159.8, 154.7, 134.4, 134.4, 131.6, 129.4,
27 127.0, 126.3, 123.3, 123.3, 115.0, 115.0, 57.7, 54.4, 45.4, 24.6; HRMS (ESI)⁺ calculated
28 for C₁₇H₁₅F₃N₃O₂S, [M+H]⁺: *m/z* 366.0888, found 366.0897; Purity: 96.0% (HPLC, *t*_R 11.32
29 min).

30
31
32 **2-(3-Bromophenyl)-7-methyl-5,6,7,8-tetrahydropyrido[4',3':4,5]thieno[2,3-d]pyrimidi**
33 **n-4(3*H*)-one (9c).** Preparation by Procedure B, off-white solid, m.p. 269-271 °C, yield
34 58.3%. ¹H-NMR (400 MHz, DMSO-*d*₆), δ (ppm): 12.83 (1H, s), 8.40 (1H, t, *J* = 1.8, 1.7 Hz),
35 8.23 (1H, ddd, *J* = 8.0, 1.4, 1.1 Hz), 7.58 (1H, m), 7.37 (1H, dd, *J* = 8.0, 7.8 Hz), 3.50 (2H,
36 s), 2.96 (2H, m), 2.63 (2H, m), 2.37 (3H, s); ¹³C-NMR (100 MHz, CF₃COOD), δ (ppm):
37 160.7, 158.4, 158.4, 140.3, 140.0, 131.1, 129.5, 129.5, 129.3, 126.5, 123.8, 123.3, 54.6,
38
39
40
41
42
43
44
45
46
47
48
49
50
51
52
53
54
55
56
57
58
59
60

54.4, 45.4, 24.7; HRMS (ESI)⁺ calculated for C₁₆H₁₅BrN₃OS, [M+H]⁺: m/z 376.0119, found 376.0126; Purity: 95.8% (HPLC, t_R 12.01 min).

2-(3-Hydroxyphenyl)-7-methyl-5,6,7,8-tetrahydropyrido[4',3':4,5]thieno[2,3-d]pyrimidin-4(3H)-one (9d). Preparation by Procedure B, off-white solid, m.p. 311-313 °C, yield 62.0%. ¹H-NMR (400 MHz, DMSO-*d*₆), δ (ppm): 12.55 (1H, s), 8.12 (2H, d, *J* = 8.0 Hz), 7.54 (2H, d, *J*=8.0 Hz), 3.12 (2H, s), 2.82 (2H, m), 2.38 (2H, m), 1.90 (3H, s); ¹³C-NMR (100 MHz, CF₃COOD), δ (ppm): 160.2, 157.5, 157.5, 151.2, 141.9, 138.8, 135.1, 132.7, 132.7, 130.0, 125.5, 124.7, 34.5, 31.3, 26.5, 21.6; HRMS (ESI)⁺ calculated for C₁₆H₁₆N₃O₂S, [M+H]⁺: m/z 314.0963, found 314.0973; Purity: 97.9% (HPLC, t_R 8.56 min).

2-(4-Hydroxyphenyl)-7-methyl-3,5,6,7,8,9-hexahydro-4H-pyrido[4',3':3,4]cyclopenta[1,2-d]pyrimidin-4-one (9e). Preparation by Procedure B, off-white solid, m.p. 316-318 °C, yield 51.8%. ¹H-NMR (400 MHz, DMSO-*d*₆), δ (ppm): 8.05 (2H, d, *J* = 8.7 Hz), 6.78 (2H, d, *J* = 8.7 Hz), 3.49 (2H, s), 2.95 (2H, m), 2.63 (2H, m), 2.36 (3H, s); ¹³C-NMR (100 MHz, CF₃COOD), δ (ppm): 165.2, 160.0, 156.5, 151.3, 141.1, 134.9, 132.6, 132.6, 123.7, 119.9, 119.9, 117.4, 34.4, 31.3, 31.1, 26.4; HRMS (ESI)⁺ calculated for C₁₇H₁₈N₃O₂, [M+H]⁺: m/z 296.1399, found 296.1402; Purity: 96.9% (HPLC, t_R 8.12 min).

2-(4-Hydroxy-3,5-dimethylphenyl)-7-methyl-5,6,7,8-tetrahydropyrido[4',3':4,5]thieno[2,3-d]pyrimidin-4(3H)-one (9f). Preparation by Procedure B, off-white solid, m.p. 329-331 °C, yield 48.7%. ¹H-NMR (400 MHz, DMSO-*d*₆), δ (ppm): 12.18 (1H, s), 8.99 (1H, s), 7.83 (2H, s), 3.56 (2H, s), 2.96 (2H, m), 2.67 (2H, m), 2.38 (3H, s), 2.23 (6H, s); ¹³C-NMR (100 MHz, CF₃COOD), δ (ppm): 160.3, 159.9, 158.9, 154.0, 131.5, 131.5, 131.5, 129.9, 129.9, 128.2, 122.1, 115.8, 54.4, 54.2, 45.4, 24.5, 16.5, 16.5; HRMS (ESI)⁺ calculated for C₁₈H₂₀N₃O₂S, [M+H]⁺: m/z 342.1276, found 342.1280; Purity: 95.6% (HPLC, t_R 8.89 min).

2-([1,1'-Biphenyl]-4-ylmethyl)-7-methyl-5,6,7,8-tetrahydropyrido[4',3':4,5]thieno[2,3-d]pyrimidin-4(3H)-one (9g). Preparation by Procedure B, off-white solid, m.p. 264-266 °C, yield 57.3%. ¹H-NMR (400 MHz, DMSO-*d*₆), δ (ppm): 12.58 (1H, s), 7.63 (4H, m), 7.44 (4H, m), 7.35 (1H, m), 3.97 (2H, s), 3.52 (2H, m), 2.91 (2H, m), 2.67 (2H, m) 2.35

(3H, s); ^{13}C -NMR (100 MHz, CF_3COOD), δ (ppm): 164.7, 159.0, 153.5, 145.9, 141.7, 132.6, 132.6, 131.4, 131.0, 131.0, 130.8, 130.8, 130.2, 130.2, 129.4, 129.0, 129.0, 128.5, 54.3, 54.1, 45.4, 40.3, 24.5; HRMS (ESI) $^+$ calculated for $\text{C}_{23}\text{H}_{22}\text{N}_3\text{OS}$, $[\text{M}+\text{H}]^+$: m/z 388.1484, found 388.1494; Purity: 95.6% (HPLC, t_{R} 11.72 min).

7-Benzyl-2-(3-methoxyphenyl)-5,6,7,8-tetrahydropyrido[4',3':4,5]thieno[2,3-d]pyrimidin-4(3H)-one (10a). Preparation by Procedure B, off-white solid, m.p. 263-265 °C, yield 55.4%. ^1H -NMR (400 MHz, $\text{DMSO}-d_6$), δ (ppm): 12.58 (1H, br s), 7.74-7.69 (2H, m), 7.45-7.28 (6H, m), 7.13 (1H, d, $J = 7.0$ Hz), 3.85 (3H, s), 3.72 (2H, s), 3.64 (2H, s), 2.98 (2H, br s), 2.79 (2H, br s); ^{13}C -NMR (100 MHz, CF_3COOD), δ (ppm): 162.8, 159.1, 154.1, 152.1, 133.8, 133.3, 132.3, 132.3, 131.7, 131.7, 130.0, 128.2, 126.5, 125.8, 122.8, 119.4, 116.5, 114.3, 63.6, 57.2, 51.7, 51.3, 24.2; HRMS (ESI) $^+$ calculated for $\text{C}_{23}\text{H}_{22}\text{N}_3\text{O}_2\text{S}$, $[\text{M}+\text{H}]^+$: m/z 404.1433, found 404.1434; Purity: 97.6% (HPLC, t_{R} 13.88 min).

7-Benzyl-2-(4-hydroxy-3,5-dimethylphenyl)-5,6,7,8-tetrahydropyrido[4',3':4,5]thieno[2,3-d]pyrimidin-4(3H)-one (10b). Preparation by Procedure B, off-white solid, m.p. 327-329 °C, yield 39.2%. ^1H -NMR (400 MHz, $\text{DMSO}-d_6$), δ (ppm): 12.19 (1H, s), 8.99 (1H, s), 7.81 (2H, s), 7.39-7.27 (5H, m), 3.72 (2H, s), 3.62 (2H, s), 2.96 (2H, br s), 2.79 (2H, br s), 2.22 (6H, s); ^{13}C -NMR (100 MHz, CF_3COOD), δ (ppm): 164.0, 157.7, 156.6, 151.7, 131.6, 130.6, 130.6, 130.0, 130.0, 129.6, 129.3, 129.3, 127.7, 127.7, 126.5, 126.4, 119.9, 113.6, 61.9, 50.0, 49.6, 22.4, 14.3, 14.3; HRMS (ESI) $^+$ calculated for $\text{C}_{24}\text{H}_{24}\text{N}_3\text{O}_2\text{S}$, $[\text{M}+\text{H}]^+$: m/z 418.1589, found 418.1597; Purity: 96.4% (HPLC, t_{R} 10.05 min).

7-Benzyl-2-phenyl-5,6,7,8-tetrahydropyrido[4',3':4,5]thieno[2,3-d]pyrimidin-4(3H)-one (10c). Preparation by Procedure B, off-white solid, m.p. 271-273 °C, yield 48.7%. ^1H -NMR (400 MHz, $\text{DMSO}-d_6$), δ (ppm): 12.57 (1H, s), 8.13 (2H, d, $J = 7.0$ Hz), 7.59-7.50 (3H, m), 7.39-7.26 (5H, m), 3.72 (2H, s), 3.64 (2H, s), 2.98 (2H, br s), 2.79 (2H, br s); ^{13}C -NMR (100 MHz, CF_3COOD), δ (ppm): 162.2, 159.2, 159.2, 153.7, 152.1, 139.1, 133.3, 132.5, 132.5, 132.3, 132.3, 131.7, 131.7, 130.0, 130.0, 129.3, 125.0, 122.7, 63.7, 51.7, 51.4, 24.2; HRMS (ESI) $^+$ calculated for $\text{C}_{22}\text{H}_{20}\text{N}_3\text{OS}$, $[\text{M}+\text{H}]^+$: m/z 374.1327, found 374.1330; Purity: 97.4% (HPLC, t_{R} 13.41 min).

7-Benzyl-2-(4-(trifluoromethyl)phenyl)-5,6,7,8-tetrahydropyrido[4',3':4,5]thieno[2,3-d]

1
2
3 **[pyrimidin-4(3H)-one (10d)**. Preparation by Procedure B, off-white solid, m.p.
4 318-321 °C, yield 59.5%. ¹H-NMR (400 MHz, DMSO-*d*₆), δ (ppm): 12.80 (1H, s), 8.33 (2H,
5 d, *J* = 8.2 Hz), 7.89 (2H, d, *J* = 8.2 Hz), 7.39-7.26 (5H, m), 3.72 (2H, s), 3.65 (2H, s), 2.89
6 (2H, t, *J* = 5.8 Hz), 2.72 (2H, t, *J* = 5.8 Hz); ¹³C-NMR (100 MHz, CF₃COOD), δ (ppm):
7 164.0, 157.9, 155.7, 155.4, 137.5, 131.1, 130.1, 130.1, 129.5, 129.5, 128.8, 128.4, 128.4,
8 128.2, 126.8, 126.0, 123.9, 121.2, 120.6, 61.3, 49.6, 49.3, 22.0; HRMS (ESI)⁺ calculated
9 for C₂₃H₁₉F₃N₃O₃S, [M+H]⁺: *m/z* 442.1201, found 442.1210; Purity: 96.5% (HPLC, *t*_R 12.96
10 min).

11
12
13
14
15
16
17
18 **7-Benzyl-2-(4-hydroxyphenyl)-5,6,7,8-tetrahydropyrido[4',3':4,5]thieno[2,3-d]pyrimi**
19 **din-4(3H)-one (10e)**. Preparation by Procedure B, off-white solid, m.p. 321-324 °C, yield
20 60.2%. ¹H-NMR (400 MHz, DMSO-*d*₆), δ (ppm): 8.08 (2H, d, *J* = 8.7 Hz), 7.39-7.26 (5H,
21 m), 6.76 (2H, d, *J* = 8.7 Hz), 3.68 (2H, s), 3.54 (2H, s), 2.89 (2H, t, *J* = 5.8 Hz), 2.72 (2H, t,
22 *J* = 5.8 Hz); ¹³C-NMR (100 MHz, CF₃COOD), δ (ppm): 164.2, 157.4, 156.6, 151.6, 131.5,
23 131.0, 131.0, 130.4, 130.4, 129.8, 129.8, 129.5, 126.5, 126.3, 120.0, 118.7, 118.7, 118.0,
24 61.8, 49.9, 49.8, 22.3; HRMS (ESI)⁺ calculated for C₂₂H₂₀N₃O₂S, [M+H]⁺: *m/z* 390.1276,
25 found 390.1280; Purity: 97.7% (HPLC, *t*_R 10.04 min).

26
27
28
29
30
31
32
33 **Protein-protein interaction (PPI) network construction and functional annotation.** To
34 create the BRD4 related protein-protein interaction (PPI) network, we collected the
35 BRD4-interacted proteins on the PrePPI database,⁴³ of which we only adopt the PPI when
36 the possibility is greater than 0.5. The PPI network was constructed by using Cytoscape.⁴⁴
37 Afterwards, we created the BRD4 related autophagic PPI subnetwork by Gene Ontology
38 (GO) annotation. All BRD4-interacted proteins were submitted to the DAVID server by
39 using the functional annotation tool to classify functional terms, referring to the GO terms
40 of the biological process (BP).^{45,46}

41
42
43
44
45
46
47
48 **Expression profiling in TCGA dataset.** The gene expression RNAseq data (polyA+
49 IlluminaHiSeq percentile) of TCGA breast cancer (BRCA) were downloaded from UCSC
50 Xena(https://tcga.xenahubs.net/download/TCGA.BRCA.sampleMap/HiSeqV2_percentile).
51 The gene expression profile was measured by using the Illumina HiSeq 2000 RNA
52 Sequencing platform. RSEM (RNASeq by Expectation-Maximization) normalized count
53
54
55
56
57
58
59
60

1
2
3 was used as gene level expression estimates in this study.

4 **Molecular docking.** The initial three dimensional geometric coordinates of the X-ray
5 crystal structure of BRD4(1) (PDB ID:: 3MXF) was downloaded from the Protein Databank
6 (PDB). The hits were screened from ZINC library by Accelrys Discovery Studio (version
7 3.5; Accelrys, SanDiego, CA, USA) using LibDock protocol.⁴⁷ Compounds were energy
8 minimized with the CHARMM force field.⁴⁸ The CDOCKER protocol was employed as
9 further docking approach to conduct semi-flexible docking to re-rank the top 20 small
10 molecule compounds.⁴⁹ The other parameters were set as default values.

11 **Molecular dynamics simulation.** Molecular dynamics (MD) simulations for **9f**-BRD4
12 complex were carried out using GROMACS (version 4.5.5) software package.⁵⁰ The
13 molecular dynamics package AMBER10 was used throughout the whole simulation
14 process as well as the minimization and equilibration protocols.⁵¹ The energy minimization
15 was firstly conducted with steepest descent method switched to conjugate gradient every
16 2500 steps totally for 5000 steps with a 0.1 kcal/mol·Å² restrains on all atoms of the
17 complexes. Following this step, another two rounds of energy minimization were
18 performed by only restraining protein and further releasing all the restrains for 5000 steps
19 of each round. Long-range Coulombic interactions were handled using the particle mesh
20 Ewald (PME) summation. For the equilibration and subsequent production runs, the
21 SHAKE algorithm was employed on all atoms covalently bonded to a hydrogen atom,
22 allowing for an integration time step of 2 fs. The system was gently annealed from 0 to 310
23 K over a period of 50 ps using a Langevin thermostat with a coupling coefficient of 1.0/ps
24 and a force constant 2.0 kcal/mol·Å² on the complex. All subsequent stages were carried
25 out in the isothermal isobaric (NPT) ensemble using a Berendsen barostat with a target
26 pressure of 1 bar and a pressure coupling constant of 2.0 ps.⁵² Additional five rounds of
27 MD (100 ps each at 310 K) were performed with the decreasing restraint weights from 2.0,
28 1.5, 1.0, 0.5 to 0.1 kcal/mol·Å². By releasing all the restrains, the system was again
29 equilibrated for 500 ps. Following the last equilibration step, the production phase of the
30 simulations was run without any restrains for a total of 20 ns.

31 **Binding free energy calculation.** MM-GBSA calculation was performed using
32
33
34
35
36
37
38
39
40
41
42
43
44
45
46
47
48
49
50
51
52
53
54
55
56
57
58
59
60

1
2
3 AMBER10.⁵¹ The first step of MM-GBSA method is the generation of multiple snapshots
4 from an MD trajectory of the protein-ligand complex, stripped of water molecules and
5 counter ions. Snapshots, equally spaced at 10 ps intervals, were extracted from the
6 equilibration section of MD trajectory. For each snapshot, the free energy is calculated for
7 each molecular species (complex, protein, and ligand). The binding free energy is
8 computed as the difference:
9

$$\Delta G_{bind} = G_{complex} - G_{protein} - G_{ligand}$$

10
11 The free energy, G , for each species can be calculated by the following scheme using the
12 MM-GBSA method⁵³:
13

$$G = E_{gas} + G_{sol} - TS$$

$$E_{gas} = E_{int} + E_{ele} + E_{vdw}$$

$$E_{int} = E_{bond} + E_{angle} + E_{torsion}$$

$$G_{sol} = G_{GB} + G_{nonpolar}$$

$$G_{nonpolar} = \gamma SAS$$

14
15
16 Here, E_{gas} is the gas-phase energy; E_{int} is the internal energy; E_{bond} , E_{angle} , and $E_{torsion}$ are
17 the bond, angle, and torsion energies, respectively; and E_{ele} and E_{vdw} are the Coulomb
18 and van der Waals energies, respectively. E_{gas} was calculated using the AMBER
19 molecular mechanics force field. G_{sol} is the solvation free energy and can be decomposed
20 into polar and nonpolar contributions. G_{GB} is the polar solvation contribution calculated by
21 solving the GB equation.⁵³ The dielectric constant of solvent and solute were set to 80 and
22 1, respectively. $G_{nonpolar}$ is the nonpolar solvation contribution and was estimated by the
23 solvent accessible surface area (SAS) determined using a water probe radius of 1.4 Å.
24 The surface tension constant γ was set to 0.0072 kcal/mol/Å².
25
26
27
28
29

30
31 **Cloning, recombinant expression, and purification of BRD4.** The catalytic core of
32 human BRD4 (residues 43-166) was PCR amplified and cloned, resulting in a construct
33 with His+thioredoxin tag (BRD4) and a TEV protease cleavage site. Proteins were
34 expressed in *E. coli* BL21 Star (DE3) cells in LB medium by adding 100ug/mL Ampicillin at
35
36
37
38
39
40
41
42
43
44
45
46
47
48
49
50
51
52
53
54
55
56
57
58
59
60

1
2
3 OD₆₀₀=0.8. Cells were incubated over night at 18 °C, disrupted with a Microfluidizer, cell
4 debris removed by centrifugation, and the supernatant supplemented with 10 mM
5 imidazole and incubated with talon resin for 1 h at 4 °C. Resin was washed with 10
6 volumes 50 mM Tris/HCl, pH 7.8, 500 mM NaCl and 10 volumes 50 mM Tris/HCl, pH 7.8,
7 200 mM NaCl, 5 mM imidazol. Recombinant proteins were eluted with 50 mM Tris/HCl, pH
8 7.8, 200 mM NaCl, 250 mM imidazol, subjected to gel filtration on a Superose 12 column
9 (GE Healthcare, Waukesha, USA) in 20 mM Tris/HCl, pH 7.8, 150 mM NaCl, concentrated,
10 and stored at -80 °C. Proteins for crystallization were digested with TEV protease
11 overnight and tags removed by affinity chromatography on talon resin prior to gel filtration.

12
13
14 **Crystallization and structure solution.** BRD4 crystals were grown at room temperature
15 by the hanging-drop, vapor-diffusion method. At beginning 9 kits were used for initial
16 crystal screening; they are INDEX, CrystalScreen, SALT, SALTRX, PEGRX, PEG/ION
17 from Hampton Company and PACT, JCSG+, CUBICPHASE1 from QIAGEN Company.
18 One microliter of LT3015 BRD4 (15 mg/mL) was mixed with 1 µL of reservoir solution.
19 After one week crystals could be found from one condition, PEG/ION 44 (0.2M ammonium
20 phosphate dibasic, 20%PEG3350). Crystals grew to a final size of 0.2 mm × 0.1 mm × 0.1
21 mm. Subsequently, BRD4 crystals were soaked into the well solution containing 5mM
22 inhibitor and growing condition for overnight. Nylon loops was used to harvest the soaked
23 brd4 crystals and then immersed the crystals in mother liquor supplemented with 15%
24 glycerol for 1 min. Synchrotron data were collected on ADSC Q315 CCD detectors at the
25 Shanghai Synchrotron Radiation Facility. HKL2000 was used to do the data processing.
26 PHASER program was used to do the Molecular replacement a probe BRD4 (PDB ID:
27 4QB3). Rigid-body refinement by maximum likelihood was run in REFMAC5. The resulting
28 model was manually rebuilt in the program COOT program before further refinement in
29 PHENIX program. BRD4 structure was analyzed by PYMOL program.

30
31
32 **Cell culture and reagents.** The non-tumorigenic epithelial cell line MCF10A, as well as
33 human breast cancer cell lines MCF-7 and MDA-MB-231 were purchased from American
34 Type Culture Collection (ATCC, Manassas, VA, USA). They were routinely cultured in
35 DMEM medium containing 10% fetal bovine serum, 100 U/ml streptomycin, 100 U/ml
36
37
38
39
40
41
42
43
44
45
46
47
48
49
50
51
52
53
54
55
56
57
58
59
60

1
2
3 penicillin, and 2 mM L-glutamine in a humidified cell incubator with an atmosphere of 5%
4 CO₂ at 37 °C. MTT (M2128), 3-MA (M9281), DAPI (D9542) and MDC (30432) were
5 purchased from Sigma-Aldrich (St. Louis, MO, USA). Bafilomycin A1 (ab120497) was
6 purchased from Abcam (Cambridge, UK). **1** (S7110) and **2a** (S7295) were purchased from
7 Selleck (Shanghai, China). Antibodies used in this study were as follow: BRD4 (13440,
8 CST, MA, USA), c-Myc (13987, CST; ab56, Abcam), AMPK α (5832, CST), p53 (2524,
9 CST), p-AMPK α ^{thr172} (2535, CST), LC3B (3868, CST), p62 (8025, CST), Akt (4691, CST),
10 p-Akt^{ser473} (4060, CST), p-Akt^{thr308} (2965, CST), mTOR (2983, CST), p-mTOR^{ser2448} (12436,
11 CST), ULK1 (8054, CST), p-ULK1^{ser317} (12753, CST), mATG13 (13273, CST),
12 p-mATG13^{ser318} (PAB19948, Abnova, Taiwan), FIP200 (12436, CST), ATG5 (12994, CST),
13 VDAC1 (4866, CST), VDAC2 (9412, CST), HMGB1 (6893, CST), p-eEF2^{thr56} (2331, CST),
14 eEF2 (2332, CST), Ki-67 (9027, CST), caspase3 (9665, CST), β -actin (66009-1-Ig,
15 Proteintech, IL, USA)

16
17
18 **AlphaScreen assay.** Assays were performed as previously described.⁵⁴ All reagents
19 were diluted in 50 mM HEPES, 100 mM NaCl, 0.1% BSA, pH 7.4 supplemented with 0.05%
20 CHAPS and allowed to equilibrate to room temperature prior to addition to plates. The
21 ligands was prepared over the range of 100-0 μ M as 1:3 serial dilution, and 4 μ L was
22 transferred to low-volume 384-well plates (ProxiPlateTM-384 Plus, PerkinElmer) followed
23 by 4 μ L of HIS-tagged protein (recombinant human BRD4(1), 250 nM). The plates were
24 sealed and incubated at room temperature for 30 min before the addition of 4 μ L of
25 biotinylated histone peptide H4 (the peptide sequence:
26 H-SGRGK(Ac)GGK(Ac)GLGK-(Ac)GGAK(Ac)RHRK(Biotin)-OH; synthesized by GL
27 Biochem, Shanghai, China). at an equimolar concentration to the protein The plates were
28 sealed and incubated for a further 30 min before the addition of 4 μ L of streptavidin-coated
29 donor beads (25 μ g/ mL) and 4 μ L of nickel chelate acceptor beads (25 μ g/mL) under
30 lowlight conditions. The plates were foil sealed to protect from light, incubated at room
31 temperature for 60 min, and read on a PHERAstar FS plate reader (BMG Labtech) using
32 an AlphaScreen 680 excitation/570 emission filter set. IC₅₀ was calculated in Prism 6.0
33 (GraphPad Software) after normalization against corresponding DMSO controls, and they
34
35
36
37
38
39
40
41
42
43
44
45
46
47
48
49
50
51
52
53
54
55
56
57
58
59
60

1
2
3 are given as the final concentration of compound in the 20 μ L reaction volume.

4 **TR-FRET bromodomain binding assay.** The BET affinity assay was performed by using
5 BRD4 (BD1) and (BD2) Inhibitor Screening Assay Kit (#32514 and #32524) purchased
6 from BPS Bioscience Inc (San Diego, CA, USA). The recombinant BRD2-BD1 (#31021),
7 BRD2-BD2 (#31023), BRD3-BD1 (#31032), BRD3-BD2 (#31033), BRDT-BD1 (#31108)
8 and BET Bromodomain Ligand (#33000) were all purchased from BPS Bioscience Inc.
9 The assay was performed by TR-FRET technology using a recombinant BRD and its
10 corresponding ligand (BET). The TR-FRET signal from the assay is correlated with the
11 amount of ligand binding to the bromodomain. The compounds final concentration of
12 DMSO is 1 % in all reactions. All of the binding reactions were conducted at room
13 temperature. The 20 μ L reaction mixture in Assay Buffer contains either bromodomains,
14 BET Ligand and the indicated amount of inhibitor. For the negative control (blank), 5 μ L of
15 the assay buffer was added instead of the BET ligand. The reaction mixture incubated for
16 120 min. After the incubation with the ligand, TR-FRET signal was measured using Tecan
17 Infinite M1000 plate reader.
18
19
20
21
22
23
24
25
26
27
28
29
30

31 **ADP-Glo™ Kinase Assay.** Kinase activity assay was performed using ADP-Glo™
32 Kinase Assay + AMPK or ULK1 Kinase Enzyme System (Promega, Madison, WI, USA) as
33 previously described.²⁶ ADP-Glo™ Kinase Assay is a luminescent kinase assay that
34 measures ADP formed from a kinase reaction; ADP is converted into ATP, which is
35 converted into light by Ultra-Glo™ Luciferase. The luminescent signal positively correlates
36 with kinase activity. The AMPK or ULK1 kinase enzyme, substrate, ATP and compound
37 were diluted in Kinase Buffer (40 mM Tris pH 7.5; 20 mM MgCl₂; 0.1 mg/ml BSA; 50 μ M
38 DTT). Then 1 μ L of compound or (5% DMSO), 2 μ L of ULK1 kinase enzyme (10 ng), 2 μ L of
39 MBP (0.1 μ g/ μ L)/ATP (10 μ M) mix were added to the wells of 384 low volume plate. After
40 incubation at room temperature for 60 minutes, 5 μ L of ADP-Glo™ Reagent was added to
41 per well. The plates were incubated at room temperature for 40 minutes, then 10 μ L of
42 Kinase Detection Reagent were added. After incubation at room temperature for 30
43 minutes, the luminescence were recorded.
44
45
46
47
48
49
50
51
52
53
54

55 **Cell viability assay.** Cell viability assay was performed following previous report with
56
57
58
59
60

1
2
3 minor modifications.⁵⁵ The MCF-7 and MDA-MB-231 cells were dispensed in 96-well flat
4 bottom micro-titer plates at a density of 5×10^4 cells/ml. After 24 h incubation, cells were
5 treated with different concentrations of compounds for the indicated time periods. Cell
6 viability was measured by the 3-(4,5-dimethylthiazol-2-yl)-2,5-diphenyltetrazolium bromide
7 (MTT) assay. 5 mg/ml MTT was added to each well. After 4 h incubation, the medium was
8 removed and 150 μ l of DMSO was added to each well to dissolve the crystal formazan dye.
9 Absorbance was measured at 570 nm on an enzyme-linked immunosorbent assay reader.

10
11
12
13
14
15
16 **Autophagy activity screening.** MCF-7 cells were treated with or without 5 μ M
17 compounds for 6 h, then cultured with 0.05 mM MDC at 37 °C for 30 min. The
18 fluorescence intensity of cells was analyzed by flow cytometry (Becton Dickinson, Franklin
19 Lakes, NJ).

20
21
22
23
24 **Co-immunoprecipitation.** Cells were lysed with RIPA buffer (40 mM Tris-HCl, pH 7.5,
25 150 mM NaCl, 0.5% NP-40, protease inhibitors protease inhibitor cocktail, 5% glycerol, 10
26 mM NaF). Whole cell lysates obtained by centrifugation were incubated with different
27 antibodies and Sepharose protein A/protein G beads (Rockland, PAG50-00-0002)
28 overnight at 4°C. The immune-complexes were then washed 3 times with RIPA buffer and
29 separated by 10% SDS-PAGE for western blot analysis.

30
31
32
33
34
35 **Autophagy assay.** The ultrastructure of cell was observed under an electron microscope
36 (Hitachi 7000, Japan). For GFP-LC3 transfection and MDC staining, cells were
37 transfected with eGFP-LC3 plasmid or stained with MDC (0.05 mM) and observed under a
38 fluorescence microscopy.

39
40
41
42
43 **Immunofluorescence analysis.** For immunofluorescence staining, nonspecific antibody
44 binding was blocked by incubating with PBS containing 1.5% goat serum. MCF-7 or
45 MDA-MB-231 cells were sequentially incubated, starting with LC3B antibody (1:200)
46 diluted in PBS containing 1% BSA incubated overnight at 4°C, followed by addition of
47 fluorescent-labeled secondary antibodies (FITC, ab6717) for 1 h at room temperature.

48
49
50
51
52 **Western blot analysis.** The MCF-7 and MDA-MB-231 cells were treated with compounds
53 for indicated times. Both adherent and floating cells were collected, and then western blot
54 analysis was carried out by the method as follow. The cell pellets were resuspended with
55
56
57
58
59
60

1
2
3 RIPA lysis buffer consisting of 1 mM PMSF and lysed at 4°C for 1 h. After 12,000 rpm
4 centrifugation for 15 min, the protein content of supernatant was determined by the
5 Bio-Rad DC protein assay (Bio-Rad Laboratories, Hercules, CA, USA). Equal amounts of
6 the total protein were separated by 10-15% SDS-PAGE and transferred to PVDF
7 membranes, the membranes were soaked in blocking buffer (5% skimmed milk or BSA).
8 Proteins were detected using primary antibodies, followed by HRP-conjugated secondary
9 antibody and visualized by using ECL as the HRP substrate.

10
11
12 **SiRNA transfection.** MCF-7 or MDA-MB-231 cells were transfected with BRD4#1
13 (s23901, Invitrogen), BRD4#2 (s23902, Invitrogen), ATG5 (6345, CST), negative control
14 (4390843, Invitrogen) siRNAs at 50nM final concentration using Lipofectamine RNAiMAX
15 reagent (Invitrogen) according to the manufacturer's instructions. The transfected cells
16 were used for subsequent experiments 48 h later.

17
18 **iTRAQ-based proteomics analyses.** Two separate iTRAQ-based proteomics analysis
19 were performed in MCF-7 and MDA-MB-231 cells. Briefly, cells were dissolved in lysis
20 buffer and labeled with iTRAQ labeling reagents. After 2D LC analysis and tandem mass
21 spectrometry analysis, protein identification and relative iTRAQ quantification were
22 performed with ProteinPilot™ Software 4.2 (AB SCIEX) using the Paragon™ algorithm for
23 the peptide identification. Results with iTRAQ ratio cutoff values of 1.2 and 0.8 for
24 fold-change and number cutoff values of 3 for quantifiable peptides for in protein
25 abundance were accepted.

26
27 **Xenograft breast cancer models.** All experiments protocols used in this study were
28 carried out in accordance with guidelines of the animal ethics committee (Sichuan
29 University). 52 female nude mice (BALB/c, 6-8 weeks, 20-22 g) were injected
30 subcutaneously with MCF-7 cells or MDA-MB-231 cells (5×10^6 cells/mouse), respectively.
31 When the tumors reached 100 mm^3 in volume ($V = L \times W^2/2$), the mice were divided into
32 four groups for each cell line. Three groups were treated with different doses of **9f** (low
33 dose, 25 mg/kg; median dose, 50 mg/kg; high dose, 100 mg/kg) once a day by intragastric
34 administration for 24 or 27 days, whereas the control group was treated with vehicle
35 control. During the treatment, the tumor volumes and body weight were measured every 3
36
37
38
39
40
41
42
43
44
45
46
47
48
49
50
51
52
53
54
55
56
57
58
59
60

1
2
3 day until the end of the study. At the end of treatment, all mice were sacrificed. The tumor
4 tissues were harvested, weighed, and photographed. Then, the tumor tissues were frozen
5 in liquid nitrogen or fixed in formalin immediately.
6
7

8 **Immunohistochemistry analysis (IHC).** Sections of the tumor were submerged into
9 EDTA antigenic retrieval buffer (pH 8.0) or citrate buffer (pH 6.0), and microwaved for
10 antigenic retrieval. Then the slides were incubated with rabbit anti-BRD4 polyclonal
11 antibody (1:400), or with anti-LC3 antibody (1:400), for 30-40 min at 37°C. Normal
12 rabbit/mouse IgG was used as a negative control. The slides were then treated by HRP
13 polymer conjugated secondary antibody for 30 min and developed with diamino-benzidine
14 solution. Meyer's hematoxylin was used as a counterstain.
15
16
17
18
19
20

21 **Zebrafish tumor xenograft assay.** Adult zebrafish (WT) were fed and kept together at
22 28.5°C with a light/dark cycle of 14/10 h following The Zebrafish Book recommendations.
23 Embryos were obtained as massive spawning and maintained in sterile dechlorinated tap
24 water (SDTW). The zebrafish xenograft model was established as previously described.⁵⁶
25 CM-Dil-labeled MCF-7 cells were transplanted into 48 hours postfertilization (hpf)
26 zebrafish embryos through perivitelline space (30 embryos each group). After
27 manipulation, zebrafish were maintained in 96 well-plates at 35°C for 1 day to favor tumor
28 cell proliferation and embryo recovering. Then, different doses of **9f** were added into
29 SDTW. On Experiments were carried out using a total number of 62 negative controls
30 (non-injected) and 71 microinjected non-treated embryos, both maintained in SDTW. On
31 the 5th day post-implantation, 10 zebrafish were randomly selected and photographed
32 using a fluorescence microscope. The fluorescence intensity was evaluated by
33 NIS-Elements D 3.10.
34
35
36
37
38
39
40
41
42
43
44
45

46 **Statistical analysis.** All cell experiments were performed independently by at least three
47 times. The data are expressed as means \pm S.E.M. and analyzed with GraphPad Prism 6.0.
48 Statistical comparisons were made by One-way ANOVA and Student's t-test. $p < 0.05$ was
49 considered statistically significant.
50
51
52
53
54
55

56 ASSOCIATED CONTENT

57
58
59
60

Supporting Information Available: candidate compound structures obtained from *in silico* virtual screening, co-immunoprecipitation assay of AMPK and c-Myc, cell viability of **9f** on normal breast cells, MD simulation results of **9f** with BRD2(1), BRD3(1), BRD4(1) and BRDT(1), autophagy associated kinase assays of **9f**, crystallization data and refinement statistics, iTRAQ datasets, original data of co-immunoprecipitation and western blot, NMR data of all compounds.

AUTHOR INFORMATION

Corresponding Authors

*B.L. E-mail: liubo2400@163.com. Phone: (+86)28-85164063.

*G.H. E-mail: hegu@scu.edu.cn. Phone: (+86)28-85503817.

Author Contributions

#These authors contributed equally.

Notes

The authors declare no competing financial interest.

ACKNOWLEDGMENTS

We are grateful to Prof. Shengyong Yang and Prof. Canhua Huang for their critical reviews on this paper. This work was supported by grants from National Key R&D Program of China (Grant No. 2017YFC0909301 and Grant No. 2017YFC0909302) and National Natural Science Foundation of China (Grant No. U1603123, Grant No. 81673455, Grant No. 81602953 and Grant No. 81402496).

ABBREVIATIONS USED

BRD4, Bromodomain-containing protein 4; BRD4(1), BRD4 domain 1 ; BET, bromodomain and extra-terminal; AMPK, AMP-activated protein kinase; ACD, autophagy-associated cell death; *Atgs*, autophagy-related genes; ULK1, UNC-51-like kinase 1; mTOR, mammalian target of rapamycin; PPI, protein-protein interactions; TCGA,

1
2
3 The Cancer Genome Atlas; GO, Gene Ontology; TR-FRET, time-resolved fluorescence
4 resonance energy transfer; MDC, Monodansylcadaverine; BafA1, Bafilomycin A1; 3-MA,
5 3-methyladenine.
6
7
8
9

10 REFERENCES

- 11
12 (1) Belkina, A. C.; Denis, G. V. BET domain co-regulators in obesity, inflammation and
13 cancer. *Nat. Rev. Cancer* **2012**, *12*, 465-477.
14
15 (2) Prinjha, R. K.; Witherington, J.; Lee, K. Place your BETs: the therapeutic potential of
16 bromodomains. *Trends Pharmacol. Sci.* **2012**, *33*, 146-153.
17
18 (3) Filippakopoulos, P.; Picaud, S.; Mangos, M. Histone recognition and large-scale
19 structural analysis of the human bromodomain family. *Cell* **2012**, *149*, 214-231.
20
21 (4) Lolli, G.; Battistutta, R. Different orientations of low-molecular-weight fragments in the
22 binding pocket of a BRD4 bromodomain. *Acta Crystallogr., Sect. D: Biol. Crystallogr.* **2013**,
23 *69*, 2161-2164.
24
25 (5) Devaiah, B. N.; Singer, D. S. Two faces of brd4: mitotic bookmark and transcriptional
26 lynchpin. *Transcription* **2013**, *4*, 13-17.
27
28 (6) Vollmuth, F.; Blankenfeldt, W.; Geyer, M. Structures of the dual bromodomains of the
29 P-TEFb-activating protein Brd4at atomic resolution. *J. Biol. Chem.* **2009**, *284*,
30 36547-36556.
31
32 (7) Shi, J.; Vakoc, C. R. The mechanisms behind the therapeutic activity of BET
33 bromodomain inhibition. *Mol. Cell.* **2014**, *54*, 728-736.
34
35 (8) Filippakopoulos, P.; Knapp, S. Targeting bromodomains: epigenetic readers of lysine
36 acetylation. *Nat. Rev. Drug Discovery* **2014**, *13*, 337-356.
37
38 (9) Liu, Z.; Wang, P.; Chen, H.; Wold, E. A.; Tian, B.; Brasier, A. R.; Zhou, J. Drug
39 discovery targeting bromodomain-containing protein 4 (BRD4). *J. Med. Chem.* **2017**, *60*,
40 4533-4558.
41
42 (10) Barbieri, I.; Cannizzaro, E.; Dawson, M. A. Bromodomains as therapeutic targets in
43 cancer. *Briefings Funct. Genomics* **2013**, *12*, 219-230.
44
45
46
47
48
49
50
51
52
53
54
55
56
57
58
59
60

- 1
2
3 (11) Farina, A.; Hattori, M.; Qin, J.; Nakatani, Y.; Minato, N.; Ozato, K. Bromodomain
4 protein Brd4 binds to GTPase-activating SPA-1, modulating its activity and subcellular
5 localization. *Mol. Cell Biol.* **2004**, *24*, 9059-9069.
6
7
8 (12) Nagarajan, S.; Hossan, T.; Alawi, M.; Najafova, Z.; Indenbirken, D.; Bedi, U.;
9 Taipaleenmäki, H.; Ben-Batalla, I.; Scheller, M.; Loges, S.; Knapp, S.; Hesse, E.; Chiang,
10 C. M.; Grundhoff, A.; Johnsen, S. A. Bromodomain protein BRD4 is required for estrogen
11 receptor-dependent enhancer activation and gene transcription. *Cell Rep.* **2014**, *8*,
12 460-469.
13
14 (13) Crawford, N. P.; Alsarraj, J.; Lukes, L.; Walker, R. C.; Officewala, J. S.; Yang, H. H.;
15 Lee, M. P.; Ozato, K.; Hunter, K. W. Bromodomain 4 activation predicts breast cancer
16 survival. *Proc. Natl. Acad. Sci. U. S. A.* **2008**, *105*, 6380-6385.
17
18 (14) Yang, Z.; Klionsky, D. J. Eaten alive: a history of macroautophagy. *Nat. Cell Biol.* **2010**,
19 *12*, 814-822.
20
21 (15) Mizushima, N.; Yoshimori, T.; Ohsumi, Y. The role of Atg proteins in autophagosome
22 formation. *Annu. Rev. Cell. Dev. Biol.* **2011**, *27*, 107-132.
23
24 (16) Chan, E. Y. Regulation and function of uncoordinated-51 like kinase proteins.
25 *Antioxid. Redox Signaling* **2012**, *17*, 775-785.
26
27 (17) Mizushima, N. The role of the Atg1/ULK1 complex in autophagy regulation. *Curr.*
28 *Opin. Cell Biol.* **2010**, *22*, 132-139.
29
30 (18) Kim, J.; Kundu, M.; Viollet, B.; Guan, K. L. AMPK and mTOR regulate autophagy
31 through direct phosphorylation of Ulk1. *Nat. Cell Biol.* **2011**, *13*, 132-141.
32
33 (19) Alers, S.; Löffler, A. S.; Wesselborg, S.; Stork, B. Role of AMPK-mTOR-Ulk1/2 in the
34 regulation of autophagy: cross talk, shortcuts, and feedbacks. *Mol. Cell Biol.* **2012**, *32*,
35 2-11.
36
37 (20) Kim, D. E.; Kim, Y.; Cho, D. H.; Jeong, S. Y.; Kim, S. B.; Suh, N.; Lee, J. S.; Choi, E.
38 K.; Koh, J. Y.; Hwang, J. J.; Kim, C. S. Raloxifene induces autophagy-dependent cell
39 death in breast cancer cells via the activation of AMP-activated protein kinase. *Mol. Cells*
40 **2015**, *38*, 138-144.
41
42 (21) Liu, B.; Wen, X.; Cheng, Y. Survival or death: disequilibrating the oncogenic and
43
44
45
46
47
48
49
50
51
52
53
54
55
56
57
58
59
60

- 1
2
3 tumor suppressive autophagy in cancer. *Cell Death Dis.* **2013**, *4*, e892.
- 4
5 (22) Ke, B.; Tian, M.; Li, J.; Liu, B.; He, G. Targeting programmed cell death using
6
7 small-molecule compounds to improve potential cancer therapy. *Med. Res. Rev.* **2016**, *36*,
8
9 983-1035.
- 10
11 (23) Filippakopoulos, P.; Qi, J.; Picaud, S.; Shen, Y.; Smith, W. B.; Fedorov, O.; Morse, E.
12
13 M.; Keates, T.; Hickman, T. T.; Felletar, I.; Philpott, M.; Munro, S.; McKeown, M. R.; Wang,
14
15 Y.; Christie, A. L.; West, N.; Cameron, M. J.; Schwartz, B.; Heightman, T. D.; La Thangue,
16
17 N.; French, C. A.; Wiest, O.; Kung, A. L.; Knapp, S.; Bradner, J. E. Selective inhibition of
18
19 BET bromodomains. *Nature* **2010**, *468*, 1067-1073.
- 20
21 (24) Jang, J. E.; Eom, J. I.; Jeung, H. K.; Cheong, J. W.; Lee, J. Y.; Kim, J. S.; Min, Y. H.
22
23 AMPK-ULK1-mediated autophagy confers resistance to BET inhibitor JQ1 in acute
24
25 myeloid leukemia stem cells. *Clin. Cancer Res.* **2017**, *23*, 2781-2794.
- 26
27 (25) Huang, M.; Garcia, J. S.; Thomas, D.; Zhu, L.; Nguyen, L. X.; Chan, S. M.; Majeti, R.;
28
29 Medeiros, B. C.; Mitchell, B. S. Autophagy mediates proteolysis of NPM1 and HEXIM1
30
31 and sensitivity to BET inhibition in AML cells. *Oncotarget* **2016**, *7*, 74917-74930.
- 32
33 (26) Zhang, L.; Fu, L. L.; Zhang, S. Y.; Zhang, J.; Zhao, Y. Q.; Zheng, Y. X.; He, G.; Yang,
34
35 S. Y.; Ouyang, L.; Liu, B. Discovery of a small molecule targeting ULK1-modulated cell
36
37 death of triple negative breast cancer *in vitro* and *in vivo*. *Chem. Sci.* **2017**, *8*, 2687-2701.
- 38
39 (27) Tang, H.; Sebti, S.; Titone, R.; Zhou, Y.; Isidoro, C.; Ross, T. S.; Hibshoosh, H.; Xiao,
40
41 G.; Packer, M.; Xie, Y.; Levine, B. Decreased BECN1 mRNA expression in human breast
42
43 cancer is associated with estrogen receptor-negative subtypes and poor prognosis.
44
45 *EBioMedicine* **2015**, *2*, 255-263.
- 46
47 (28) Stratikopoulos, E. E.; Dendy, M.; Szabolcs, M.; Khaykin, A. J.; Lefebvre, C.; Zhou, M.
48
49 M.; Parsons, R. Kinase and BET inhibitors together clamp inhibition of PI3K signaling and
50
51 overcome resistance to therapy. *Cancer Cell* **2015**, *27*, 837-851.
- 52
53 (29) Sakamaki, J. I.; Wilkinson, S.; Hahn, M.; Tasdemir, N.; O'Prey, J.; Clark, W.; Hedley,
54
55 A.; Nixon, C.; Long, J. S.; New, M.; Van Acker, T.; Tooze, S. A.; Lowe, S. W.; Dikic, I.; Ryan,
56
57 K. M. Bromodomain protein BRD4 is a transcriptional repressor of autophagy and
58
59 lysosomal function. *Mol. Cell* **2017**, *66*, 517-532.
- 60

- 1
2
3 (30) Picaud, S.; Wells, C.; Felletar, I.; Brotherton, D.; Martin, S.; Savitsky, P.; Diez-Dacal,
4 B.; Philpott, M.; Bountra, C.; Lingard, H.; Fedorov, O.; Müller, S.; Brennan, P. E.; Knapp, S.;
5 Filippakopoulos, P. RVX-208, an inhibitor of BET transcriptional regulators with selectivity
6 for the second bromodomain. *Proc. Natl. Acad. Sci. U. S. A.* **2013**, *110*, 19754-19759.
7
8 (31) Liu, B.; Zhang, S.; Guo, M.; Tian, M. PDB code: 4ZW1. DOI: 10.2210/pdb4zw1/pdb.
9
10 (32) Milhas, S.; Raux, B.; Betzi, S.; Derviaux, C.; Roche, P.; Restouin, A. Protein-protein
11 interaction inhibition (2p2i)-oriented chemical library accelerates hit discovery. *ACS Chem.*
12 *Biol.* **2016**, *11*, 2140-2148.
13
14 (33) Wu, S. Y.; Lee, A. Y.; Lai, H. T.; Zhang, H.; Chiang, C. M. Phospho switch triggers
15 Brd4 chromatin binding and activator recruitment for gene-specific targeting. *Mol. Cell*
16 **2013**, *49*, 843-857.
17
18 (34) Nieminen, A. I.; Eskelinen, V. M.; Haikala, H. M.; Tervonen, T. A.; Yan, Y.; Partanen, J.
19 I.; Klefström, J. Myc-induced AMPK-phospho p53 pathway activates Bak to sensitize
20 mitochondrial apoptosis. *Proc. Natl. Acad. Sci. U. S. A.* **2013**, *110*, E1839-E1848.
21
22 (35) Fu, L. L.; Tian, M.; Li, X.; Li, J. J.; Huang, J.; Ouyang, L.; Zhang, Y.; Liu, B. Inhibition
23 of BET bromodomains as a therapeutic strategy for cancer drug discovery. *Oncotarget*
24 **2015**, *6*, 5501-5516.
25
26 (36) Gilham, D.; Wasiak, S.; Tsujikawa, L. M.; Halliday, C.; Norek, K.; Patel, R. G.;
27 Kulikowski, E.; Johansson, J.; Sweeney, M.; Wong, N. C. RVX-208, a BET-inhibitor for
28 treating atherosclerotic cardiovascular disease, raises ApoA-I/HDL and represses
29 pathways that contribute to cardiovascular disease. *Atherosclerosis* **2016**, *247*, 48-57.
30
31 (37) Waring, M. J.; Chen, H.; Rabow, A. A.; Walker, G.; Bobby, R.; Boiko, S.; Bradbury, R.
32 H.; Callis, R.; Clark, E.; Dale, I.; Daniels, D. L.; Dulak, A.; Flavell, L.; Holdgate, G.; Jowitt, T.
33 A.; Kikhney, A.; McAlister, M.; Méndez, J.; Ogg, D.; Patel, J.; Petteruti, P.; Robb, G. R.;
34 Robers, M. B.; Saif, S.; Stratton, N.; Svergun, D. I.; Wang, W.; Whittaker, D.; Wilson, D. M.;
35 Yao, Y. Potent and selective bivalent inhibitors of BET bromodomains. *Nat. Chem. Biol.*
36 **2016**, *12*, 1097-1104.
37
38 (38) Fu, L. L.; Xie, T.; Zhang, S. Y.; Liu, B. Eukaryotic elongation factor-2 kinase (eEF2K):
39 a potential therapeutic target in cancer. *Apoptosis* **2014**, *19*, 1527-1531.
40
41
42
43
44
45
46
47
48
49
50
51
52
53
54
55
56
57
58
59
60

1
2
3 (39) Wang, X. Regufe da Mota S, Liu R, Moore CE, Xie J, Lanucara F, Agarwala U, Pyr Dit
4 Ruys S, Vertommen D, Rider MH, Eyers CE, Proud CG. Eukaryotic elongation factor 2
5 kinase activity is controlled by multiple inputs from oncogenic signaling. *Mol. Cell Biol.*
6 **2014**, *34*, 4088-4103.
7
8

9
10 (40) Cheng, Y.; Ren, X.; Zhang, Y.; Patel, R.; Sharma, A.; Wu, H.; Robertson, G. P.; Yan,
11 L.; Rubin, E.; Yang, J. M. eEF-2 kinase dictates cross-talk between autophagy and
12 apoptosis induced by Akt inhibition, thereby modulating cytotoxicity of novel Akt inhibitor
13 MK-2206. *Cancer Res.* **2011**, *71*, 2654-2663.
14
15

16 (41) Sun, Y.; Vashisht, A. A.; Tchieu, J.; Wohlschlegel, J. A.; Dreier, L. Voltage-dependent
17 anion channels (VDACs) recruit Parkin to defective mitochondria to promote mitochondrial
18 autophagy. *J. Biol. Chem.* **2012**, *287*, 40652-40660.
19
20

21 (42) Geisler, S.; Holmström, K. M.; Skujat, D.; Fiesel, F. C.; Rothfuss, O. C.; Kahle, P. J.;
22 Springer, W. PINK1/Parkin-mediated mitophagy is dependent on VDAC1 and
23 p62/SQSTM1. *Nat. Cell Biol.* **2010**, *12*, 119-131.
24
25

26 (43) Zhang, Q. C.; Petrey, D.; Garzón, J. I.; Deng, L.; Honig, B. PrePPI: a
27 structure-informed database of protein-protein interactions. *Nucleic Acids Res.* **2013**, *41*,
28 D828-D833.
29

30 (44) Shannon, P.; Markiel, A.; Ozier, O.; Baliga, N. S.; Wang, J. T.; Ramage, D.; Amin, N.;
31 Schwikowski, B.; Ideker, T. Cytoscape: a software environment for integrated models of
32 biomolecular interaction networks. *Genome Res.* **2003**, *13*, 2498-2504.
33
34

35 (45) Huang, D. W.; Sherman B. T.; Lempicki, R. A. Systematic and integrative analysis of
36 large gene lists using DAVID bioinformatics resources. *Nat. Protoc.* **2009**, *4*, 44-57.
37
38

39 (46) Huang, D. W.; Sherman B. T.; Lempicki, R. A. Bioinformatics enrichment tools: paths
40 toward the comprehensive functional analysis of large gene lists. *Nucleic Acids Res.* **2009**,
41 *37*, 1-13.
42
43

44 (47) Diller, D. J.; Merz, K. M. Jr. High throughput docking for library design and library
45 prioritization. *Proteins* **2001**, *43*, 113-124.
46
47

48 (48) Vanommeslaeghe, K.; Hatcher, E.; Acharya, C.; Kundu, S.; Zhong, S.; Shim, J.;
49 Darian, E.; Guvench, O.; Lopes, P.; Vorobyov, I.; Mackerell, A. D. CHARMM general force
50
51
52
53
54
55
56
57
58
59
60

1
2
3 field: A force field for drug-like molecules compatible with the CHARMM all-atom additive
4 biological force fields. *J. Comput. Chem.* **2010**, *31*, 671-690.

5
6 (49) Wu, G. S.; Robertson, D. H.; Brooks, C. R.; Vieth, M. Detailed analysis of grid-based
7 molecular docking: A case study of CDOCKER-A CHARMM-based MD docking algorithm.
8
9
10 *J. Comput. Chem.* **2003**, *24*, 1549-1562.

11
12 (50) Pronk, S.; Páll, S.; Schulz, R.; Larsson, P.; Bjelkmar, P.; Apostolov, R.; Shirts, M. R.;
13 Smith, J. C.; Kasson, P. M.; van der Spoel, D.; Hess, B.; Lindahl, E. GROMACS 4.5: a
14 high-throughput and highly parallel open source molecular simulation toolkit.
15
16
17 *Bioinformatics* **2013**, *29*, 845-854.

18
19 (51) Case, D. A.; Cheatham, T. E. 3rd.; Darden, T.; Gohlke, H.; Luo, R.; Merz, K. M. Jr.;
20 Onufriev, A.; Simmerling, C.; Wang, B.; Woods, R. J. The Amber biomolecular simulation
21 programs. *J. Comput. Chem.* **2005**, *26*, 1668-1688.

22
23 (52) Berendsen, H. J. C.; Postma, J. P. M.; Gunsteren, W. F. v.; DiNola, A.; Haak, J. R.
24
25
26
27
28
29
30 Molecular dynamics with coupling to an external bath. *J. Chem. Phys.* **1984**, *81*,
31 3684-3690.

32
33 (53) Kollman, P. A.; Massova, I.; Reyes, C.; Kuhn, B.; Huo, S.; Chong, L.; Lee, M.; Lee, T.;
34 Duan, Y.; Wang, W.; Donini, O.; Cieplak, P.; Srinivasan, J.; Case, D. A.; Cheatham, T. E.
35
36
37
38
39
40
41
42
43
44
45 3rd. Calculating structures and free energies of complex molecules: combining molecular
46 mechanics and continuum models. *Acc. Chem. Res.* **2000**, *33*, 889-897.

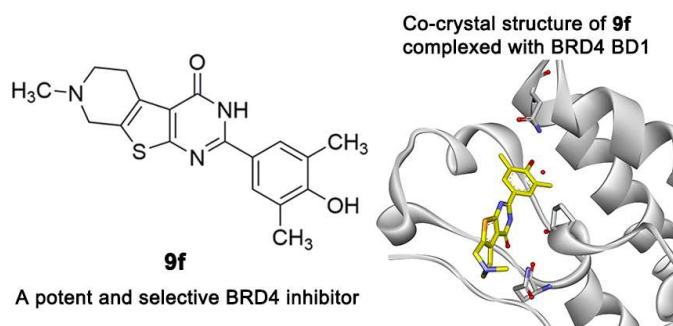
46
47 (54) Vidler, L. R.; Filippakopoulos, P.; Fedorov, O.; Picaud, S.; Martin, S.; Tomsett, M.;
48 Woodward, H.; Brown, N.; Knapp, S.; Hoelder, S. Discovery of novel small-molecule
49
50
51
52
53
54
55
56
57
58
59
60 inhibitors of BRD4 using structure-based virtual screening. *J. Med. Chem.* **2013**, *56*,
8073-8088.

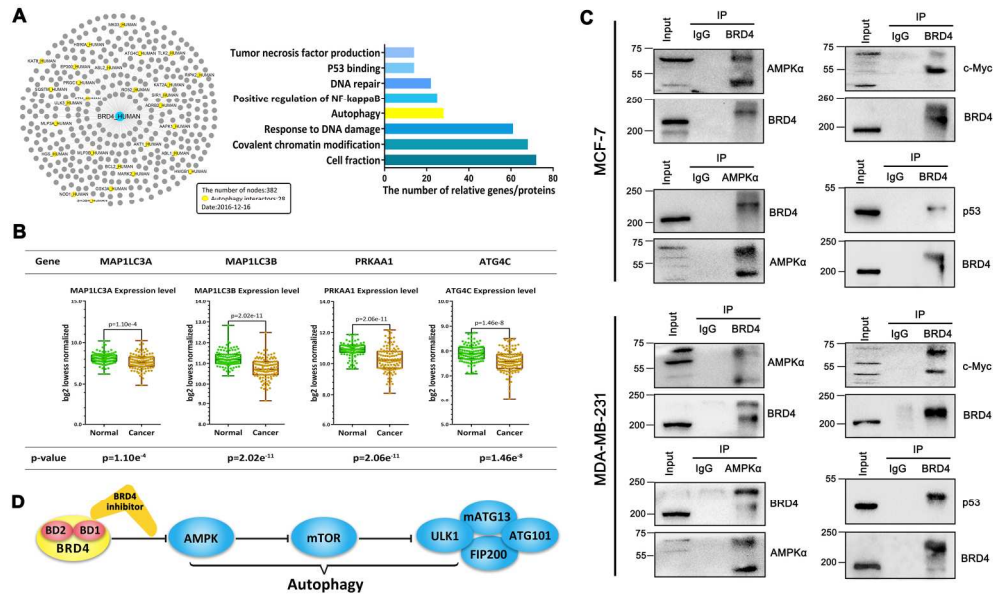
(55) Fu, L.; Zhang, S.; Zhang, L.; Tong, X.; Zhang, J.; Zhang, Y.; Ouyang, L.; Liu, B.;
Huang, J. Systems biology network-based discovery of a small molecule activator
BL-AD008 targeting AMPK/ZIPK and inducing apoptosis in cervical cancer. *Oncotarget*
2015, *6*, 8071-8088.

(56) Pan, Y.; Zheng, M.; Zhong, L.; Yang, J.; Zhou, S.; Qin, Y.; Xiang, R.; Chen, Y.; Yang, S.
Y. A preclinical evaluation of SKLB261, a multikinase inhibitor of EGFR/Src/VEGFR2, as a

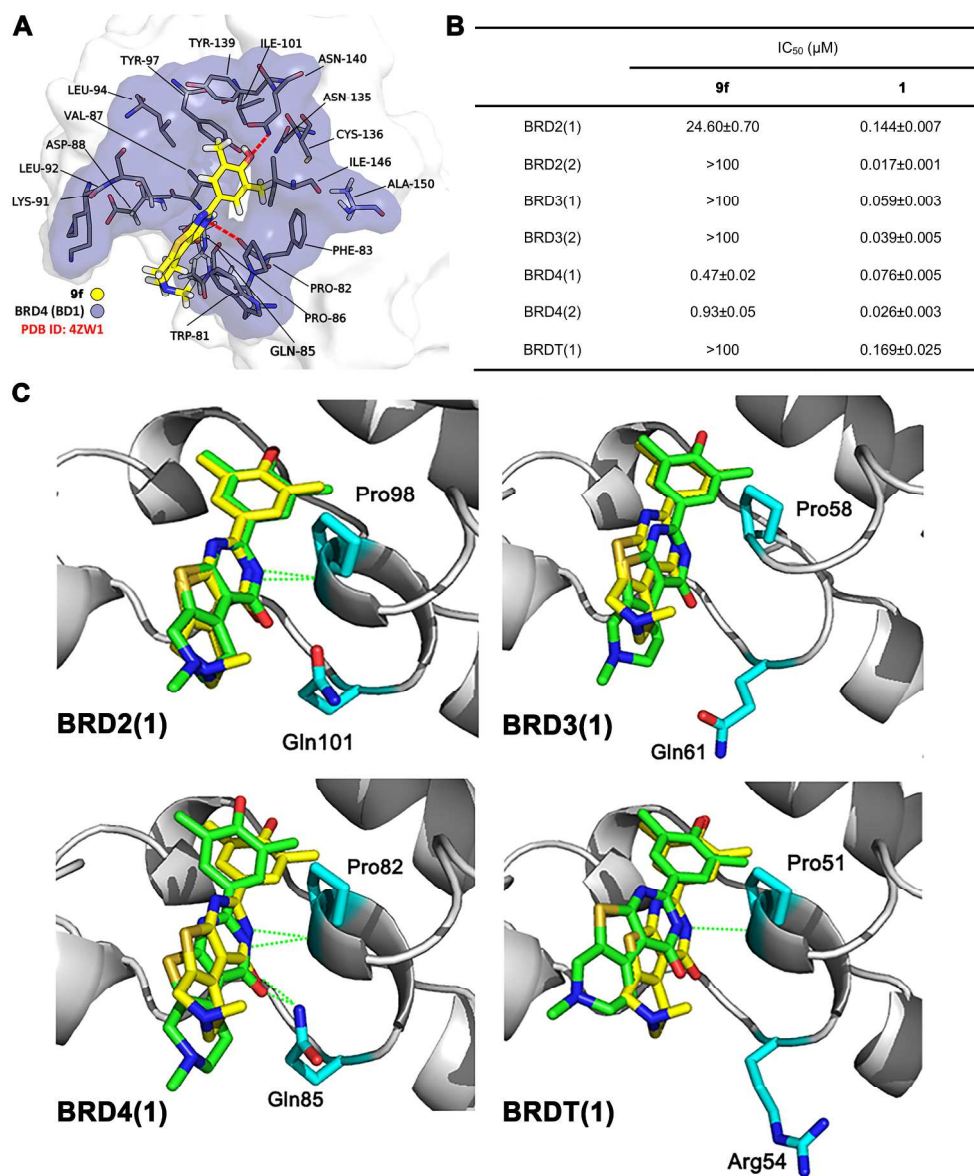
1
2
3 therapeutic agent against pancreatic cancer. *Mol. Cancer Ther.* **2015**, *14*, 407-418.
4
5
6
7
8
9

10
11 **Table of Contents graphic**
12

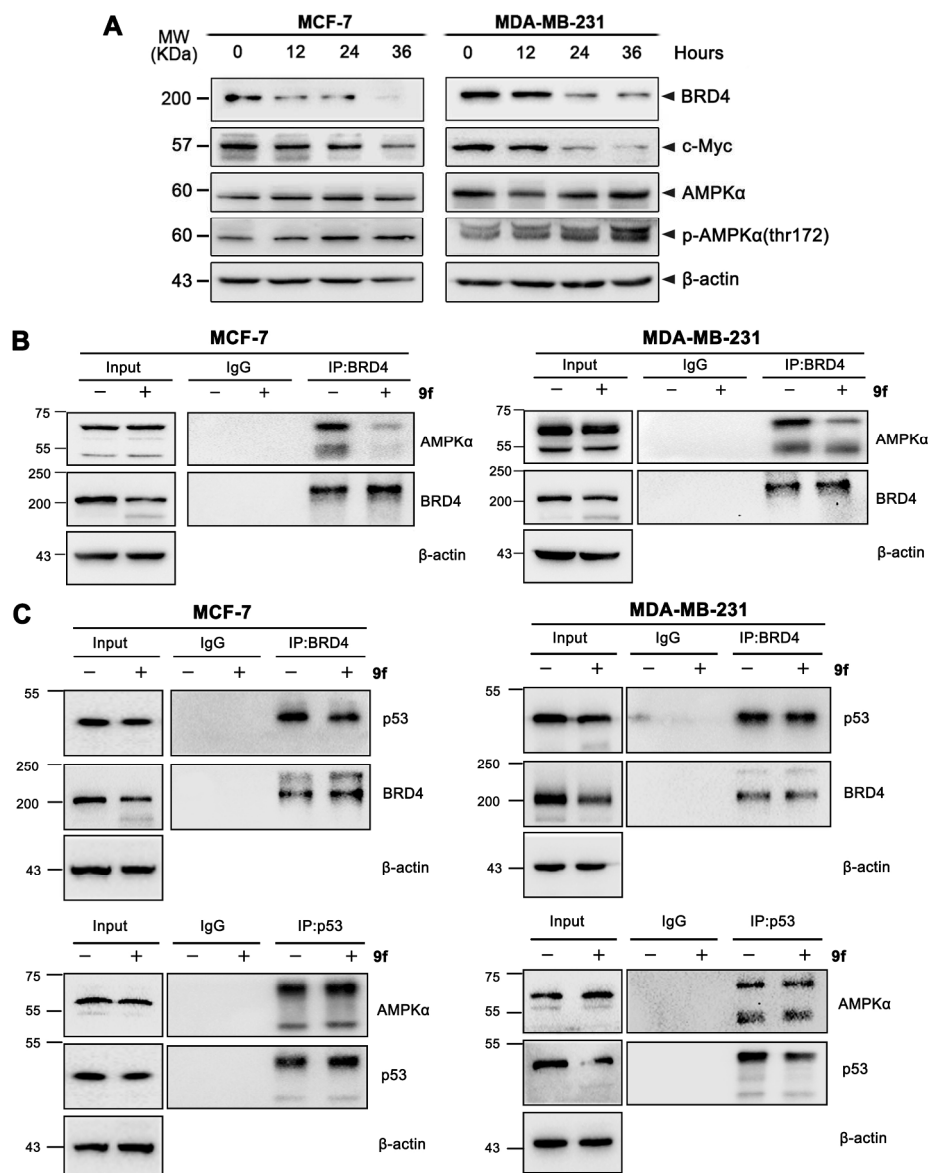




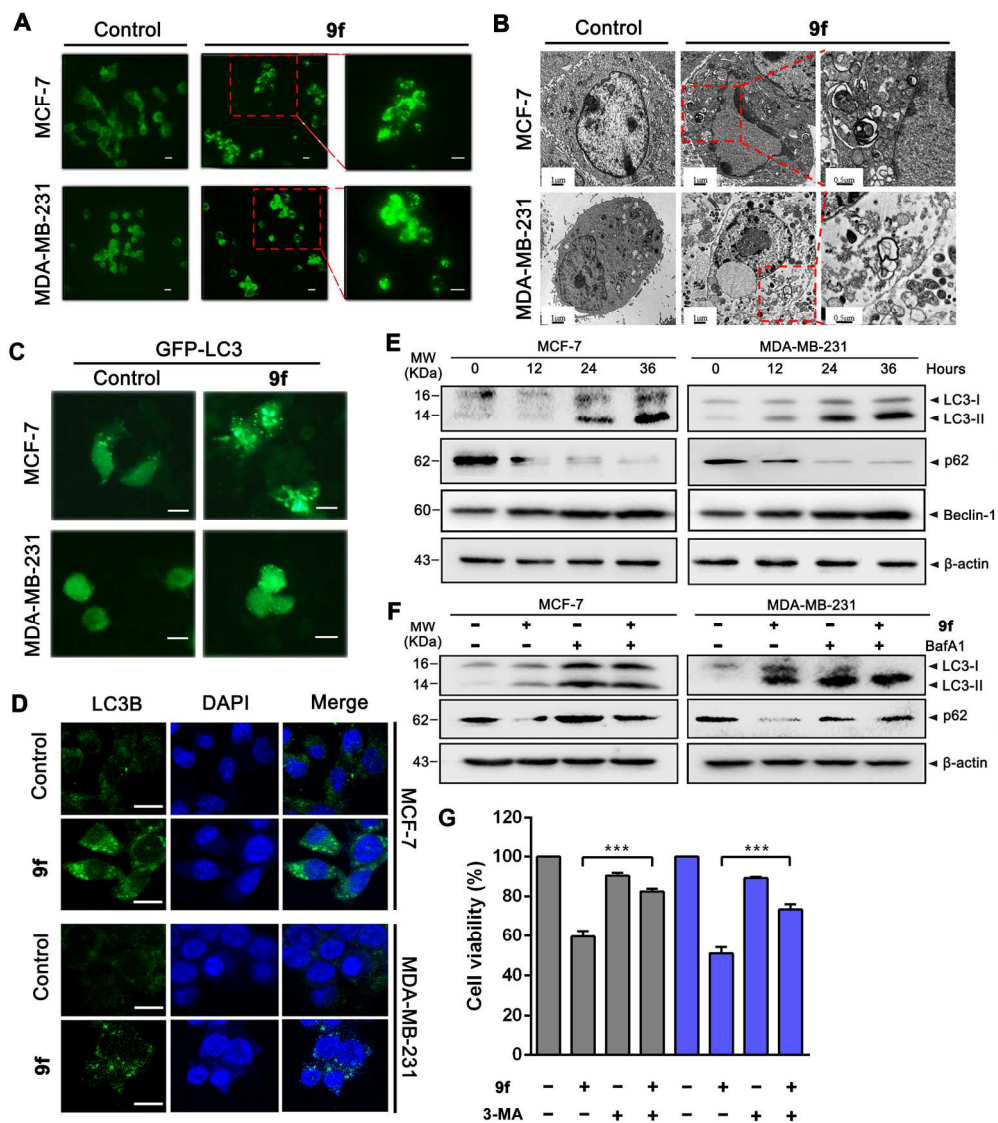
197x118mm (300 x 300 DPI)



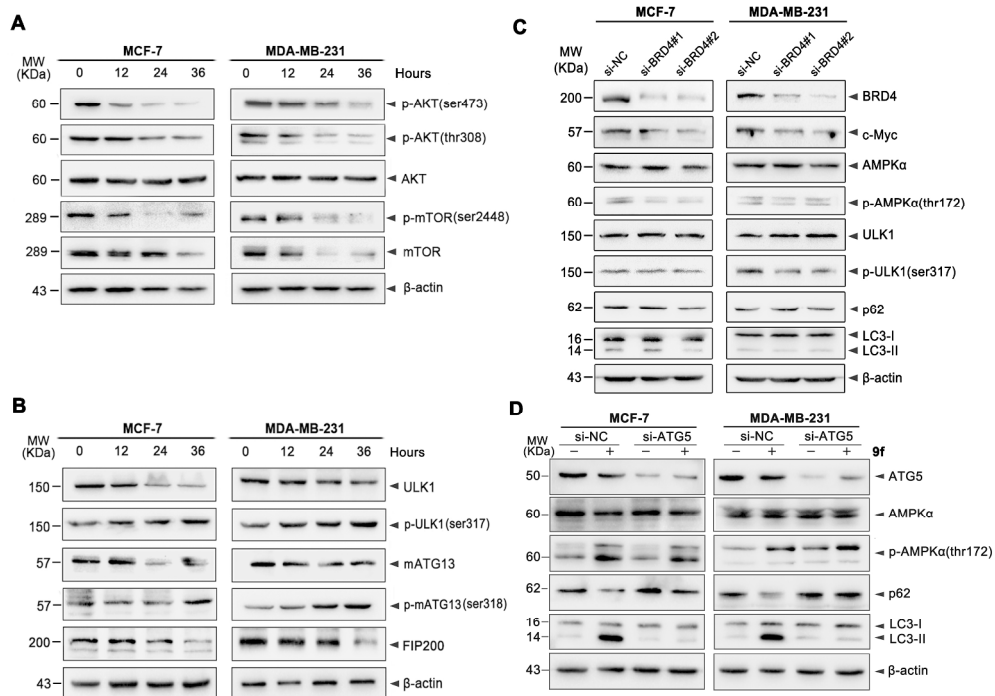
235x279mm (300 x 300 DPI)



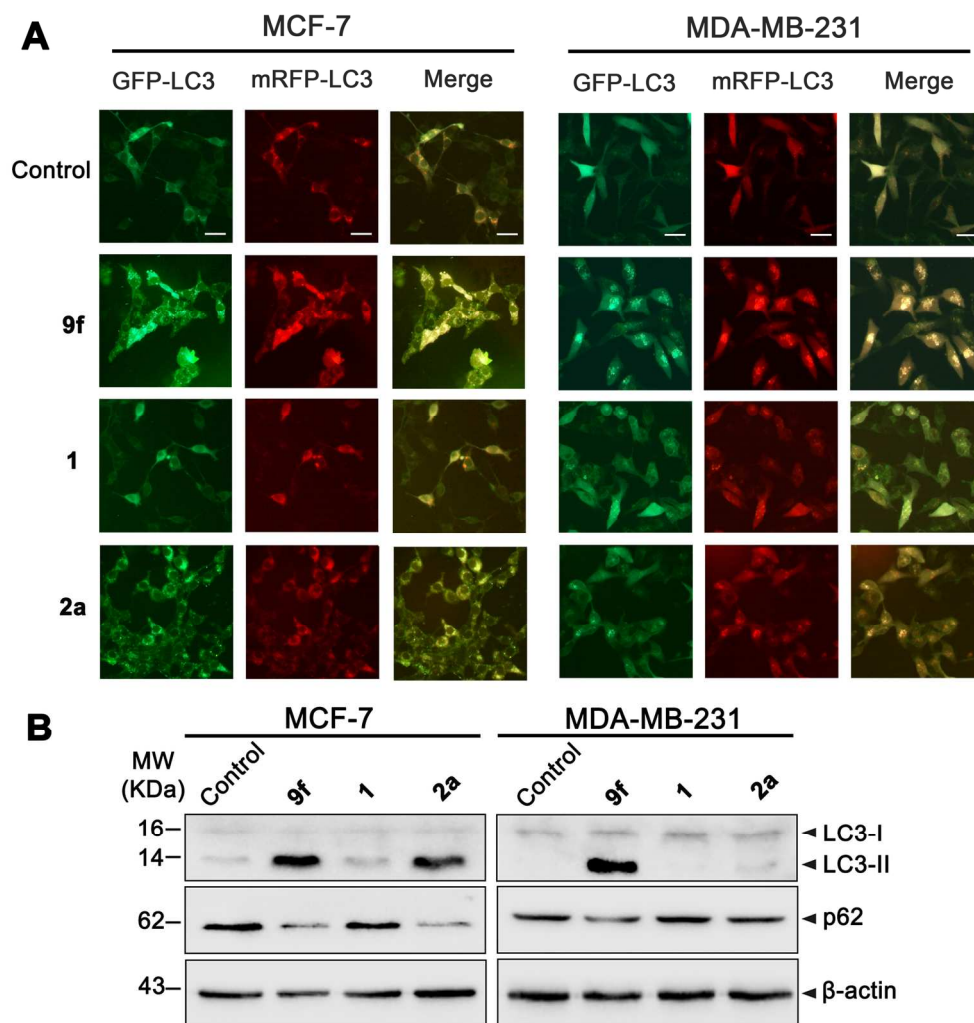
217x273mm (300 x 300 DPI)



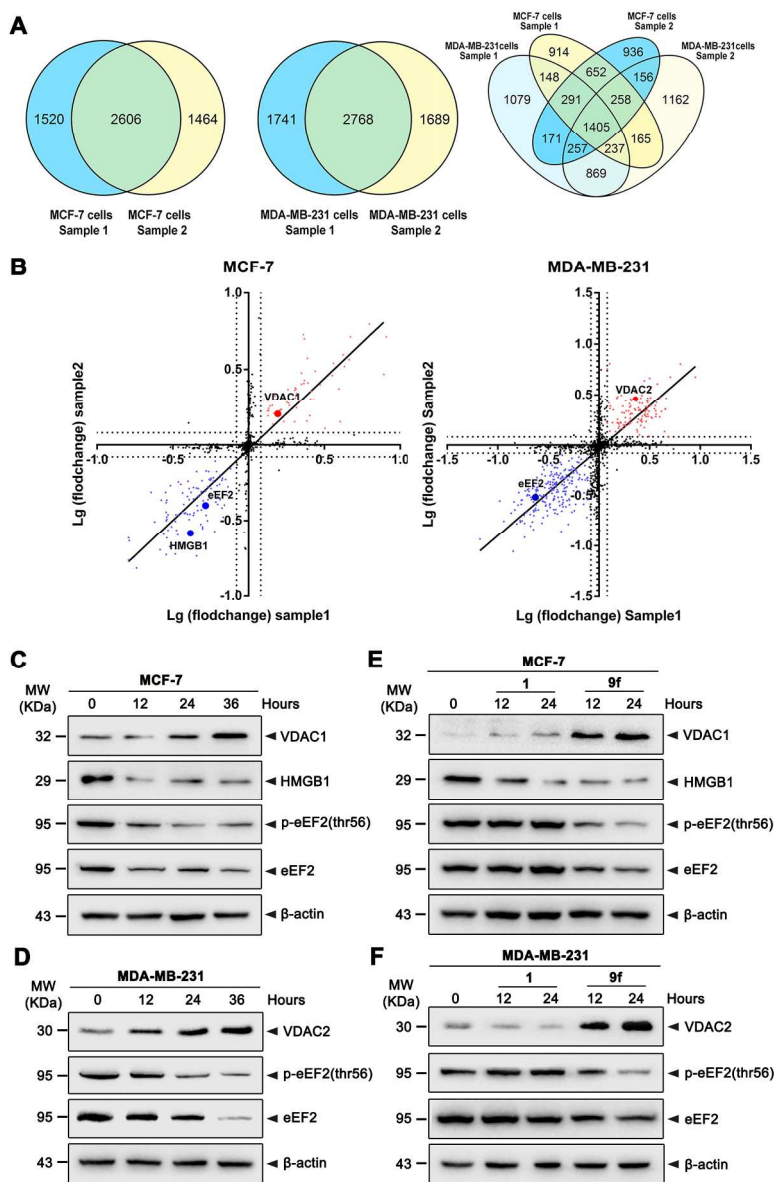
203x231mm (300 x 300 DPI)



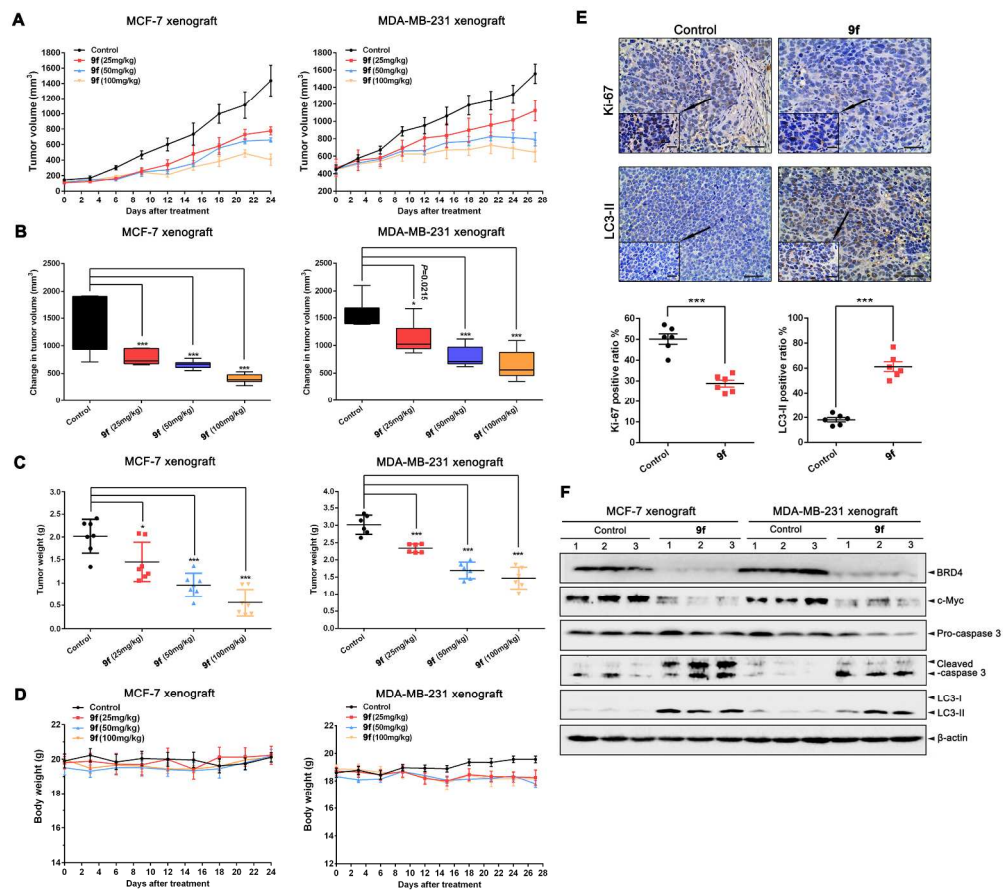
245x177mm (300 x 300 DPI)



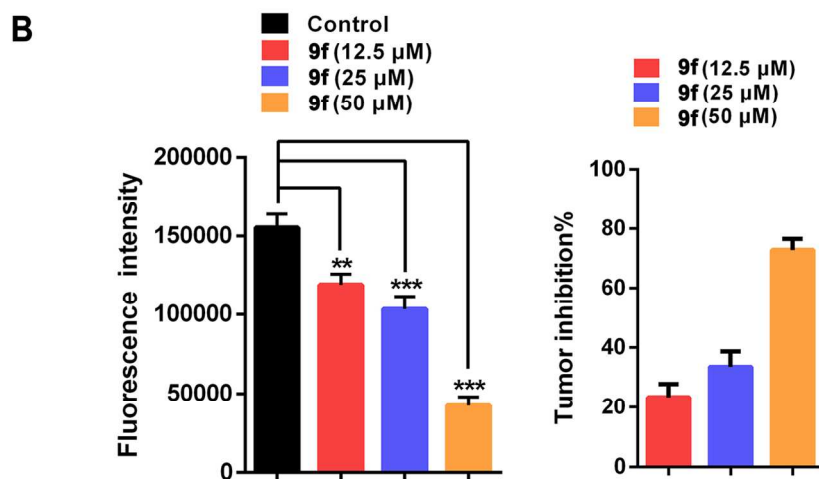
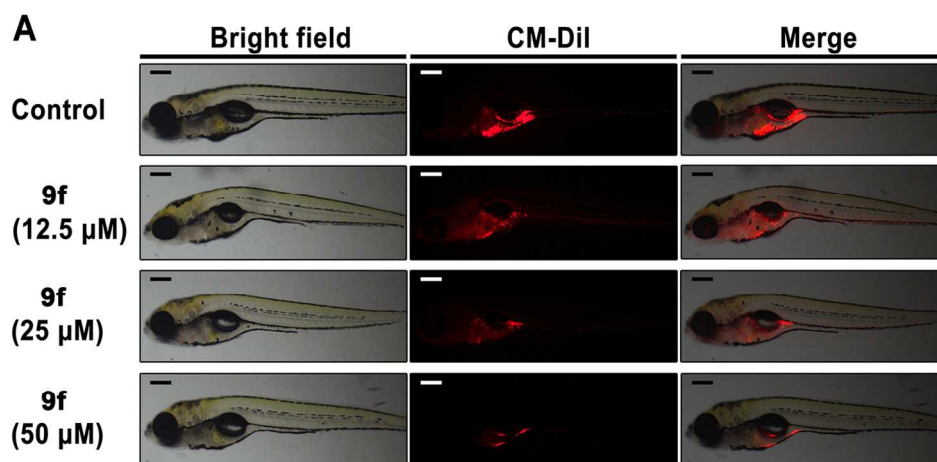
78x82mm (600 x 600 DPI)



162x248mm (300 x 300 DPI)



245x219mm (300 x 300 DPI)



131x130mm (300 x 300 DPI)